ELECTROKINETIC SEPARATIONS ON MICROFLUIDIC DEVICES FOR N-GLYCAN PROFILING

Zexi Zhuang

Submitted to the faculty of the University Graduate School
in partial fulfillment of the requirements
for the degree
Doctor of Philosophy
in the Department of Chemistry
Indiana University
August 2010

Accepted by the Graduate Faculty, Indiana University, in partial fulfillment of the requirements for the degree of Doctor of Philosophy.

Doctoral Committee

_____

Stephen C. Jacobson, Ph.D.

_____

Gary M. Hieftje, Ph.D.

_____

Milos V. Novotny, Ph.D.

_____

Bogdan Dragnea, Ph.D.

June 25, 2010

This dissertation is dedicated to my mother, Rongshen Xu, who loves and supports me unconditionally and wholeheartedly.

Acknowledgements

Communication and collaboration is fundamental for a Ph.D. to complete and present scientific research. I would like to acknowledge the many people who were involved in this work. Most directly, I would like to thank my supervisor, Professor Stephen C. Jacobson, for his support throughout my graduate career here at IU. His conscientious manner in scientific research is a model. The time spent in his research group has had a strong impact on my life. I also thank my committee members, Professors Gray M. Hieftje, Milos V. Novotny, and Bogdan Dragnea. They are extraordinary scientists, and their perspectives have been inspiring.

I greatly appreciate the opportunities to collaborate with many talented scientists: Professor Milos Novotny, Dr. Yehia Mechref, and Dr. Jason A. Starkey contributed to the glycan separation projects; Slavica Isailovic helped with glycan sample preparation and comparing the separation results with capillary electrophoresis; and Indranil Mitra contributed to the glycan separations on the serpentine microchannels. I would also like to thank Electronic Instrument Services, Mechanical Instrumentation Services, and the glass shop for their help on various projects.

I thank my co-workers for scientific discussions and help on improving presentation skills, especially Seth Madren for discussions on monolith development, Maggie Donoghue for discussions on one- and two-dimensional microfluidic separations, and Dr. Yan Liu for encouraging me to be optimistic. I am privileged to have made many friends here, and I enjoyed the time to study and learn together. I give my gratitude to them, especially Peng Du.

I cannot be grateful enough to my mother, Rongshen Xu. She supported me unconditionally throughout my life and encouraged me to pursue research and a scientific career; and to my wife, Yi He, and my son, Hunter Zhuang, for their important roles in my day to day life, sacrificing time for me to graduate with my doctorate, and keeping me pleasant. I thank my aunts, Rongyin Xu, and Rongyan Xu, for their suggestions about my career and communication skills, based on their rich experience and sincere support.

Zexi Zhuang

ELECTROKINETIC SEPARATIONS ON MICROFLUIDIC DEVICES FOR N-GLYCAN PROFILING

Microfluidic devices have been employed for various chromatographic and electrophoretic separations of biomolecules. However, the inherent complexity of analyzing real biological samples requires faster and more efficient separation techniques. N-glycans are essential molecules in many living systems and may become important biomarkers for cancer and other diseases in humans. In this work, we developed several microfluidic platforms for separation and analysis of N-glycans. On microfluidic devices, channels with high separation efficiencies can be incorporated while maintaining a small footprint. However, incorporating turns with small radii of curvature can cause significant band broadening. We explored two options to minimize the turn-induced band broadening: a spiral channel with a large radius of curvature and serpentine channels with asymetrically tapered turns. The latter serpentine design offers a more compact footprint than the spiral design. Using separation lengths of ~20 cm and electric field strengths up to 1500 V/cm, analysis times were less than 1.2 min, and separation efficiencies were between 500,000 and 655,000 plates for the N-glycans. These high efficiencies are necessary to separate structural isomers that exist in these samples. A direct comparison between microchip and capillary electrophoresis demonstrated the separation performance on microchips was as good as or better than on capillaries. Statistical analysis of the glycan profiles derived from blood serum samples revealed differences between healthy individuals and cancer patients, and relevant glycan structures may be

used as biomarkers for early stage screening and prognosis. To further increase the separation peak capacity, microfluidic platforms with serial-to-parallel interfaces were evaluated for two-dimensional N-glycan profiling. Three designs and operation modes were investigated, and an interface with a gated valve provided the highest performance and reproducibility. Capillary electrochromatography with monolithic stationary phases and capillary electrophoresis were coupled together as first and second dimensions, respectively.

_____	_____
Stephen C. Jacobson, Ph.D.	Gary M. Hieftje, Ph.D.
_____	_____
Milos V. Novotny, Ph.D.	Bogdan Dragnea, Ph.D.

Table of Contents

List of Figures and Tables

Chapter 2. Pressure Controlled Gated Valving on a Microfluidic Device

Chapter 3. Electrophoretic Analysis of N-Glycans on a Spiral Microchannel

Chapter 1. Introduction to Separations on Microfluidic Devices and Glycan Analysis

1.1. Microfluidic Devices Background and Applications

The field of microfluidics has proliferated during the past two decades. More and more applications have been developed with microfluidic devices or micro total analysis systems. The field originated from the concepts of scaling down the conventional analytical environments, where the chemical processes take place, from millimeters to micrometers. The down scaling not only reduces the intrinsic characteristics of the device, e.g., footprint, reagent consumption, waste generation, cost, and analysis time; but also makes the control of the device much easier and faster, e.g., heat dissipation, pressure, temperature, and flow velocities.

To fabricate of the microfluidic devices, photolithography and wet chemical etching techniques were initially adapted from the fabrication of microelectromechanical systems. Other techniques have also been developed rapidly, e.g., dry etching, embossing, laser ablation, and microcontact printing. The materials that are commonly used for microfluidic device fabrication include glass,[1] silicon,[2] and polymers,[3-4] e.g., poly(dimethylsiloxane) (PDMS)[5] and poly(methylmethacrylate) (PMMA).[6] Glass and silicon have good chemical and mechanical stabilities. Glass devices have shown overall the best performance and stability for chemical separations. Silicon is opaque and common detection methods such as ultraviolet absorbance or fluorescence cannot be easily integrated. PDMS, an elastomer, has shortened fabrication time by more than 50%; the good gas permeability allows cells to breathe and permits *in vitro* cell studies; and the elasticity allows pneumatic pressure controlled valving[7] and complex three dimensional

flow networks[8] to be fabricated. However, the surface chemistry of the polymer needs to be controlled to achieve long term stability, similar to glass and silicon. The polymer also swells when organic solvents are present. For our applications where separation performance is the highest priority, glass is the most suitable material. Consequently, glass has been used for fabricating all of the microfluidic devices in this dissertation.

As the dimension shrinks, challenges arise for sensitive detection of analytes. Electrochemical, mass spectrometry, and optical methods including absorption, refractive index, and fluorescence are commonly used.[9-11] Laser induced fluorescence (LIF) is one of the most sensitive methods and provides high temporal and spatial resolution data acquisition when coupled with photo-detectors and CCD cameras. A fluorescence detection setup was assembled and coupled to an inverted optical microscope for monitoring transient events at a single point in a microchannel.

The development of microfluidics field was spurred by and later expanded to many applications, most of which are related to biological and life sciences.[12] Chemical separation was one of the earliest applications and started with the miniaturized gas chromatograph in 1979.[13] Other applications have been developed rapidly, e.g., creating bubbles or droplets,[14-15] chemical reaction,[16] integration of multifunctions,[17] point of care devices,[18-19] single cell or single molecule analysis,[20-22] cytometry,[23] and drug delivery.[24] The work in this dissertation is directed towards improving the efficiency and analysis time of biomolecular separations, e.g., N-glycans, on a microfluidic platform.

1.2. Separation of Biomolecules on Microfluidic Devices

Separation is a fundamental step to analyze an unknown mixture. Separation science and technologies have been making vital contributions to various aspects of human life, among which the most widely used are chromatography and electrophoresis. The platform of separation has shifted from macro-column to micro-column because the smaller scale reduces sample band dispersion contributions to the plate height and improves the separation efficiency significantly. When the channel dimension is reduced, Reynolds numbers *Re* are usually much less than 100. Turbulent flow diminishes when *Re* is less than 2000. With laminar flow the molecules can be transported with a more predictable manner.

Various separation techniques have been demonstrated on microchips,[25] including capillary electrophoresis (CE), capillary electrochromatography (CEC),[26] micellar electrokinetic chromatography (MEKC),[27] isoelectric focusing (IEF),[28] and free-flow electrophoresis (FFE).[29] These techniques provided better performance compared to their macro-scale equivalents and benefit from the advantages of the microfluidic platforms: the smaller dimensions reduce the time for molecules to diffuse; the flat profile of electroosmotic flow reduces band broadening compared to the parabolic profile of the pressure-driven flow; and the larger surface to volume ratio facilitates heat transfer and reduces Joule heating. While the advantages are apparent, for chromatographic separations, the pressure needed increases substantially when the column dimensions decrease, which also makes pressure driven chromatography in nanofluidic channels impractical. Although pressure drop increases with decreasing channel cross section, voltage requirements for electrically driven systems remain unchanged. This condition

favors electrokinetically driven separations, which constitutes the majority of separations on microfluidic platforms. For buffers and solvents for which electrokinetic transport cannot be used, such as pure organic solvents, high conductivity solutions, and low pH buffers, pressure-driven flow control and valving on microfluidic devices was developed. A microfluidic system with a pressure-driven gated valve was demonstrated to dispense small-volume injections and is discussed in Chapter 2.

The development of the separation techniques has been largely driven by the complexity of the biomolecular samples, which includes DNA[30], amino acids[31], peptides[32], proteins[33], and glycoconjugates. In recent years, glycans have received a great deal of attention. Genomic sequences are the central structures of biological systems and are translated to produce proteins, which are the actual functional molecules in biological processes, such as cell development, cell recognition, and signal transport. A majority of eukaryotic proteins are believed to be glycosylated.[34] Glycans and glycoconjugates, such as glycoproteins and glycolipids, play important roles in many biological processes as mentioned above. Development of analytical glycomics have focused on separation and identification of the glycan mixtures to facilitate understanding of their biological functions.

1.3. Glycan Analysis Technologies

Glycan mixtures are inherently more complex than DNA and proteins because the structures can be composed of different monosaccharides components, the oligosaccharides contain branches, and the linkages between the monosaccharides can vary. Glycans can be attached to proteins that contain the appropriate sequence in their

peptide chains by two types of linkages. N-linked sugars are added to the amide side-chain of some asparagine residues, which form part of the tripeptide sequence asparagines-any amino acid-serine/threonine, while O-linked sugars are added to the hydroxyl side-chain of some serine or threonine residues. Recent glycomic studies have analyzed unfractionated samples obtained from blood serum or tissue biopsies. The large dynamic range and complexity of the samples require separation methods with excellent structural resolution and detection methods with high sensitivity.

Traditionally, gel electrophoresis[35] is used for carbohydrate separations, and exoglycosidase enzymes are used for identifying the monosaccharide sequence. More recently, chromatographic techniques including reverse phase, hydrophobic and hydrophilic interaction, and ion exchange chromatography have been applied to resolve complex glycan samples.[36] In addition, capillary electrophoretic[37-40] and electrochromatographic[41-45] methods are used to separate glycoconjugates and glycans. In particular, capillary electrophoresis combined with mass spectrometry[46] has been used in several applications because of thehigh separation efficiency, ability to resolve structural isomers, direct mass and structure information, and high sensitivity. Over the past several years, a lectin-based microarray technique has been developed for glycan analysis.[47] This technique relies on using a group of lectins that selectively interact with certain glycan structures and bioinformatics for data processing to deconvolute the signal.

For chromatographic and electrophoretic glycan separations, detection is usually facilitated by a fluorescent tag, which is coupled to the glycans prior to analysis. A variety of molecules have been explored for this purpose and includes 2-aminopyridine,[48] 8-aminopyrene-1,3,6-trisulfonic acid (APTS),[49] and 2-aminoacridone (2-AMAC).[50] The

fluorescent label is typically connected to the reducing end of the glycans by reductive amination. The reaction results in one fluorescent label per glycan molecule and makes quantitative analysis possible. The APTS label adds three negative charges to the glycans, which enhances their electrophoretic mobilities and permits fast CE separations. 2-AMAC is neutral, and the labeled sugars can be separated by either hydrophilic or hydrophobic chromatographic techniques.

1.4. Glycan Profiling on Microfluidic Platforms

Compared to traditional HPLC and capillaries, microfluidic platforms offer precise fluidic handling, improved heat dissipation, and integration of multiple functions. Consequently, faster and more efficient glycan separations are expected. Microchip electrophoretic characterization of sugar isomers using polymethyl methacrylate (PMMA) chips and methylcellulose containing buffers to minimize the analyte adsorption was demonstrated.[51-54] Blood serum glycans were separated with 4% polyacrylamide gel sieving matrix.[55] Labeled hexosamines at the C-2 amino groups and monosaccharides were analyzed as phosphate or borate complexes with UV detection on quartz chips made by Shimadzu.[56-57]

The studies above have demonstrated glycan separations, but the plate numbers generated are low and not sufficient to resolve positional and linkage isomers. The separation channels incorporated had short lengths (3.3-7.0 cm). On microfluidic devices, channels with high separation efficiencies can be incorporated while maintaining a small footprint. However, incorporating turns with small radii of curvature can lead to significant band broadening. We explored two options to generate high efficiency

separation of N-glycans and to minimize the turn-induced band broadening: (1) a spiral channel with a large radius of curvature[58] and (2) serpentine channels with asymetrically tapered turns.[59-60] The latter serpentine design offers a more compact footprint than the spiral design. The electric field strengths used in previous studies were lower than 300 V/cm. However, in microchip electrophoresis, separation efficiency increases with electric field strength. On the serpentine microchannels separations with field strengths of up to ~1500 V/cm were investigated. As expected, separation efficiencies increased substantially as the field strength was increased up to 1000 V/cm and began to level off above 1000 V/cm. The electrophoretic separations on the spiral and serpentine channel designs are reported in Chapters 3 and 4, respectively.

To further increase the separation peak capacity, microfluidic platforms with serial-to-parallel interfaces were developed and evaluated for two-dimensional N-glycan separation. Two most common formats of joining two dimensional separations on microfluidic devices are serial and planar coupling.[61-65] To date, serial coupling systems have offered superior peak capacities. However, serial coupling requires the second dimensional separation to be operated ~10 times faster than the first dimensional separation in order to sample the first dimension effluent sufficiently. With the serial-to-parallel interfaces, we combine the fluid handling capabilities of microfluidic devices as seen in the serially coupled separations with the array format for the 2D separation on the planar devices. In Chapter 5, three designs and operation modes were discussed, and an interface with a gated valve provided the highest performance and reproducibility. In Chapter 6, CEC with monolithic stationary phases[66] and CE were coupled together as first and second dimensions on the gated serial-to-parallel interface, respectively.

1.5. References

1. Jacobson, S. C.; Hergenroder, R.; Moore, A. W.; Ramsey, J. M., Precolumn Reactions with Electrophoretic Analysis Integrated on a Microchip. *Anal. Chem.* **1994,** *66* (23), 4127-4132.
2. Manz, A.; Miyahara, Y.; Miura, J.; Watanabe, Y.; Miyagi, H.; Sato, K., Design of an Open-Tubular Column Liquid Chromatograph Using Silicon Chip Technology. *Sens. Actuators B Chem.* **1990,** *1* (1-6), 249-255.
3. Becker, H.; Gartner, C., Polymer Microfabrication Technologies for Microfluidic Systems. *Anal. Bioanal. Chem.* **2008,** *390* (1), 89-111.
4. Becker, H.; Gartner, C., Polymer Microfabrication Methods for Microfluidic Analytical Applications. *Electrophoresis* **2000,** *21* (1), 12-26.
5. McDonald, J. C.; Duffy, D. C.; Anderson, J. R.; Chiu, D. T.; Wu, H. K.; Schueller, O. J. A.; Whitesides, G. M., Fabrication of Microfluidic Systems in Poly(Dimethylsiloxane). *Electrophoresis* **2000,** *21* (1), 27-40.
6. Martynova, L.; Locascio, L. E.; Gaitan, M.; Kramer, G. W.; Christensen, R. G.; MacCrehan, W. A., Fabrication of Plastic Microfluid Channels by Imprinting Methods. *Anal. Chem.* **1997,** *69* (23), 4783-4789.
7. Unger, M. A.; Chou, H. P.; Thorsen, T.; Scherer, A.; Quake, S. R., Monolithic Microfabricated Valves and Pumps by Multilayer Soft Lithography. *Science* **2000,** *288* (5463), 113-116.
8. Wu, H. K.; Odom, T. W.; Chiu, D. T.; Whitesides, G. M., Fabrication of Complex Three-Dimensional Microchannel Systems in Pdms. *J. Am. Chem. Soc.* **2003,** *125* (2), 554-559.
9. Mogensen, K. B.; Klank, H.; Kutter, J. P., Recent Developments in Detection for Microfluidic Systems. *Electrophoresis* **2004,** *25* (21-22), 3498-3512.
10. Vandaveer, W. R.; Pasas-Farmer, S. A.; Fischer, D. J.; Frankenfeld, C. N.; Lunte, S. M., Recent Developments in Electrochemical Detection for Microchip Capillary Electrophoresis. *Electrophoresis* **2004,** *25* (21-22), 3528-3549.
11. Johnson, M. E.; Landers, J. P., Fundamentals and Practice for Ultrasensitive Laser-Induced Fluorescence Detection in Microanalytical Systems. *Electrophoresis* **2004,** *25* (21-22), 3513-3527.
12. Auroux, P. A.; Iossifidis, D.; Reyes, D. R.; Manz, A., Micro Total Analysis Systems. 2. Analytical Standard Operations and Applications. *Anal. Chem.* **2002,** *74* (12), 2637-2652.
13. Terry, S. C.; Jerman, J. H.; Angell, J. B., Gas-Chromatographic Air Analyzer Fabricated on a Silicon-Wafer. *IEEE Trans. Electron Devices* **1979,** *26* (12), 1880-1886.
14. Prakash, M.; Gershenfeld, N., Microfluidic Bubble Logic. *Science* **2007,** *315* (5813), 832-835.
15. Fuerstman, M. J.; Garstecki, P.; Whitesides, G. M., Coding/Decoding and Reversibility of Droplet Trains in Microfluidic Networks. *Science* **2007,** *315* (5813), 828-832.
16. deMello, A. J., Control and Detection of Chemical Reactions in Microfluidic Systems. *Nature* **2006,** *442* (7101), 394-402.

17. Ohno, K.; Tachikawa, K.; Manz, A., Microfluidics: Applications for Analytical Purposes in Chemistry and Biochemistry. *Electrophoresis* **2008,** *29* (22), 4443-4453.
18. Weigl, B.; Domingo, G.; LaBarre, P.; Gerlach, J., Towards Non- and Minimally Instrumented, Microfluidics-Based Diagnostic Devices. *Lab Chip* **2008,** *8* (12), 1999-2014.
19. Myers, F. B.; Lee, L. P., Innovations in Optical Microfluidic Technologies for Point-of-Care Diagnostics. *Lab Chip* **2008,** *8* (12), 2015-2031.
20. Bennett, M. R.; Hasty, J., Modelling Microfluidic Devices for Measuring Gene Network Dynamics in Single Cells. *Nat. Rev. Genet.* **2009,** *10* (9), 628-638.
21. El-Ali, J.; Sorger, P. K.; Jensen, K. F., Cells on Chips. *Nature* **2006,** *442* (7101), 403-411.
22. Craighead, H., Future Lab-on-a-Chip Technologies for Interrogating Individual Molecules. *Nature* **2006,** *442* (7101), 387-393.
23. Yan, H.; Zhang, B. Y.; Wu, H. K., Chemical Cytometry on Microfluidic Chips. *Electrophoresis* **2008,** *29* (9), 1775-1786.
24. Tao, S. L.; Desai, T. A., Microfabricated Drug Delivery Systems: From Particles to Pores. *Adv. Drug Deliver. Rev.* **2003,** *55* (3), 315-328.
25. Wu, D. P.; Qin, J. H.; Lin, B. C., Electrophoretic Separations on Microfluidic Chips. *J. Chromatogr. A* **2008,** *1184* (1-2), 542-559.
26. Svec, F., Cec: Selected Developments That Caught My Eye since the Year 2000. *Electrophoresis* **2009,** *30*, S68-S82.
27. Kitagawa, F.; Otsuka, K., Micellar Eletrokinetic Chromatography on Microchips. *J. Sep. Sci.* **2008,** *31* (5), 794-802.
28. Sommer, G. J.; Hatch, A. V., Ief in Microfluidic Devices. *Electrophoresis* **2009,** *30* (5), 742-757.
29. Kohlheyer, D.; Eijkel, J. C. T.; van den Berg, A.; Schasfoort, R. B. M., Miniaturizing Free-Flow Electrophoresis - a Critical Review. *Electrophoresis* **2008,** *29* (5), 977-993.
30. Szantai, E.; Guttman, A., Genotyping with Microfluidic Devices. *Electrophoresis* **2006,** *27* (24), 4896-4903.
31. Pumera, M., Microfluidics in Amino Acid Analysis. *Electrophoresis* **2007,** *28* (13), 2113-2124.
32. Kasicka, V., Recent Advances in Ce and Cec of Peptides (2007-2009). *Electrophoresis* **2010,** *31* (1), 122-146.
33. Tran, N. T.; Ayed, I.; Pallandre, A.; Taverna, M., Recent Innovations in Protein Separation on Microchips by Electrophoretic Methods: An Update. *Electrophoresis* **2010,** *31* (1), 147-173.
34. Apweiler, R.; Hermjakob, H.; Sharon, N., On the Frequency of Protein Glycosylation, as Deduced from Analysis of the Swiss-Prot Database. *Biochim. Biophys. Acta* **1999,** *1473* (1), 4-8.
35. Jackson, P., The Analysis of Fluorophore-Labeled Glycans by High-Resolution Polyacrylamide-Gel Electrophoresis. *Anal. Biochem.* **1994,** *216* (2), 243-252.
36. El Rassi, Z., *Carbohydrate Analysis-High Performance Liquid Chromatography and Capillary Electrophoresis*. Elsevier Science B.V.: Amsterdam, The Ntherlands, 1995.

37. Liu, J. P.; Shirota, O.; Wiesler, D.; Novotny, M., Ultrasensitive Fluorometric Detection of Carbohydrates as Derivatives in Mixtures Separated by Capillary Electrophoresis. *Proc. Natl. Acad. Sci. U. S. A.* **1991,** *88* (6), 2302-2306.
38. Nashabeh, W.; Elrassi, Z., Capillary Zone Electrophoresis of Linear and Branched Oligosaccharides. *J. Chromatogr. A* **1992,** *600* (2), 279-287.
39. Kakehi, K.; Susami, A.; Taga, A.; Suzuki, S.; Honda, S., High-Performance Capillary Electrophoresis of O-Glycosidically Linked Sialic Acid-Containing Oligosaccharides in Glycoproteins as Their Alditol Derivatives with Low-Wavelength Uv Monitoring. *J. Chromatogr. A* **1994,** *680* (1), 209-215.
40. Hutterer, K. M.; Birrell, H.; Camilleri, P.; Jorgenson, J. W., High Resolution of Oligosaccharide Mixtures by Ultrahigh Voltage Micellar Electrokinetic Capillary Chromatography. *J. Chromatogr. B* **2000,** *745* (2), 365-372.
41. Palm, A.; Novotny, M. V., Macroporous Polyacrylamide Poly(Ethylene Glycol) Matrixes as Stationary Phases in Capillary Electrochromatography. *Anal. Chem.* **1997,** *69* (22), 4499-4507.
42. Yang, C. M.; El Rassi, Z., Capillary Electrochromatography of Derivatized Mono- and Oligosaccharides. *Electrophoresis* **1998,** *19* (12), 2061-2067.
43. Suzuki, S.; Yamamoto, M.; Kuwahara, Y.; Makiura, K.; Honda, S., Separation of 1-Phenyl-3-Methyl-5-Pyrazolone Derivatives of Monosaccharides by Capillary Electrochromatography. *Electrophoresis* **1998,** *19* (15), 2682-2688.
44. Que, A. H.; Mechref, Y.; Huang, Y. P.; Taraszka, J. A.; Clemmer, D. E.; Novotny, M. V., Coupling Capillary Electrochromatography with Electrospray Fourier Transform Mass Spectrometry for Characterizing Complex Oligosaccharide Pools. *Anal. Chem.* **2003,** *75* (7), 1684-1690.
45. Tegeler, T. J.; Mechref, Y.; Boraas, K.; Reilly, J. P.; Novotny, M. V., Microdeposition Device Interfacing Capillary Electrochromatography and Microcolumn Liquid Chromatography with Matrix-Assisted Laser Desorption/Ionization Mass Spectrometry. *Anal. Chem.* **2004,** *76* (22), 6698-6706.
46. Mechref, Y.; Novotny, M. V., Glycomic Analysis by Capillary Electrophoresis-Mass Spectrometry. *Mass Spectrom. Rev.* **2009,** *28* (2), 207-222.
47. Kuno, A.; Uchiyama, N.; Koseki-Kuno, S.; Ebe, Y.; Takashima, S.; Yamada, M.; Hirabayashi, J., Evanescent-Field Fluorescence-Assisted Lectin Microarray: A New Strategy for Glycan Profiling. *Nat. Methods* **2005,** *2* (11), 851-856.
48. Tomiya, N.; Awaya, J.; Kurono, M.; Endo, S.; Arata, Y.; Takahashi, N., Analyses of N-Linked Oligosaccharides Using a Two-Dimensional Mapping Technique. *Anal. Biochem.* **1988,** *171* (1), 73-90.
49. Evangelista, R. A.; Liu, M. S.; Chen, F. T. A., Characterization of 9-Aminopyrene-1,4,6-Trisulfonate-Derivatized Sugars by Capillary Electrophoresis with Laser-Induced Fluorescence Detection. *Anal. Chem.* **1995,** *67* (13), 2239-2245.
50. Greenaway, M.; Okafo, G. N.; Camilleri, P.; Dhanak, D., A Sensitive and Selective Method for the Analysis of Complex-Mixtures of Sugars and Linear Oligosaccharides. *J. Chem. Soc. Chem. Comm.* **1994,** (14), 1691-1692.
51. Dang, F.; Zhang, L.; Hagiwara, H.; Mishina, Y.; Baba, Y., Ultrafast Analysis of Oligosaccharides on Microchip with Light-Emitting Diode Confocal Fluorescence Detection. *Electrophoresis* **2003,** *24* (4), 714-721.

52. Dang, F. Q.; Kakehi, K.; Cheng, J. J.; Tabata, O.; Kurokawa, M.; Nakajima, K.; Ishikawa, M.; Baba, Y., Hybrid Dynamic Coating with N-Dodecyl Beta-D-Maltoside and Methyl Cellulose for High-Performance Carbohydrate Analysis on Poly(Methyl Methacrylate) Chips. *Anal. Chem.* **2006,** *78* (5), 1452-1458.
53. Dang, F. Q.; Kakehi, K.; Nakajima, K.; Shinohara, Y.; Ishikawa, M.; Kaji, N.; Tokeshi, M.; Baba, Y., Rapid Analysis of Oligosaccharides Derived from Glycoproteins by Microchip Electrophoresis. *J. Chromatogr. A* **2006,** *1109* (2), 138-143.
54. Dang, F. Q.; Zhang, L. H.; Jabasini, M.; Kaji, N.; Baba, Y., Characterization of Electrophoretic Behavior of Sugar Isomers by Microchip Electrophoresis Coupled with Videomicroscopy. *Anal. Chem.* **2003,** *75* (10), 2433-2439.
55. Callewaert, N.; Contreras, R.; Mitnik-Gankin, L.; Carey, L.; Matsudaira, P.; Ehrlich, D., Total Serum Protein N-Glycome Profiling on a Capillary Electrophoresis-Microfluidics Platform. *Electrophoresis* **2004,** *25* (18-19), 3128-3131.
56. Suzuki, S.; Shimotsu, N.; Honda, S.; Arai, A.; Nakanishi, H., Rapid Analysis of Amino Sugars by Microchip Electrophoresis with Laser-Induced Fluorescence Detection. *Electrophoresis* **2001,** *22* (18), 4023-4031.
57. Suzuki, S.; Ishida, Y.; Arai, A.; Nakanishi, H.; Honda, S., High-Speed Electrophoretic Analysis of 1-Phenyl-3-Methyl-5-Pyrazolone Derivatives of Monosaccharides on a Quartz Microchip with Whole-Channel Uv Detection. *Electrophoresis* **2003,** *24* (21), 3828-3833.
58. Culbertson, C. T.; Jacobson, S. C.; Ramsey, J. M., Microchip Devices for High-Efficiency Separations. *Anal. Chem.* **2000,** *72* (23), 5814-5819.
59. Griffiths, S. K.; Nilson, R. H., Band Spreading in Two-Dimensional Microchannel Turns for Electrokinetic Species Transport. *Anal. Chem.* **2000,** *72* (21), 5473-5482.
60. Molho, J. I.; Herr, A. E.; Mosier, B. P.; Santiago, J. G.; Kenny, T. W.; Brennen, R. A.; Gordon, G. B.; Mohammadi, B., Optimization of Turn Geometries for Microchip Electrophoresis. *Anal. Chem.* **2001,** *73* (6), 1350-1360.
61. Ramsey, J. D.; Jacobson, S. C.; Culbertson, C. T.; Ramsey, J. M., High-Efficiency, Two-Dimensional Separations of Protein Digests on Microfluidic Devices. *Anal. Chem.* **2003,** *75* (15), 3758-3764.
62. Gottschlich, N.; Jacobson, S. C.; Culbertson, C. T.; Ramsey, J. M., Two-Dimensional Electrochromatography/Capillary Electrophoresis on a Microchip. *ANAL CHEM* **2001,** *73* (11), 2669-2674.
63. Chen, X. X.; Wu, H. K.; Mao, C. D.; Whitesides, G. M., A Prototype Two-Dimensional Capillary Electrophoresis System Fabricated in Poly(Dimethylsiloxane). *Anal. Chem.* **2002,** *74* (8), 1772-1778.
64. O'Farrell, P. H., High Resolution Two-Dimensional Electrophoresis of Proteins. *J. Biol. Chem.* **1975,** *250* (10), 4007-21.
65. Emrich, C. A.; Medintz, I. L.; Chu, W. K.; Mathies, R. A., Microfabricated Two-Dimensional Electrophoresis Device for Differential Protein Expression Profiling. *Anal. Chem.* **2007,** *79* (19), 7360-7366.

66. Zhong, H. W.; El Rassi, Z., Neutral Polar Methacrylate-Based Monoliths for Normal Phase Nano-Lc and Cec of Polar Species Including N-Glycans. *J. Sep. Sci.* **2009,** *32* (1), 10-20.

Chapter 2. Pressure Controlled Gated Valving on a Microfluidic Device

2.1. Introduction to Microchip Hydrodynamic Chromatography

Interest in microfluidic devices, also called lab-on-a-chip" or micro total analysis systems (μTAS), is growing rapidly. Capillary electrophoresis (CE),[1-3] liquid chromatography (LC), micellar electrokinetic chromatography (MEKC),[4-5] capillary gel electrophoresis (CGE),[6-7] hydrodynamic chromatography (HDC)[8-10] and several other separation techniques have been demonstrated on chips.[11-12] With on-chip separations, higher efficiencies and shorter analysis times can be achieved. Since the pioneering work of Terry et al.[13] in 1979 for a miniaturized gas chromatography, a large fraction of research on microfluidic devices has been directed toward developing electrokinetically driven separations, especially for genomics and proteomics. Meanwhile, for systems that cannot support electrokinetic transport, such as organic solvents, high conductivity solutions, and low pH buffers, pressure-driven flow control and valving on microfluidic devices is necessary.

A pressure difference, Δp, along a liquid filled microchannel results in a parabolic flow profile with an average velocity u. The velocity of the liquid is fastest in the center of the channel and zero at the channel wall. Between the center and the wall a velocity gradient du/dr is established due to frictional forces. In a capillary with a circular cross-section, the velocity gradient is determined by the well-known Hagen-Poiseuille equation.

$$u(r) = \frac{\Delta p}{4\eta l}(R^2 - r^2) \quad (1)$$

where R is the radius of the channel, r is the distance from the center, l is the length, and η is the viscosity. One consequence is larger molecules move faster in the channel than smaller molecules because the larger molecules cannot access low velocity regions near the channel wall.

Several groups have directed their work towards pressure-driven flow in microfluidic channels. Whitesides and coworkers have demonstrated a pressure-driven flow control switch on a three-dimensional elastomeric microchip based on tangential contact microchannels[14] and some other applications.[15-17] Burns and coworkers developed a method to thermopneumatically pump discrete drops in microchannels by heating trapped air in a pressure-generating chamber.[18] Hong et al. presented an on-chip pressure generator utilizing energy from solid chemical propellant.[19] Chang et al. demonstrated a bi-directional airflow driving microfluidic system combing suction and exclusion.[20] van den Berg et al.[8-10] developed a microfluidic system for hydrodynamic separation. The chip was clamped to a macroflow-actuating system, and solvent was pressed through the gas-pressurized vessels. Gesmet et al. discussed the sidewall-induced band broadening effect in pressure-driven microfabricated columns and possible solutions to reduce it.[21] Haswell's group demonstrated several organic syntheses in pressure-driven micro reactors.[22-24] Most recently, van de Goor et al. developed a microfluidic system for peptide analysis with an integrated HPLC column, sample enrichment column, and nanoelectrospray tip.[25]

In this work, we developed a simple, on-chip pressure-driven microfluidic valve capable of generating reproducible, small-volume injections in microchannels and providing flexible control of pressure-driven flows. Fluid velocities were calculated for

various applied pressures, and a linear relationship between velocity and pressure was observed.

2.2. Experimental Section

Microchip Design and Fabrication. The microchip was fabricated in white crown glass by standard photolithographic methods and wet chemical etching, as previously described.[26-27] Briefly, a positive photomask (Telic Co.) was fabricated on a chrome-coated soda lime glass substrate from a CAD design. The microchip substrate was white crown glass covered with a thin chromium film (100nm), an anti-reflective coating, and a positive photoresist. The microchip design then was transferred onto the glass substrate by UV flood exposure (Optical Associates, Inc.). The photoresist was developed (Microposit MF 319; Rohm and Haas Electronic Materials, Inc.), and the chromium film of the channel pattern was etched (Cr etchant 1020; Transene Company, Inc.). Channels were etched with a dilute, stirred buffered oxide etchant (Transene Company, Inc.). Access holes for reservoirs were drilled at the ends of the channels with a sandblaster (Paasche Airbrush Co.). The drilled substrate and cover plate were then hydrolyzed, brought into contact with each other, ramped, and heated at 550° C for 10 h to permanently bond the substrate and the cover plate. Short segments of glass tubing (1/4" o.d. x 1/4" i.d. x 1/4" tall) were epoxied to the drilled side of the bonded substrate for reservoirs. The channel dimensions were measured with a stylus profiler (Dektak 6M; Veeco Instruments, Inc.) and were 9.7 μm deep and 39.4 μm wide at the top.

Instrumentation. A nitrogen gas cylinder was used as the pressure source. Pressure was applied to the chip through a stainless steel gas manifold, on which solenoids were

mounted for gas control. The output of the manifold was connected through a tee fitting (Swagelok Co.) to the chip and to the pressure transducers (PX137-015DV; OMEGA Engineering INC.). The signals from the pressure transducers were sampled at 100 Hz with a National Instruments PCI-6032E multifunction I/O card. A schematic of the chip design is shown in **Figure 1-1**. Pressure was applied to the buffer and sample reservoirs. To make a pressure injection, the solenoid was switched to a lower pressure at the buffer reservoir, which allowed sample to move onto the separation channel. The solenoids were computer controlled through an analog output board (PCI-6713 AO card; National Instruments Corp., Austin, TX) LabView program, and a simple transistor switch circuit. The degree of venting was manually controlled by needle valves (Swagelok Co.) on the gas manifold.

Solutions. A 10 mM sodium tetraborate (Sigma-Aldrich) solution was used as the buffer. 1 M Sodium hydroxide solution was used for cleaning the chip. 50 mM sodium chloride (Fluka) and 10 mM sodium tetraborate solution was used for conductivity measurements. 10 μM Rhodamine B (Aldrich) in 10 mM sodium tetraborate solution was used for imaging and single point detection. All water used was 18 MΩ·cm and filtered (0.2 μm filter).

Conductivity Measurements. The channel lengths were measured on an inverted microscope (Nikon Eclipse TE200-U) equipped with linear scales (Microcode II, Boeckeler Instruments) attached to the stage. Channel resistances were measured with the 10 mM sodium tetraborate and 50 mM sodium chloride solution as the buffer. A potential of 10 V (Keithley 6487) was applied to each pair of channels, and the current

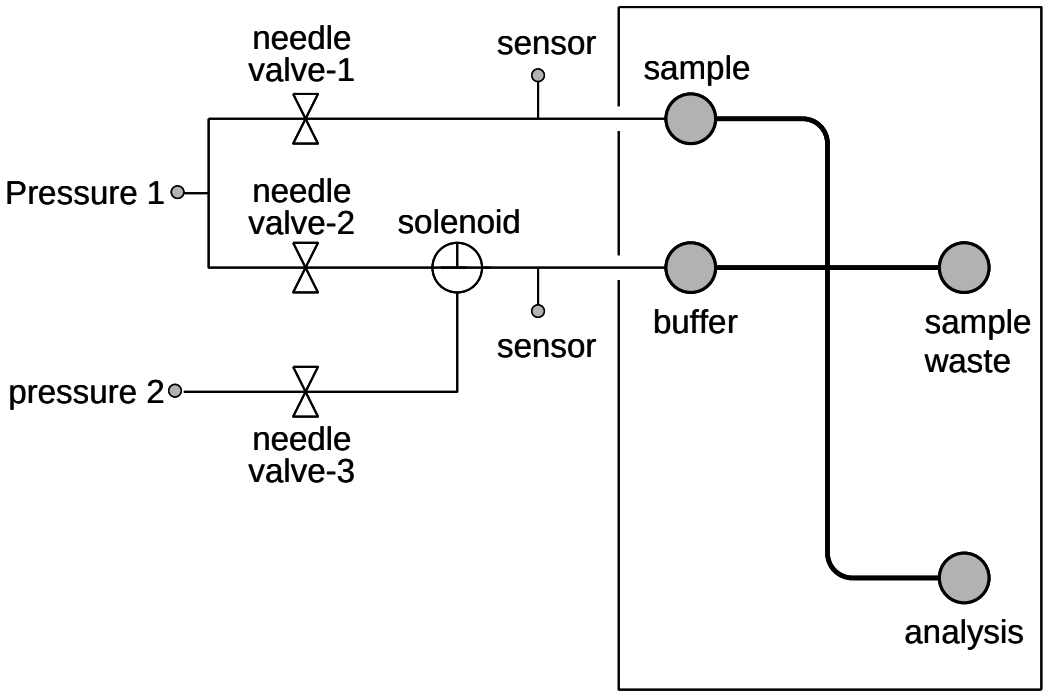

Figure 1-1. Schematic of the microfluidic device design and experimental setup. Pressures were applied at the sample and buffer reservoirs of the chip with needle valves in-lineto control relative pressures. A solenoid was employed to control whether a higher pressure (1) or lower pressure (2) was applied at the buffer reservoir. Two pressure sensors were integrated to monitor the pressures.

Table 1-1. Microchannel lengths and resistances

Channel	Buffer	Sample	Sample Waste	Waste
Length (mm)	6.62	16.60	6.56	36.62
Resistance (MΩ)	28.7	72.5	23.8	156

was measured with a picoammeter (Keithley 6485). Channel lengths and resistances are shown in **Table 1-1**.

Microchip Operation. Microchips were initially cleaned with a 1 M sodium hydroxide solution with applying vacuum for 5 min at each reservoir. The chips were then rinsed with water to clean out the sodium hydroxide. Pressure-driven injections were tested by lowering pressure applied at the buffer reservoir. For load mode, appropriate pressures were applied at both sample and buffer reservoirs. For dispense mode, the pressure at the buffer reservoir was lowered by switching the solenoid (controlled by LabView) for a short period of time (100–500 ms) and then returning the solenoid to its original state. Images of the pressure-driven injections were taken with a CCD camera (Micromax; Roper Scientific, Inc., Princeton Instruments) and movies were captured with a digital camera (SONY IEEE 1394, DFW-V500).

Injections of 100, 300 and 500 ms of 10 μM rhodamine B were tested at different pressures (approximately 1, 2, 4, and 8 psi). Ten injections were made for each condition. For each applied pressure, the fluorescence signals were detected at two points (1 mm and 10 mm downstream from the cross intersection).

Pressure-driven injections were monitored at a single location in the microchannel with laser induced fluorescence (LIF) detection.[28] The 514.5-nm line of an argon ion laser (MELLES GRIOT, 543-AP-A01) was used as the excitation source at 5 mW. A similar setup was constructed on one camera port of the inverted microscope as shown in **Figure 2-2**. With a 40-mm focal length biconvex lens (ThorLabs, LB1027), a parfocal image was formed at a pinhole (600 μm, ThorLabs). A microscope coverslip was placed

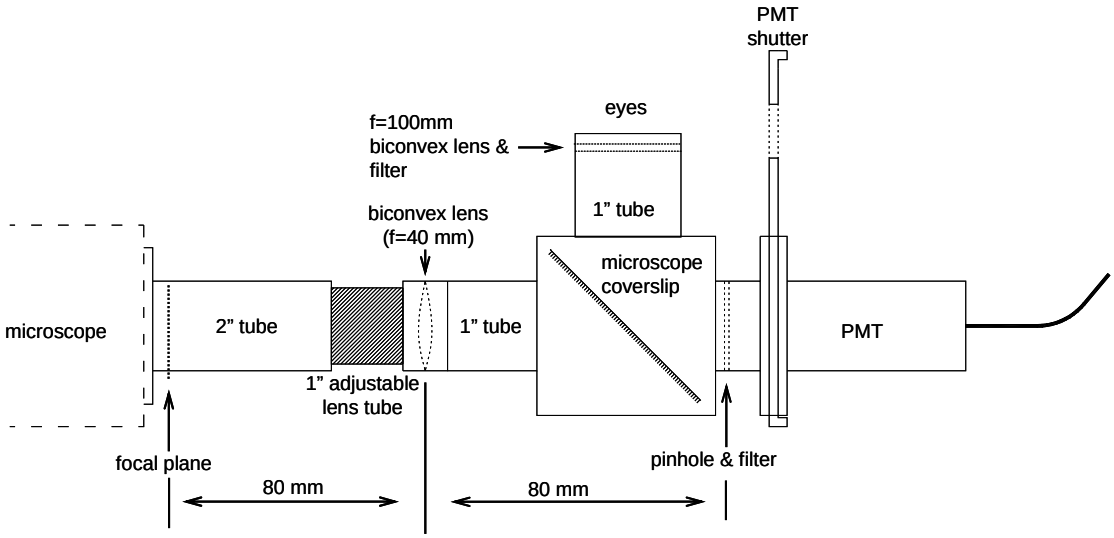

Figure 2-2. Schematic of the single point detection scheme attached to a camera port of the microscope. 2" and 1" lens tubes and a 1" adjustable lens tube were mounted onto the camera port of the microscope. A biconvex lens (f = 40 mm) was secured in the 1" adjustable lens tube. Position of the 1" adjustable lens tube was set such that the lens was located 80 mm from both the microscope focal plane and the pinhole plane. Position of the 1" adjustable lens tube was then finely adjusted to achieve the best focus. A microscope coverslip was placed at 45° before the pinhole (parfocal image plane) to facilitate alignment.

at 45° before the pinhole to provide an image of the channel over the pinhole. The laser beam was reflected and focused onto the channel with a 20x microscope objective, and the fluorescence was collected through the same objective. The signal passing through the pinhole was spectrally filtered with a 550 nm cut off filter (Thorlabs, Inc.) before being measured at a photomultiplier tube (PMT; H5783-01, Hamamatsu Corp.). The signal from the PMT was amplified (SR570, Stanford Research Systems). The signal from the amplifier was sampled at 100 Hz with the multifunction I/O card. Data acquisition was accomplished in the same LabView program that was used for pressure measurements.

2.3. Results and Discussion

Theory. For the cross microchip used for this project, the cross sections of the channels were considered as rectangles. The total fluid flow velocities into and out of the intersection are equal. Because the cross-sectional area in each of the channels was approximately the same, the pressure generated flow rate down each branch of the channels is given by the following equations:[29]

$$u_s + u_b + u_w + u_{sw} = 0 \qquad (2)$$

$$u_i = \frac{\Delta P_i d^2}{\eta l_i}\left(\frac{1}{12} - \frac{16d}{\pi^5 w}\right) \qquad (3)$$

where ΔP_i is the pressure drop from the reservoir i to the intersection, d is the depth of the channel, w is the width of channel, and l_i is the length of channel i. The subscripts designate the channel from the cross intersection to the corresponding reservoir: s for sample, b for buffer, sw for sample waste, and w for waste. Equation 3 describes the

average flow velocity when the channel aspect ratio satisfies $w > 3d$. If $w >> d$, then the second term in the parenthetical expression in equation 3 approaches zero, and the equation simplifies to the equation presented by Giddings[30] for thin rectangular channels. The pressure generated at the intersection was calculated by inserting equation 3 into equation 2 and solving for P_i as shown in equation 4, where P_s, P_{sw}, P_b, and P_w are the pressures applied at the reservoirs, and l_s, l_{sw}, l_b, and l_w are for channel lengths as defined above. Pressures at the intersection for load and dispense modes were calculated by substituting the pressures measured by the pressure transducers into equation 4.

$$P_i = \frac{\left(\frac{P_s}{L_s} + \frac{P_b}{L_b} + \frac{P_{sw}}{L_{sw}} + \frac{P_w}{L_w}\right)}{\left(\frac{1}{L_s} + \frac{1}{L_b} + \frac{1}{L_{sw}} + \frac{1}{L_w}\right)} \qquad (4)$$

By substituting pressures calculated from equation 4 into equation 3, the pressure induced linear velocities can be calculated.

Pressure Valving Images. A sequence of images for a pressure-driven injection is shown in **Figure 2-3**. Image (a) is a white light image of the microchannel intersection showing the channel layout. Sample loading is shown in image (b), where similar pressures were applied to the sample and buffer reservoirs. Because the analysis channel was longer than the sample waste channel, flow resistance in the channel was higher, and thus, sample was pushed towards the sample waste reservoir. To make an injection, as shown in image (c), the pressure applied at the buffer reservoir was switched to a lower pressure. To terminate the injection, the higher pressure was reapplied by switching the

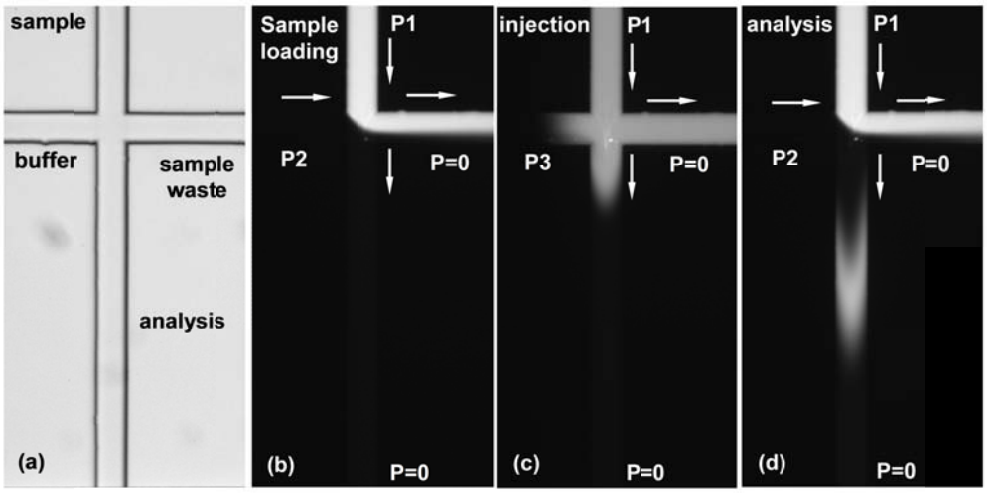

Figure 2-3. Image sequence for a 100-ms pressure-driven injection. The pressures applied for the injection were 1.97 psi to the sample reservoir and 1.43 psi to the buffer reservoir. (a) White light image. (b) Sample loading. (c) Injection. (d) Analysis. In (b), (c), and (d), the bright areas are the rhodamine B sample, and the dark areas are the background. The arrows indicate the relative direction of the sample and buffer flows.

solenoid back to its initial state. The pressure-driven parabolic flow profile is shown in image (d).

Pressure and Fluorescence Profiles. Pressure-driven injections were detected by the single point LIF detection setup described above As shown in **Figure 2-4**, pressure (line profile 1) at the buffer reservoir was lowered to 0 for 100 ms and returned to the initial state to make an injection. After an average 1.283 s, an injected sample plug arrived at the detection point (line profile 2), and a peak was detected. Four of 10 peaks are shown in the figure.

In **Figure 2-5**, ten injections from one series of injections with an applied pressure of ~ 1 psi are overlaid, and injections with injections times of 100, 300, and 500 ms are aligned at the falling edges of the injection pulses. The rising edges of the peaks were aligned as expected, and peak areas and peak heights of the injections increased as the injection time increased. The figure shows how well ten temporal profiles overlay with respect to position and shape and demonstrated reproducibility of the device. Relative standard deviations of integrated peak areas were less than 0.7%.

Variation of Velocity with Applied Pressure. Transit time of the sample from the intersection to the single point detection point (10 mm downstream from intersection point) was evaluated by taking the time from start of the injection to the leading edge of the injected peak. First derivatives of the peaks were calculated and plotted to find the leading edges. During the peak transit time, the sample traveled at two different velocities corresponding to the two different pressures applied at the buffer reservoir for sample loading mode and dispense mode (see equation 5).

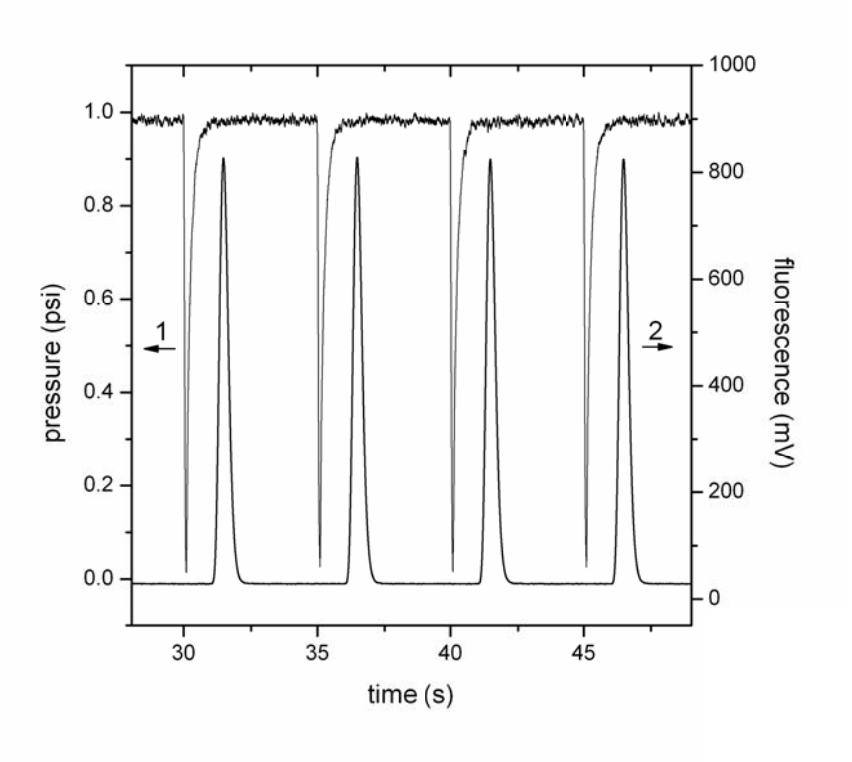

Figure 2-4. Pressure transducer and fluorescence signals for the 100-ms injections. The detection point was 1 mm downstream from the intersection. The pressures applied for these injections were ~2 psi to the sample reservoir and ~1 psi to the buffer reservoir. Four of ten peaks are shown. Curve 1 represents the pressure profile, and curve 2 shows the fluorescence signal.

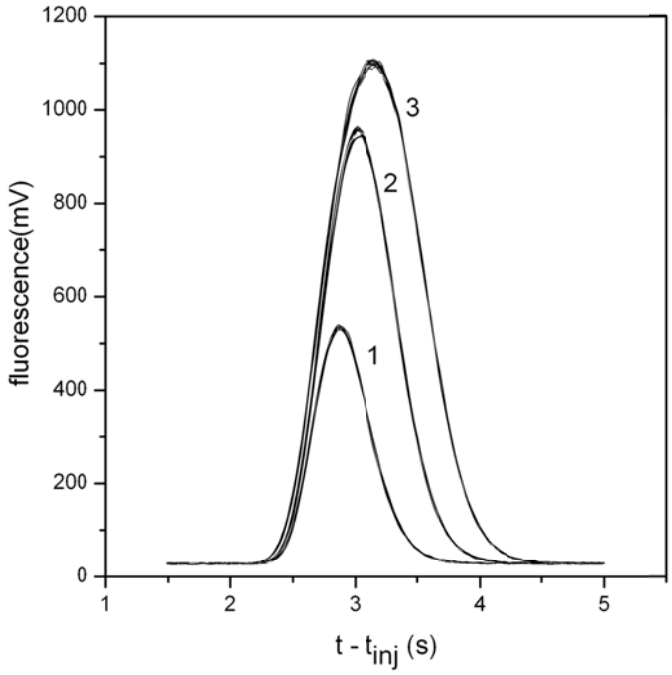

Figure 2-5. Fluorescence signals for the 100-ms (curve 1), 300-ms (curve 2), and 500-ms (curve 3) injections. The detection point was 1 mm downstream from the intersection. The pressures applied for these injections were ~1 psi to the sample reservoir and ~0.5 psi to the buffer reservoir. Data were aligned at the falling edges of the injections.

$$v_1 t_1 + v_2 t_2 = 10 \text{ mm} \qquad (5)$$

$$t_1 = 100,300, \text{ or } 500 \text{ ms} \qquad (6)$$

$$t_{total} = t_1 + t_2 \qquad (7)$$

where t_1 is injection time, t_2 is time from the end of the injection to the leading edge of the peak, t_{total} is the total time from the start of the injection to the leading edge of the peak, v_1 is the velocity in the dispense mode during injection time t_1, and v_2 is the velocity in the sample loading mode during time t_2.

With a simplified equation 3 (w > 3d),

$$v_1 = \frac{\Delta P_1 d^2}{\eta l}\left(\frac{1}{12}\right) \qquad (8)$$

$$v_2 = \frac{\Delta P_2 d^2}{\eta l}\left(\frac{1}{12}\right) \qquad (9)$$

where Δp_1 and Δp_2 are the pressures at the intersection calculated with equation 4. Because the pressure at the waste reservoir is 0 psi, the pressure at the intersection is the same as the pressure drop across the analysis channel.

Dividing equation 8 by equation 9,

$$v_1 / v_2 = \Delta p_1 / \Delta p_2 \qquad (10)$$

Flow velocities for these two modes can be calculated by solving equations 5 to 10 simultaneously. Velocities were calculated for 100-ms injections at different pressures

from fluorescence signals obtained 10 mm downstream from the cross intersection. Variation of the velocity for these injections with applied pressure are plotted in **Figure 2-6**. The velocity had a linear relationship with the pressure which is in agreement with equation 3.

Variation of the Amount of Injected Sample with Applied Pressure. The amount of sample injected can be calculated by multiplying concentration and injection volume. Injection volume V was calculated by multiplying injection time t, flow velocity v_1 during dispense mode, and channel cross-sectional area A. Thus, amounts of sample injected were calculated as shown in equation 11, where c is concentration, and n is number of moles of sample injected.

$$n = A \times c \times t \times v_1 \qquad (11)$$

The channel cross-section area A was constant with the assumption that the channels etched uniformly. Because the fluorescence signal was proportional to sample concentration, areas under the temporal profiles (i.e., time-integrated fluorescence) were proportional to the product of sample concentration and time. Therefore, the product of peak area and dispense mode velocity was proportional to the number of moles of injected sample. **Figure 2-7** shows this product increased with injection time and applied pressure and the injected amount increased as injection time or applied pressure increased.

2.4. Conclusion

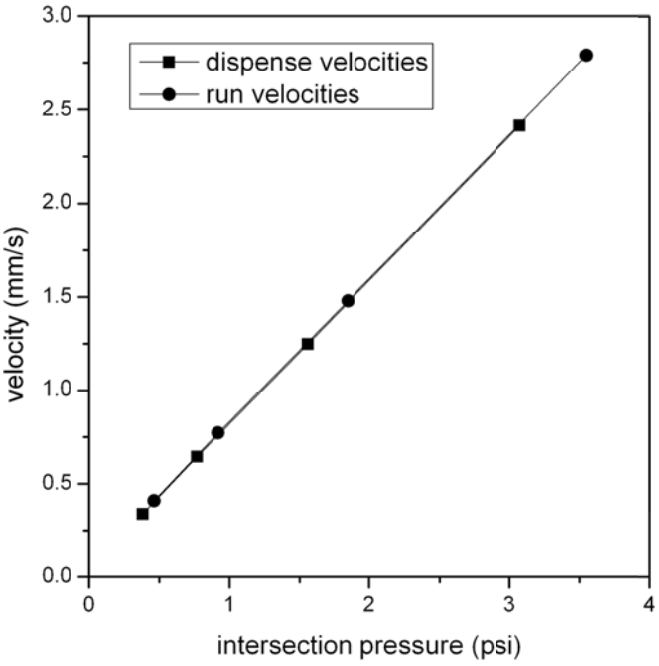

Figure 2-6. Variation of the velocity with pressure profile at the cross intersection for 100-ms Pressures applied to the sample reservoir were ~1, 2, 4, and 8 psi.

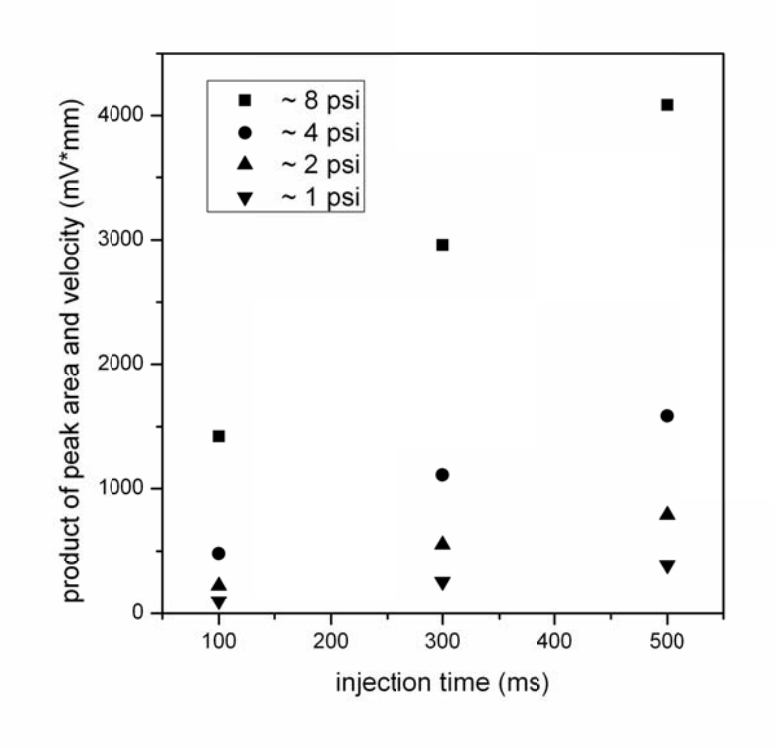

Figure 2-7. Variation of the product of peak area and velocity during sample loading modewith injection time. Fluorescence signals were obtained 10 mm downstream from the cross intersection. The pressures applied to the sample reservoir were ~1, 2, 4, and 8 psi.

A microfluidic device capable of generating pressure-driven injections was demonstrated. Injection pulses were controlled precisely and reproducibly. From detection data, flow velocities, intersection pressures, and injection sample amounts have been calculated and evaluated. The flow velocity scaled linearly with applied pressure, as expected from theory. Also, the injected amount increased as injection time and applied pressure increased. Pressure and injection time can be easily controlled to maximize injection performance.

2.5. References:

1. Effenhauser, C. S.; Manz, A.; Widmer, H. M., Glass Chips for High-Speed Capillary Electrophoresis Separations with Submicrometer Plate Heights. *Anal. Chem.* **1993,** *65* (19), 2637-2642.
2. Harrison, D. J.; Manz, A.; Fan, Z. H.; Ludi, H.; Widmer, H. M., Capillary Electrophoresis and Sample Injection Systems Integrated on a Planar Glass Chip. *Anal. Chem.* **1992,** *64* (17), 1926-1932.
3. Jacobson, S. C.; Culbertson, C. T.; Daler, J. E.; Ramsey, J. M., Microchip Structures for Submillisecond Electrophoresis. *Anal. Chem.* **1998,** *70* (16), 3476-3480.
4. Kutter, J. P.; Jacobson, S. C.; Ramsey, J. M., Integrated Microchip Device with Electrokinetically Controlled Solvent Mixing for Isocratic and Gradient Elution in Micellar Electrokinetic Chromatography. *Anal. Chem.* **1997,** *69* (24), 5165-5171.
5. Moore, A. W.; Jacobson, S. C.; Ramsey, J. M., Microchip Separations of Neutral Species Via Micellar Electrokinetic Capillary Chromatography. *Anal. Chem.* **1995,** *67* (22), 4184-4189.
6. Effenhauser, C. S.; Paulus, A.; Manz, A.; Widmer, H. M., High-Speed Separation of Antisense Oligonucleotides on a Micromachined Capillary Electrophoresis Device. *Anal. Chem.* **1994,** *66* (18), 2949-2953.
7. Waters, L. C.; Jacobson, S. C.; Kroutchinina, N.; Khandurina, J.; Foote, R. S.; Ramsey, J. M., Microchip Device for Cell Lysis, Multiplex Pcr Amplification, and Electrophoretic Sizing. *Anal. Chem.* **1998,** *70* (1), 158-162.
8. Blom, M. T.; Chmela, E.; Gardeniers, J. G. E.; Tijssen, R.; Elwenspoek, M.; van den Berg, A., Design and Fabrication of a Hydrodynamic Chromatography Chip. *Sens. Actuator B-Chem.* **2002,** *82* (1), 111-116.
9. Blom, M. T.; Chmela, E.; Oosterbroek, R. E.; Tijssen, R.; van den Berg, A., On-Chip Hydrodynamic Chromatography Separation and Detection of Nanoparticles and Biomolecules. *Anal. Chem.* **2003,** *75* (24), 6761-6768.

10. Chmela, E.; Tijssen, R.; Blom, M.; Gardeniers, H.; van den Berg, A., A Chip System for Size Separation of Macromolecules and Particles by Hydrodynamic Chromatography. *Anal. Chem.* **2002,** *74* (14), 3470-3475.
11. Auroux, P. A.; Iossifidis, D.; Reyes, D. R.; Manz, A., Micro Total Analysis Systems. 2. Analytical Standard Operations and Applications. *Anal. Chem.* **2002,** *74* (12), 2637-2652.
12. Reyes, D. R.; Iossifidis, D.; Auroux, P. A.; Manz, A., Micro Total Analysis Systems. 1. Introduction, Theory, and Technology. *Anal. Chem.* **2002,** *74* (12), 2623-2636.
13. Terry, S. C.; Jerman, J. H.; Angell, J. B., Gas-Chromatographic Air Analyzer Fabricated on a Silicon-Wafer. *IEEE Trans. Electron Devices* **1979,** *26* (12), 1880-1886.
14. Ismagilov, R. F.; Rosmarin, D.; Kenis, P. J. A.; Chiu, D. T.; Zhang, W.; Stone, H. A.; Whitesides, G. M., Pressure-Driven Laminar Flow in Tangential Microchannels: An Elastomeric Microfluidic Switch. *Anal. Chem.* **2001,** *73* (19), 4682-4687.
15. Stroock, A. D.; Dertinger, S. K.; Whitesides, G. M.; Ajdari, A., Patterning Flows Using Grooved Surfaces. *Anal. Chem.* **2002,** *74* (20), 5306-5312.
16. Stroock, A. D.; Dertinger, S. K. W.; Ajdari, A.; Mezic, I.; Stone, H. A.; Whitesides, G. M., Chaotic Mixer for Microchannels. *Science* **2002,** *295* (5555), 647-651.
17. Stroock, A. D.; Whitesides, G. M., Controlling Flows in Microchannels with Patterned Surface Charge and Topography. *Accounts Chem. Res.* **2003,** *36* (8), 597-604.
18. Handique, K.; Burke, D. T.; Mastrangelo, C. H.; Burns, M. A., On-Chip Thermopneumatic Pressure for Discrete Drop Pumping. *Anal. Chem.* **2001,** *73* (8), 1831-1838.
19. Hong, C. C.; Murugesan, S.; Kim, S.; Beaucage, G.; Choi, J. W.; Ahn, C. H., A Functional on-Chip Pressure Generator Using Solid Chemical Propellant for Disposable Lab-on-a-Chip. *Lab Chip* **2003,** *3* (4), 281-286.
20. Jen, C. P.; Lin, Y. C.; Wu, W. D.; Wu, C. Y.; Wu, G. G.; Chang, C. C., Improved Design and Experimental Demonstration of a Bi-Directional Microfluidic Driving System. *Sens. Actuator B-Chem.* **2003,** *96* (3), 701-708.
21. Vervoort, N.; Billen, J.; Gzil, P.; Baron, G. V.; Desmet, G., Importance and Reduction of the Sidewall-Induced Band-Broadening Effect in Pressure-Driven Microfabricated Columns. *Anal. Chem.* **2004,** *76* (15), 4501-4507.
22. Feng, X. Z.; Haswell, S. J.; Watts, P., Organic Synthesis in Micro Reactors. *Curr. Top. Med. Chem.* **2004,** *4* (7), 707-727.
23. Haswell, S. J.; O'Sullivan, B.; Styring, P., Kumada-Corriu Reactions in a Pressure-Driven Microflow Reactor. *Lab Chip* **2001,** *1* (2), 164-166.
24. Wiles, C.; Watts, P.; Haswell, S. J.; Pombo-Villar, E., Stereoselective Alkylation of an Evans Auxiliary Derivative within a Pressure-Driven Micro Reactor. *Lab Chip* **2004,** *4* (3), 171-173.
25. Yin, N. F.; Killeen, K.; Brennen, R.; Sobek, D.; Werlich, M.; van de Goor, T. V., Microfluidic Chip for Peptide Analysis with an Integrated Hplc Column, Sample

Enrichment Column, and Nanoelectrospray Tip. *Anal. Chem.* **2005,** *77* (2), 527-533.
26. Jacobson, S. C.; Ermakov, S. V.; Ramsey, J. M., Minimizing the Number of Voltage Sources and Fluid Reservoirs for Electrokinetic Valving in Microfluidic Devices. *Anal. Chem.* **1999,** *71* (15), 3273-3276.
27. Jacobson, S. C.; Hergenroder, R.; Moore, A. W.; Ramsey, J. M., Precolumn Reactions with Electrophoretic Analysis Integrated on a Microchip. *Anal. Chem.* **1994,** *66* (23), 4127-4132.
28. Jacobson, S. C.; Ramsey, J. M., Integrated Microdevice for DNA Restriction Fragment Analysis. *Anal. Chem.* **1996,** *68* (5), 720-723.
29. White, F. M., *Viscous Fluid Flow*. 2 ed.; McGraw-Hill: New York, 1991; p 118-120.
30. Giddings, J. C., *Unified Separation Science*. 1 ed.; John Wiley and Sons, Inc.: New York, 1991; p 59-61.

Chapter 3. Electrophoretic Analysis of N-Glycans on a Microfluidic Device with a Spiral Separation Channel[1]

3.1. Introduction to Glycan Analysis

The biological importance of glycoproteins in eukaryotic systems has been recognized in the recent literature.[2-5] From relatively simple roles in protein stabilization and proper folding to the sophisticated ways in which the glycan chains participate in cell differentiation and development, cell-to-cell recognition, and adhesion-based cellular organization, protein glycosylation is a very essential biological process. However, the molecular details and roles of these important processes have been largely hindered due to methodological difficulties.

The field of analytical glycobiology increasingly demands methods with higher sensitivity and structural information content, as the glycomic and glycoproteomic measurements must be obtained from small quantities of isolated glycoproteins. Additionally, the recent emphasis on functional glycomic measurements in complex unfractionated biological mixtures, e.g., tissue biopsies and physiological fluids, promises development of new diagnostic and prognostic methods for human diseases.[6-8] Combining high measurement sensitivity with structural resolution of numerous glycan entities is thus critical in modern biomedical research focused on diseases that potentially feature aberrant structures.

While modern mass spectrometry (MS) often provides the necessary sensitivity for biomedical and clinical applications of glycan analysis[9-10] at minute sample volumes or quantities, the methods based solely on MS experience difficulties in distinguishing

glycan isomers. In contrast, capillary electrophoresis combined with laser-induced fluorescence detection generally provides exquisite resolution of isomers and sensitivity, albeit structural identification capabilities are limited.[10] In addressing the analytical needs for a complete structural analysis of complex glycan pools, there is a distinct need for combining several analytical approaches, typically those involving MS as well as capillary separation techniques.[9-10]

Capillary electrophoresis (CE),[11-13] capillary gel electrophoresis,[14-16] micellar electrokinetic chromatography,[17-19] and capillary electrochromatography[20-26] represent different electromigration principles capable of resolving small structural differences in isomeric glycan structures. In combination with fluorescence detection, these techniques provide the microscale capabilities needed for analyzing glycan samples from tissue extracts and physiological fluids where glycoproteins are present over a wide concentration range. CE represents perhaps the most easily predictable electromigration principle because structural isomer separations in this format are dependent on the hydrodynamic volumes of the glycans. Consequently, structures that differ only by the antenna location where a particular monosaccharide, e.g., galactose, is attached can be readily distinguished.[27]

Although a few groups have analyzed glycan mixtures using microchip electrophoresis[28-29] and microchip gel electrophoresis,[30] these studies lack the separation efficiencies necessary to resolve positional and linkage isomers. The plate numbers generated are low primarily because short separation lengths, e.g., 3.3 to 7.0 cm, are used. In order to increase the absolute plate numbers to resolve structural isomers, we used a spiral channel design,[31] which provides high separation performance by minimizing

issues associated with the "racetrack" effect. Other channel designs which also minimize the racetrack effect include serpentine channel layouts incorporating low dispersion turns with symmetric[32] and asymmetric[33-35] tapering of the channel in the turns.

In addition to using the spiral channel design, we coated the microchannels with polyacrylamide to minimize electroosmotic flow, labeled the glycan samples with 8-amino-1,3,6-trisulfonic acid (APTS)[36-37] to impart charge on the glycans and permit fluorescence detection, and employed a modified pinched injection[38] to inject variable volumes. These operating conditions along with electric field strengths up to 750 V/cm generated separations 8 to 50 times more efficient than what have been previously reported for glycan separations on microfluidic devices[28-30] and some of the highest efficiencies yet reported for microchip electrophoresis. This enhanced efficiency allowed structural isomers to be resolved easily. Also, we present the first head-to-head comparison between microchip and capillary electrophoresis, demonstrating that the microchips perform as well as capillaries for high performance separations.

3.2. Experimental Section

Materials. Acetic acid, acetonitrile, α_1-acid glycoprotein, ammonium bicarbonate, ammonium persulfate, asialofetuin, citric acid, dimethylsulfoxide (DMSO), disodium fluorescein, dithiothreitol (DTT), fetuin, 4-(2-hydroxyethyl)-1-piperazine-ethanesulfonic acid (HEPES), iodoacetamide (IAA), β-mercaptoethanol, γ-methacryloxypropyltrimethoxysilane (MAPTOS), methanol, methylene dichloride, potassium phosphate monobasic, ribonuclease B (RNase B), sodium cyanoborohydride, sodium tetraborate, N,N,N',N'-tetramethylethylenediamine (TEMED), trifluoroacetic

acid (TFA), trifluoroethanol (TFE), and tris(hydroxymethyl)aminomethane hydrochloride (Tris-HCl) were purchased from Sigma-Aldrich. High-purity 8-amino-1,3,6-trisulfonic acid (APTS) was obtained from Beckman Coulter, Inc., and peptide-N-glycosidase F (PNGase) of *Chryseobacterium menigosepticum* (EC 3.2.2.18) from Northstar BioProducts. Sodium hydroxide was purchased from Fisher Scientific, Microposit MF 319 developer from Rohm and Haas Electronic Materials, and Chromium Etchant 1020 and buffered oxide etchant (BOE) from Transene Co., Inc. Fused silica capillary (25-μm i.d. and 250-μm o.d.) was received from Polymicro Technologies, LLC and B270 glass substrates and cover plates from Telic Co.

Microfluidic Device Fabrication. The microfluidic device with the spiral separation channel, depicted in **Figure 3-1**, was fabricated by standard photolithography and wet chemical etching.[39] Borosilicate glass substrates (B270) coated with 120 nm of Cr and 530 nm of AZ1518 photoresist were exposed to 200 mJ/cm^2 UV radiation through a photogenerated mask (HTA Photomask) on a mask aligner (205S, Optical Associates, Inc.). Substrates were then developed for 2 min in MF-319 developer and rinsed with water. After development, the channel pattern was transferred to the chromium layer by etching in Cr Etchant 1020 and subsequently to the glass layer by etching in buffered oxide etchant until the channels were 15 μm deep. The channel widths at the top were 240 μm for the wide channels and 60 μm for the narrow channels. These dimensions were measured using a stylus-based profiler (Dektak 6M, Veeco Instruments, Inc.). Fluid access holes were sandblasted at the ends of the channels (AEC Air Eraser, Paasche Airbrush Co.). Following sandblasting, the photoresist layer was removed by rinsing in acetone for 2 min, and the chromium layer was removed by etching in Cr Etchant 1020.

The drilled substrate was then bonded to a cover plate by hydrolyzing both pieces in a solution of NH_4OH, H_2O_2, and H_2O (2:1:2), bringing the substrate and coverplate into contact, ramping to 550° C, and annealing for 10 h. Short segments of glass tubing (6 mm o.d. x 4 mm i.d. x 6 mm tall) were affixed over the sandblasted holes using epoxy (353NDT, Epoxy Technology).

Channel Coating. The microchannels and capillaries were coated with linear polyacrylamide to minimize electroosmotic flow, and the coating procedure was modified slightly from Hjertén's method.[40] Briefly, the microchannels and capillaries were cleaned sequentially with 1.0 M sodium hydroxide solution, water, and methanol for 20 min each. The microchannels and capillaries were then filled with a solution of 45 μL MAPTOS dissolved in 1.5 mL methylene dichloride with 0.02 M acetic acid. After 45 min, the microchannels and capillaries were rinsed with methanol and water for 15 min each to remove residual silane solution. The channels were then filled with an aqueous solution containing 2.4% (w/w) acrylamide, 1.0 μL/mL TEMED, and 1.0 mg/mL ammonium persulfate. After 2 h, the microchannels and capillaries were flushed with water for 20 min and filled with buffer. To introduce the various solutions, a subambient pressure was used to draw solutions through the microchannels, and a pressure of 50 psi was applied to the capillary inlet to introduce the solutions.

Sample Preparation. 1-μg aliquots of dried glycoprotein (RNase B or asialofetuin) were suspended in 2.5 μL phosphate buffer (pH 7) with 1% β-mercaptoethanol and thermally denatured at 95 ºC for 10 min. The solution was cooled to room temperature prior to the addition of a 0.5-μL aliquot of PNGase in phosphate buffer, and the reaction

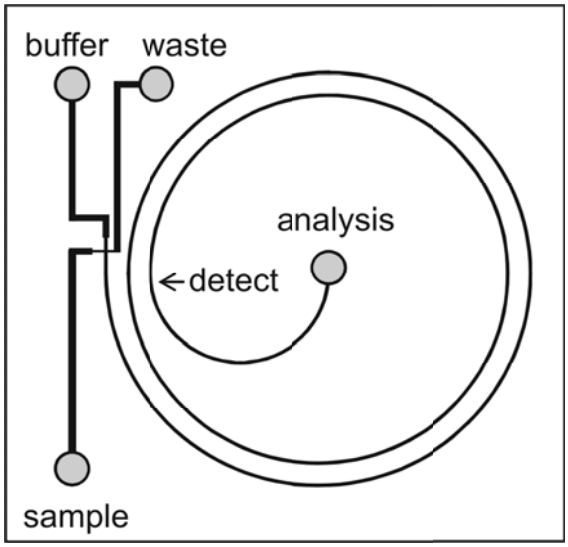

Figure 3-1. Schematic of the microfluidic device with the spiral channel design used for glycan analysis. The effective separation length was 22 cm from the cross intersection to the detection point indicated by the arrow. The reservoirs and corresponding channels are labeled with their functions. The microchip substrate was 5 cm by 5 cm. The narrow and wide channels were 60 and 240 μm wide at the top, respectively.

mixture was then incubated overnight at 37 ºC. Next, the released glycans were collected and dried in vacuum and labeled with APTS by adding a 2-μL aliquot of 100 μM APTS solution prepared in 0.9 M citric acid and a 1-μL aliquot of 1 M sodium cyanoborohydride prepared in DMSO. The reaction was allowed to proceed for 2 h at 55 ºC. The derivatization mixture was dialyzed overnight at room temperature using a 1000-Da cut-off cellulose membrane to reduce the amount of unreacted APTS. Finally, the dialyzed mixture was dried and resuspended in 15 μL of 1 mM phosphate and 20 mM HEPES buffer (pH 6.8) prior to electrophoretic analysis.

Human serum samples were reduced and alkylated as previously described.[41] Briefly, a 10-μL aliquot of human blood serum was lyophilized and then resuspended in 25 μL of 25 mM ammonium bicarbonate, 25 μL of TFE, and 2.5 μL of 200 mM DTT prior to incubation at 60 °C for 45 min. A 10-μL aliquot of 200 mM IAA was then added and allowed to react at room temperature for 1 h in the dark. Subsequently, a 2.5-μL aliquot of DTT was added to react with the excess IAA. Next, the reaction mixture was diluted with 300 μL of water and 100 μL of 25 mM ammonium bicarbonate to adjust the pH to 7.5-8.0, making the solution suitable for the enzymatic release of N-glycans using PNGase according to our previously published procedure.[42] A 5 mU aliquot of PNGase F was added to the reaction mixture and incubated overnight (18-22 h) at 37 °C.

The volume of enzymatically released glycans was adjusted to 1 mL by adding deionized water. Samples were then applied to both C18 Sep-Pak® cartridges (Waters Corp., Milford, MA) and activated charcoal cartridges (Harvard Apparatus, Holliston, MA). The use of C18 Sep-Pak® cartridges is necessary to isolate the glycans from peptides and proteins, which would otherwise interfere with trapping on the activated

charcoal cartridges. The reaction mixture was first applied to C18 Sep-Pak® cartridge that had been preconditioned with ethanol and deionized water according to the manufacturer's recommendation. The reaction mixture was circulated through the C18 Sep-Pak® cartridge 5 times prior to washing with water. Peptides and O-linked glycopeptides were retained on the C18 Sep-Pak® cartridge, while the released glycans were collected in the eluent. Next, the C18 Sep-Pak® cartridge was washed with 1 mL of deionized water. The combined eluent containing the released N-glycans were then passed over activated charcoal microcolumns. The columns were pre-conditioned with 1 mL of acetonitrile and 1 mL of 0.1% TFA aqueous solution, as recommended by the manufacturer. After applying the sample, the microcolumn was washed with 1 mL of 0.1% TFA aqueous solution. The samples were then eluted with a 1-mL aliquot of 50% ACN aqueous solution containing 0.1% TFA. Finally, the purified glycans were evaporated to dryness using vacuum CentriVap Concentrator (Labconco Corp., Kansas City, MO) prior to APTS derivatization as described above.

Microchip Electrophoresis. The microfluidic device with the spiral separation channel is depicted in **Figure 3-1**. For the electrophoretic separations, a fast-slewing high voltage power supply (0-10 kV) developed in-house was used to control the potentials applied to the sample, buffer, and waste reservoirs, and a commercial high voltage power supply (0-30 kV; CZE 1000R, Spellman High Voltage Electronics Corp.) was used to control the potential applied at the analysis reservoir. The high voltage outputs were controlled using a program written in LabView 8.0 (National Instruments Corp.) and an analog output board (PCI-6713, National Instruments Corp.). Electric field strengths in the analysis channel of 75, 130, 250, 330, 510, and 750 V/cm were used to evaluate the

separation performance on the microfluidic devices. The buffer used for the microchip separations was 1 mM phosphate and 20 mM HEPES (pH 6.8).

To monitor the injections and separations, an inverted optical microscope (TE-2000U, Nikon, Inc.) was configured for epifluorescence and equipped with 20x and 40x objectives and an HQ FITC filter cube (Chroma Technology Corp.). For imaging experiments, a metal halide lamp (X-Cite 120, EXFO, Inc.) was used for excitation, the fluorescence signal was detected with a CCD camera (Cascade 512B, Photometrics), and images were captured and processed using IPLab software (BD Biosciences Bioimaging). For measurements at a single point in the analysis channel, the same microscope was used. The 488-nm line of an argon ion laser (Melles Griot, Inc.) was attenuated to 0.5 mW with neutral density filters and focused to a point in the analysis channel 22 cm downstream from the cross intersection. The fluorescence signal was spatially filtered with a 600 μm pinhole, detected with a photomultiplier tube (H5783-01, Hamamatsu Corp.), amplified by a low-noise current preamplifier (SR570, Stanford Research Systems, Inc.), and recorded using a multifunction data acquisition board (PCI-6032E, National Instruments Corp.) and software written with LabView. The sampling frequency was 100 Hz.

Modified Pinched Injections. A modified pinched injection[38] was used to dispense samples for the microchip electrophoresis, and the injection process is shown in **Figure 3-2**. The sample stream was confined to the cross intersection during the sample loading similar to a standard pinched injection.[39] For the loading mode, the potentials applied to the sample, buffer, waste, and analysis reservoirs were 0, 0.22, 0.6, and 0 kV, respectively. To inject variable volumes, the sample was gated into the separation

channel for a period of time, e.g., 0.1 to 6 s, by raising the potential at the analysis reservoir to either 4 or 6 kV and keeping the other voltages constant. To dispense the sample plug into the spiral analysis channel for separation, the potential applied on the sample reservoir was raised to 0.4 kV. To image the injection process shown in **Figure 3-2**, the buffer was 1 mM borate and 20 mM HEPES, and the sample was disodium fluorescein (10 μM) in this buffer. The phosphate-HEPES buffer, noted above, was used for all other experiments. The sample preparation procedures are outlined in the Supporting Information.

Capillary Electrophoresis. Capillary electrophoresis was performed on a commercial capillary electrophoresis system (P/ACE^{TM} MDQ, Beckman Coulter, Inc.) equipped with a laser-induced fluorescence detection module with a 488-nm line from an argon ion laser. The capillary had a total length of 32 cm and an effective separation length of 22 cm, which was equal to the effective separation length on the microfluidic device. Sample injections were pressure-induced, and potentials of 2, 4, 8, 10, 16, and 24 kV were applied across the capillary to obtain electric field strengths of 60, 130, 250, 310, 500, and 750 V/cm. These separation field strengths were similar to those used for the microchip electrophoresis. Also, the buffer used for the capillary separations was the same as the microchip separations, which was 1 mM phosphate and 20 mM HEPES.

Data Analysis. To calculate the separation efficiencies, the data for selected peaks were fitted with a Gaussian function using OriginPro 7.5 software (OrignLab Corp., Northampton, MA). The peak parameters obtained were used to calculate the velocity, plate height, plate number, and plates per time.

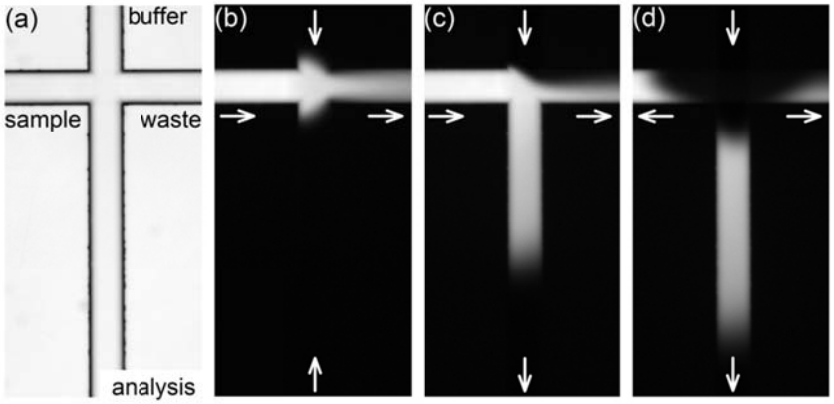

Figure 3-2. (a) Transmitted light image of the cross intersection and fluorescence images of fluorescein during (b) sample loading, (c) injection, and (d) analysis for the modified pinched injection. The injection time in (c) was 1 s. In the fluorescence images, the bright areas represent the sample, and the arrows depict the direction of flow.

3.3. Results and Discussion

Microchip Electrophoresis. We used the spiral channel design and electric field strengths ranging from 75 to 750 V/cm to evaluate the separation performance of N-glycan samples from several model glycoproteins including ribonuclease B (RNase B), fetuin, and $_1$-acid glycoprotein. A typical electropherogram on the microfluidic device at 750 V/cm is shown in **Figure 3-3** for N-glycans released from RNase B (see **Table 3-1** for structures) and labeled with APTS for fluorescence detection. In this and other glycan separations, the faster migrating components in the separation (≤ 1.8 min) were associated with the APTS labeling reaction, and the slower migrating components (> 1.8 min) were the glycans of interest. As seen in **Figure 3-3** and **Table 3-2**, the separation efficiencies were excellent with the label by-product peak (L1) approaching 1,000,000 plates and the three high-mannose glycan peaks (Mannose 5, Mannose 6, and Mannose 9) between 400,000 and 470,000 plates. Man 5, Man 6, and Man 9 were also used to compare the separation performance on the microchip and capillary platforms (discussed below). Moreover, the linear velocities of Man 5, Man 6, and Man 9 had a relative standard deviation less than 1% over the range of field strengths evaluated. The phosphate-HEPES buffer helped to provide this very good run-to-run reproducibility and excellent linearity of the velocity with electric field strength (R^2 > 0.9999), especially at the higher field strengths, e.g., 750 V/cm, where Joule heating can be a concern.

Structural Isomer Separations. An advantage of electrophoretic separations is the ability to resolve structural isomers in glycan mixtures, which cannot be easily resolved standard deviation less than 1% over the range of field strengths evaluated. The phosphate-HEPES buffer helped to provide this very good run-to-run reproducibility and

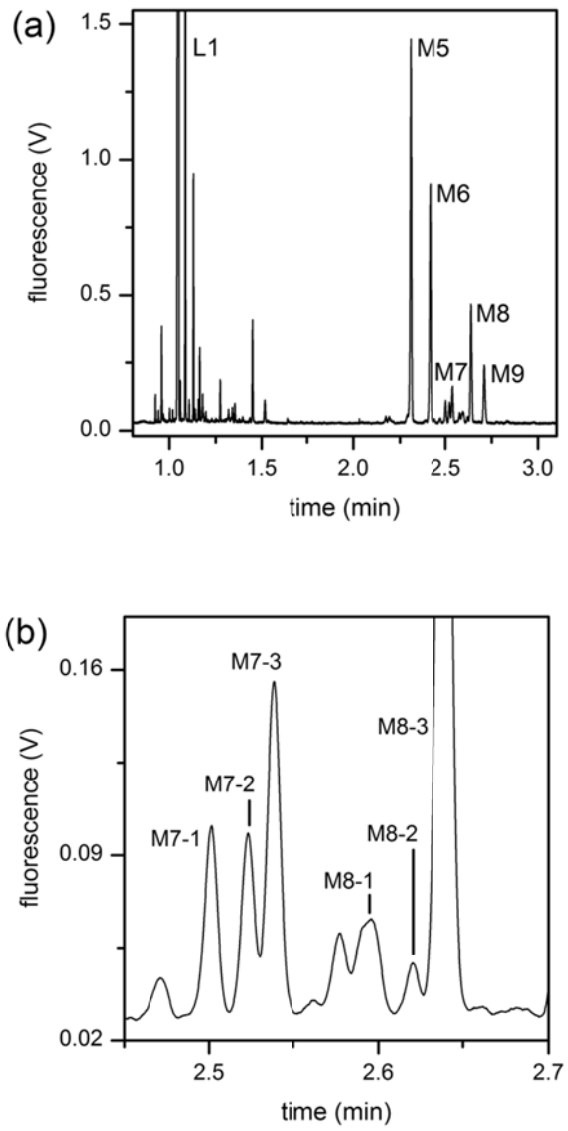

Figure 3-3. (a) Electropherogram of the N-glycans derived from ribonuclease B separated on the microfluidic device. The separation field strength was 750 V/cm, and the separation length was 22 cm. The labeled peaks are a label by-product (L1), Mannose 5 (M5), Mannose 6 (M6), Mannose 7 (M7), Mannose (M8), and Mannose 9 (M9). The glycan structures are listed in **Table 3-1**, and the separation efficiencies are listed in **Table 3-2**. (b) Enlarged view of (a) showing separation of the positional isomers of Mannose 7 and Mannose 8.

Table 3-1. Structures of N-glycans derived from ribonuclease B labeled in **Figure 3-3**. The symbols are ○ for mannose (Man) and ■ for N-acetylglucosamine (GlcNAc).

Name	Label	Structure
Mannose 5	M5	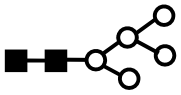
Mannose 6	M6	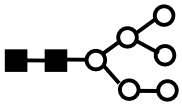
Mannose 7-1	M7-1	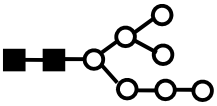
Mannose 7-2	M7-2	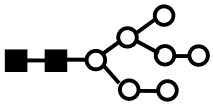
Mannose 7-3	M7-3	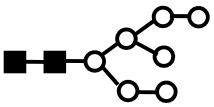
Mannose 8-1	M8-1	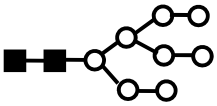
Mannose 8-2	M8-2	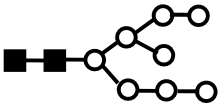
Mannose 8-3	M8-3	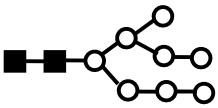
Mannose 9	M9	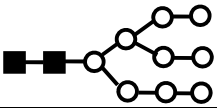

Table 3-2. Velocities (*u*), plate heights (*H*), plate numbers (*N*), plate numbers per time (*N*/s), and diffusion coefficients (*D*) for microchip electrophoresis.

Component	*u* (cm/min)	*H* (μm)	*N*	*N*/s (s^{-1})	*D* (cm^2/s) x 10^6
L1	20.5	0.232	958,000	14,700	4.00
M5	9.43	0.474	467,000	3310	2.41
M6	9.02	0.467	473,000	3200	2.41
M9	8.03	0.554	400,000	2420	2.11
C1	11.5	0.336	655,000	5730	-
C2	9.98	0.443	446,000	3370	-
C3	8.19	0.534	412,000	2550	-

Note: All parameters except *D* were measured with a separation field strength of 750 V/cm, and *D* was calculated using Equation 1 fitted to data in **Figure 3-6**.

excellent linearity of the velocity with electric field strength (R^2 > 0.9999), especially at the higher field strengths, e.g., 750 V/cm, where Joule heating can be a concern.

Structural Isomer Separations. An advantage of electrophoretic separations is the ability to resolve structural isomers in glycan mixtures, which cannot be easily resolved by mass spectrometry. To confirm that the microchip separations provided sufficiently high separation efficiencies, we analyzed both positional and linkage isomers. For the separation of N-glycans released from RNase B, **Figure 3-3b** shows a separation of the positional isomers of Man 7 and Man 8, and the structures are listed in **Table 3-1**. In each case, the three isomers differ only by the position of the antenna location where the terminal mannose is connected.

Also, the separation of N-glycans released from asialofetuin was used to demonstrate resolution of linkage isomers (see **Figure 3-4**). The difference between the isomers labeled A2 and A3 is the linkage between the terminal galactose (Gal) and N-acetylglucosamine (GlcNAc) on the middle antenna. The isomer in peak A2 had a β1,3-linkage where GlcNAc is labeled with a shaded square, and the isomer in peak A3 had a β1,4-linkage. The elution sequence of the three positional isomers for RNase B glycans was validated with a theoretical calculation of the hydrodynamic volume, and the elution sequence of the two linkage isomers was confirmed using specific linkage glycosidase enzymes.[43] Both the positional and linkage isomers shown separated here using microchip electrophoresis were not resolved in data reported previously because the peak capacities were too low.[28-29]

Cancer Sample Analysis. An application for these separations is to determine

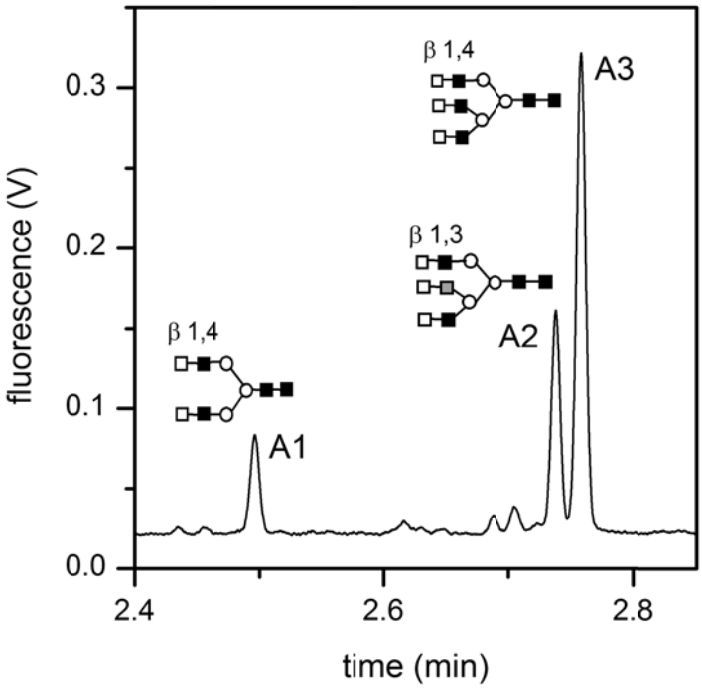

Figure 3-4. Electropherogram of the N-glycans derived from asialofetuin separated on the microfluidic device. The peaks are labeled with their corresponding glycan structures, and peaks A2 and A3 are linkage isomers. The symbols are □ for galactose (Gal), ○ for mannose (Man), and ■ for N-acetylglucosamine (GlcNAc). The separation field strength was 750 V/cm, and the separation length was 22 cm.

glycan profiles from blood sera of patients with and without cancer. The N-glycans derived from a blood sample of a Stage IV breast cancer patient were electrophoretically separated on the microchip using a separation length of 22 cm and field strength of 750 V/cm, and the electropherogram is shown in **Figure 3-5**. Most of the N-glycans have been identified by enzymatic sequencing, and several of the structures including some positional isomers are shown in the figure. Plate heights and plate numbers were calculated for fast (C1), intermediate (C2), and slow (C3) migrating peaks (see **Table 3-2**). The plate heights for these peaks show that the separation of these clinically-derived samples was comparable to the test mixtures of RNase B. In addition, the microchip separations were 8 times faster than capillary separations with similar efficiencies. With the fast and efficient separations on the microfluidic devices, comparative glycan maps could potentially be developed as a rapid screening or prognosis tool.

Comparison of Microchip and Capillary Electrophoresis. The separation performance was compared for microchip and capillary electrophoresis using the same effective separation length of 22 cm and electric field strengths from 60 to 750 V/cm. The plate heights were calculated and plotted as a function of the analyte velocity in **Figure 3-6**. The open symbols represent the data points from the capillary separations, and the solid symbols represent those from the microchip separations. The figure shows that at low separation velocities ($\leq$ 4 cm/min) the microfluidic device and the capillary offered similar separation performance. This result was expected because the separations are diffusion-limited in this velocity range. However, at higher linear velocities, e.g., $\geq$ 4 cm/min, the microchip exhibited better separation performance. For the fastest separations at 750 V/cm, Man 5, Man 6, and Man 9 had an average plate height of

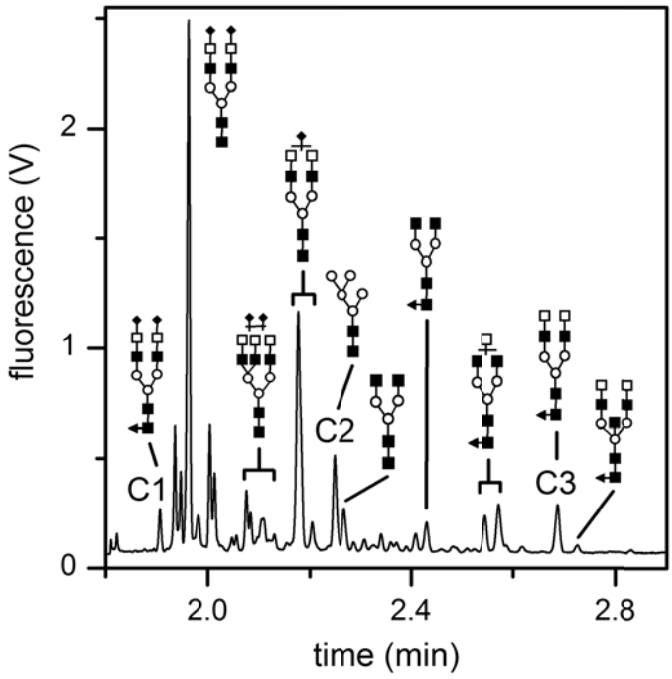

Figure 3-5. Electropherogram of N-glycans released from a blood serum sample from a stage IV breast cancer patient separated on the microfluidic device. The separation length was 22 cm, and the separation field strength was 750 V/cm. The separation efficiencies for components C1, C2, and C3 are listed in **Table 2**. The symbols are □ for galactose (Gal), ○ for mannose (Man), ■ for N-acetylglucosamine (GlcNAc), ▲ for fucose (Fuc), and ♦ for N-acetylneuraminic acid (NeuAC).

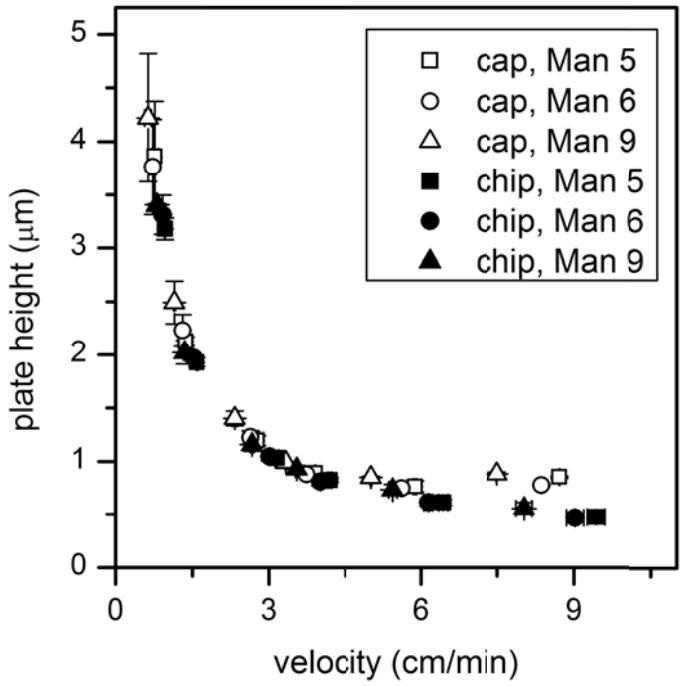

Figure 3-6. Variation of plate height with velocity for microchip and capillary electrophoresis of glycans from ribonuclease B. Separation field strengths ranged from 60 to 750 V/cm. Data are open symbols for the capillary (cap) and solid symbols for the microchip (chip). The error bars are $\pm\sigma$ for plate height and velocity.

0.836 μm and average plate number of 264,000 for the capillary separations and an average plate height of 0.498 μm and an average plate number of 440,000 for the microfluidic separations. Consequently, the microchip separations were up to 1.7 times more efficient than the capillary separations allowing the microchip separations to be run at least 3 times faster for the same applied potential.

This performance difference can be seen in the plate height data in **Figure 3-6**, which were fitted with Equation 1,

$$H = \frac{\sigma_{diff}^2}{L} + \frac{\sigma_{inj}^2}{L} = \frac{2D}{u} + \frac{l_{inj}^2}{12L} \quad (1)$$

where σ_{diff}^2 and σ_{inj}^2 are the variances due to diffusion and injection, respectively, while D is the diffusion coefficient, u is the velocity, and l_{inj} is the injection length. We assumed that the primary contributions to the plate height were from axial diffusion and the injection length. Curve fittings were performed with OriginPro 7.5 software, and $R^2 >$ 0.999 for the microfluidic data and $R^2 > 0.99$ for the capillary data were calculated. From the fits, the diffusion coefficients are listed in **Table 3-2** and are reasonable for the molecular weights of the labeled glycans. Also, the estimated injection lengths were consistently higher for the capillary data than for the microchip data. This suggested that the overall performance of the capillary separations was limited by the injection process, at least for the instrument used. We optimized the injections for both the microchips and capillaries, but higher quality injections on capillaries may be possible on other instruments. Moreover, the injection lengths on the microchip were slightly overestimated from the fits implying that additional dispersion processes such as

adsorption or Joule heating could be occurring for these separations. However, the contribution was small, e.g., less than 10% of the total plate height, and therefore, the source of additional dispersion was difficult to pinpoint.

Higher Separation Performance. The separations on both the microchips and capillaries can be pushed to be more efficient. To illustrate, the label by-product peak in **Figure 3-3a** had a plate height of 0.232 μm corresponding to a plate number of 958,000, which was more than double the average plate number (444,000) for Man 5, Man 6, and Man 9 (see **Table 3-1**). In addition, the migration time of the label by-product (1.09 min) was 2.1 times shorter than the migration time for Man 5 (2.31 min). These data suggested that the separation performance and analysis time on the microfluidic device can be further improved by using higher electric field strengths. By doubling the field strength to 1500 V/cm, the resolution could be increased by 40%, and the analysis time reduced to less than 1.5 min.

3.4. Conclusion

With the spiral channel design, we demonstrated for the first time the ability to electrophoretically separate complex glycan mixtures containing structural isomers (both linkage and positional) in less than 3 min with an excellent average peak capacity of approximately 200. Although microfluidic separations of glycans have been demonstrated before, their poor separation efficiencies hampered isomeric resolution.[28-29] We may be able to push the separation performance further on the microfluidic device by increasing the separation field strength, e.g., 1500 V/cm, and integrating longer separation channels. To our knowledge, this work included the first head-to-head

comparison between microchips and capillaries for separating small molecules. We were pleased to see that the microfluidic devices performed at least as well as the capillaries under all conditions evaluated and the non-circular cross-section of the microchannels did not adversely impact the separation performance.

3.5. References

1. This chapter reproduced in part with permission from Zhuang, Z., Starkey, J. A., Mechref, Y., Novotny, M. V., and Jacobson, S. C., Electrophoretic Analysis of N-Glycans on Microfluidic Devices. *Anal. Chem.* **2007,** *79* (18), 7170-7175. Copyright 2007 American Chemical Society.
2. Apweiler, R.; Hermjakob, H.; Sharon, N., On the Frequency of Protein Glycosylation, as Deduced from Analysis of the Swiss-Prot Database. *Biochim. Biophys. Acta-Gen. Subj.* **1999,** *1473* (1), 4-8.
3. Fukui, S.; Feizi, T.; Galustian, C.; Lawson, A. M.; Chai, W. G., Oligosaccharide Microarrays for High-Throughput Detection and Specificity Assignments of Carbohydrate-Protein Interactions. *Nat. Biotechnol.* **2002,** *20* (10), 1011-1017.
4. Dennis, J. W.; Granovsky, M.; Warren, C. E., Protein Glycosylation in Development and Disease. *Bioessays* **1999,** *21* (5), 412-421.
5. Lowe, J. B.; Marth, J. D., A Genetic Approach to Mammalian Glycan Function. *Annu. Rev. Biochem.* **2003,** *72*, 643-691.
6. An, H. J.; Miyamoto, S.; Lancaster, K. S.; Kirmiz, C.; Li, B. S.; Lam, K. S.; Leiserowitz, G. S.; Lebrilla, C. B., Profiling of Glycans in Serum for the Discovery of Potential Biomarkers for Ovarian Cancer. *J. Proteome Res.* **2006,** *5* (7), 1626-1635.
7. Kyselova, Z.; Mechref, Y.; Kang, P.; Goetz, J. A.; Dobrolecki, L. E.; Sledge, G. W.; Schnaper, L.; Hickey, R. J.; Malkas, L. H.; Novotny, M. V., Breast Cancer Diagnosis and Prognosis through Quantitative Measurements of Serum Glycan Profiles. *Clin. Chem.* **2008,** *54* (7), 1166-1175.
8. Kyselova, Z.; Mechref, Y.; Al Bataineh, M. M.; Dobrolecki, L. E.; Hickey, R. J.; Vinson, J.; Sweeney, C. J.; Novotny, M. V., Alterations in the Serum Glycome Due to Metastatic Prostate Cancer. *J. Proteome Res.* **2007,** *6* (5), 1822-1832.
9. Mechref, Y.; Novotny, M. V., Structural Investigations of Glycoconjugates at High Sensitivity. *Chem. Rev.* **2002,** *102*, 321-369.
10. Mechref, Y.; Novotny, M. V., Miniaturized Separation Techniques in Glycomic Investigations. *Journal of Chromatography B* **2006,** *841* (1-2), 65-78.
11. Honda, S.; Makino, A.; Suzuki, S.; Kakehi, K., Analysis of the Oligosaccharides in Ovalbumin by High-Performance Capillary Electrophoresis. *Analytical Biochemistry* **1990,** *191* (2), 228-234.

12. Liu, J. P.; Shirota, O.; Wiesler, D.; Novotny, M., Ultrasensitive Fluorometric Detection of Carbohydrates as Derivatives in Mixtures Separated by Capillary Electrophoresis. *Proc. Natl. Acad. Sci. U. S. A.* **1991,** *88* (6), 2302-2306.
13. Nashabeh, W.; El Rassi, Z., Capillary Zone Electrophoresis of Linear and Branched Oligosaccharides. *J Chromatogr A* **1992,** *600* (2), 279-287.
14. Guttman, A.; Pritchett, T., Capillary Gel-Electrophoresis Separation of High-Mannose Type Oligosaccharides Derivatized by 1-Aminopyrene-3,6,8-Trisulfonic Acid. *Electrophoresis* **1995,** *16* (10), 1906-1911.
15. Callewaert, N.; Geysens, S.; Molemans, P.; Contreras, R., Ultrasensitive Profiling and Sequencing of N-Linked Oligosaccharides Using Standard DNA-Sequencing Equipment. *Glycobiology* **2001,** *11* (4), 275-281.
16. Guttman, A., High-Resolution Carbohydrate Profiling by Capillary Gel Electrophoresis. *Nature* **1996,** *380* (6573), 461-462.
17. Greenaway, M.; Okafo, G. N.; Camilleri, P.; Dhanak, D., A Sensitive and Selective Method for the Analysis of Complex-Mixtures of Sugars and Linear Oligosaccharides. *Chem. Commun.* **1994,** (14), 1691-1692.
18. Kakehi, K.; Susami, A.; Taga, A.; Suzuki, S.; Honda, S., High-Performance Capillary Electrophoresis of O-Glycosidically Linked Sialic Acid-Containing Oligosaccharides in Glycoproteins as Their Alditol Derivatives with Low-Wavelength Uv Monitoring. *J. Chromatogr. A* **1994,** *680* (1), 209-215.
19. Hutterer, K. M.; Birrell, H.; Camilleri, P.; Jorgenson, J. W., High Resolution of Oligosaccharide Mixtures by Ultrahigh Voltage Micellar Electrokinetic Capillary Chromatography. *J. Chromatogr. B* **2000,** *745* (2), 365-372.
20. Palm, A.; Novotny, M. V., Macroporous Polyacrylamide Poly(Ethylene Glycol) Matrixes as Stationary Phases in Capillary Electrochromatography. *Anal. Chem.* **1997,** *69* (22), 4499-4507.
21. Yang, C. M.; El Rassi, Z., Capillary Electrochromatography of Derivatized Mono- and Oligosaccharides. *Electrophoresis* **1998,** *19* (12), 2061-2067.
22. Suzuki, S.; Yamamoto, M.; Kuwahara, Y.; Makiura, K.; Honda, S., Separation of 1-Phenyl-3-Methyl-5-Pyrazolone Derivatives of Monosaccharides by Capillary Electrochromatography. *Electrophoresis* **1998,** *19* (15), 2682-2688.
23. Que, A. H.; Novotny, M. V., Structural Characterization of Neutral Oligosaccharide Mixtures through a Combination of Capillary Electrochromatography and Ion Trap Tandem Mass Spectrometry. *Anal. Bioanal. Chem.* **2003,** *375* (5), 599-608.
24. Que, A. H.; Mechref, Y.; Huang, Y. P.; Taraszka, J. A.; Clemmer, D. E.; Novotny, M. V., Coupling Capillary Electrochromatography with Electrospray Fourier Transform Mass Spectrometry for Characterizing Complex Oligosaccharide Pools. *Anal. Chem.* **2003,** *75* (7), 1684-1690.
25. Que, A. H.; Novotny, M. V., Separation of Neutral Saccharide Mixtures with Capillary Electrochromatography Using Hydrophilic Monolithic Columns. *Anal. Chem.* **2002,** *74* (20), 5184-5191.
26. Tegeler, T. J.; Mechref, Y.; Boraas, K.; Reilly, J. P.; Novotny, M. V., Microdeposition Device Interfacing Capillary Electrochromatography and Microcolumn Liquid Chromatography with Matrix-Assisted Laser Desorption/Ionization Mass Spectrometry. *Anal. Chem.* **2004,** *76* (22), 6698-6706.

27. Mechref, Y.; Muzikar, J.; Novotny, M. V., Comprehensive Assessment of N-Glycans Derived from a Murine Monoclonal Antibody: A Case for Multimethodological Approach. *Electrophoresis* **2005,** *26* (10), 2034-2046.
28. Dang, F. Q.; Zhang, L. H.; Jabasini, M.; Kaji, N.; Baba, Y., Characterization of Electrophoretic Behavior of Sugar Isomers by Microchip Electrophoresis Coupled with Videomicroscopy. *Anal. Chem.* **2003,** *75* (10), 2433-2439.
29. Dang, F. Q.; Kakehi, K.; Nakajima, K.; Shinohara, Y.; Ishikawa, M.; Kaji, N.; Tokeshi, M.; Baba, Y., Rapid Analysis of Oligosaccharides Derived from Glycoproteins by Microchip Electrophoresis. *J. Chromatogr. A* **2006,** *1109* (2), 138-143.
30. Callewaert, N.; Contreras, R.; Mitnik-Gankin, L.; Carey, L.; Matsudaira, P.; Ehrlich, D., Total Serum Protein N-Glycome Profiling on a Capillary Electrophoresis-Microfluidics Platform. *Electrophoresis* **2004,** *25* (18-19), 3128-3131.
31. Culbertson, C. T.; Jacobson, S. C.; Ramsey, J. M., Microchip Devices for High Efficiency Separations. *Anal. Chem.* **2000,** *72* (23), 5814-5819.
32. Paegel, B. M.; Emrich, C. A.; Weyemayer, G. J.; Scherer, J. R.; Mathies, R. A., High Throughput DNA Sequencing with a Microfabricated 96-Lane Capillary Array Electrophoresis Bioprocessor. *Proc. Natl. Acad. Sci. U. S. A.* **2002,** *99* (2), 574-579.
33. Griffiths, S. K.; Nilson, R. H., Low-Dispersion Turns and Junctions for Microchannel Systems. *Anal. Chem.* **2001,** *73*, 272-278.
34. Molho, J. I.; Herr, A. E.; Mosier, B. P.; Santiago, J. G.; Kenny, T. W.; Brennen, R. A.; Gordon, G. B.; Mohammadi, B., Optimization of Turn Geometries for Microchip Electrophoresis. *Anal. Chem.* **2001,** *73*, 1350-1360.
35. Ramsey, J. D.; Jacobson, S. C.; Culbertson, C. T.; Ramsey, J. M., High-Efficiency, Two-Dimensional Separations of Protein Digests on Microfluidic Devices. *Anal. Chem.* **2003,** *75*, 3758-3764.
36. Evangelista, R. A.; Liu, M. S.; Chen, F. T. A., Characterization of 9-Aminopyrene-1,4,6-Trisulfonate-Derivatized Sugars by Capillary Electrophoresis with Laser-Induced Fluorescence Detection. *Anal. Chem.* **1995,** *67* (13), 2239-2245.
37. Evangelista, R. A.; Chen, F. T. A.; Guttman, A., Reductive Amination of N-Linked Oligosaccharides Using Organic Acid Catalysts. *J Chromatogr A* **1996,** *745* (1-2), 273-280.
38. Kovarik, M. L.; Jacobson, S. C., Attoliter-Scale Dispensing in Nanofluidic Channels. *Anal. Chem.* **2007,** *79*, 1655-1660.
39. Jacobson, S. C.; Hergenröder, R.; Koutny, L. B.; Warmack, R. J.; Ramsey, J. M., Effects of Injection Schemes and Column Geometry on the Performance of Microchip Electrophoresis Devices. *Anal. Chem.* **1994,** *66* (7), 1107-1113.
40. Hjerten, S., High-Performance Electrophoresis. Elimination of Electroendosmosis and Solute Adsorption. *J. Chromatogr.* **1985,** *347*, 191-198.
41. Canelle, L.; Bousquet, J.; Pionneau, C.; Hardouin, J.; Choquet-Kastylevsky, G.; Joubert-Caron, R.; Caron, M., A Proteomic Approach to Investigate Potential Biomarkers Directed against Membrane-Associated Breast Cancer Proteins. *Electrophoresis* **2006,** *27* (8), 1609-1616.

42. Mechref, Y.; Novotny, M. V., Mass Spectrometric Mapping and Sequencing of N-Linked Oligosaccharides Derived from Submicrogram Amounts of Glycoproteins. *Anal. Chem.* **1998,** *70* (3), 455-463.
43. Starkey, J. A.; Mechref, Y.; Novotny, M. V., unpublished data.

Chapter 4. Microchip Electrophoresis of N-Glycans on Serpentine Separation Channels with Turn Taper Ratios of 1, 2, and 3

4.1. Introduction to Glycan Analysis and Turn-Induced Band Broadening

Glycans have long been viewed as essential molecules for many living organisms, and more recently, are receiving substantial attention since alteration in the glycosylation of proteins has been implicated in many inflammatory diseases and cancer [1-6]. Glycan-protein and glycan-glycan interactions are fundamentally important in protein structure modulation and localization, transporting signals in multicellular systems, and cell-cell recognition, including bacterial and viral infections and cancer pathogenesis [7-9]. The field of analytical glycobiology has begun to focus on these functionalities, biological processes, and the associated diseases.

Many glycans have high molecular masses and complex chemical structures stemming from vast diversity in composition, branching, and linkages. A small change in these structures may be indicative of significant pathological alterations. Recent studies on the glycomic structures found in complex biological mixtures, such as physiological fluids [10-12], illustrated the demand for separation methods with excellent structural resolution and detection methods at high sensitivity. Chromatographic techniques including reverse phase, hydrophobic and hydrophilic interaction, and ion exchange chromatography have been used for carbohydrate separations [13]. More recently, capillary electrophoresis [14-17] and electrochromatography [18-22] have been applied to the separation of glycoconjugates and glycans. In particular, capillary electrophoresis combined with mass spectrometry [23] has been used in several applications because of its high separation

efficiency, ability to resolve structural isomers, direct mass and structural information, and high sensitivity.

Microfluidic devices have been used for analyzing glycan structures [24-26] with the benefits of shorter analysis times and precise sample control. These studies showed lower separation efficiencies compared to capillary separations, primarily due to shorter channel lengths. To increase the resolution of these separations, longer separation channels need to be fabricated on microchips where turns must be integrated in the channels without introducing significant sample dispersion, i.e., the "racetrack" effect. A spiral channel is one such design that minimizes turn-induced band broadening by incorporating large radius turns[27]. Previously, we reported high efficiency electrophoretic separations of N-glycans on a 22-cm spiral microchannel [28] and demonstrated comparable performance to conventional capillary electrophoresis, but with shorter analysis times. Serpentine channels with symmetric [29] and asymmetric [30-31] turns not only minimize turn-induced dispersion but also reduce the device footprint. Consequently, serpentine channels can easily be multiplexed [32] to increase the sample throughput, and additional separation length can be incorporated without substantially increasing the overall device size.

We designed and fabricated microfluidic devices with serpentine separation channels and asymmetric turns that had taper ratios of 1, 2, and 3. We define the taper ratio as the ratio of the width of the straight channel (straight width) to the width of the channel in the turn (turn width). The primary goals of this study were (i) to evaluate the contribution of different taper ratios to band dispersion, (ii) to push separations of N-glycans to higher electric field strengths and longer separation lengths, and (iii) to demonstrate separations

of clinically relevant N-glycan samples had similar efficiencies to model samples. We show that serpentine channels having turns with taper ratios 2 and 3 did not exhibit a substantial "racetrack" effect, excellent separation efficiencies were achieved at 750-1750 V/cm field strengths , and 22- and 36-cm long serpentine channels allowed analysis times under 1.25 and 3.1 min, respectively.

4.2. Experimental Section

Materials. We purchased acetic acid, acetonitrile (ACN), ammonium bicarbonate, ammonium persulfate, citric acid, dimethylsulfoxide (DMSO), 4-(2-hydroxyethyl)-1-piperazine-ethanesulfonic acid (HEPES), β-mercaptoethanol, γ-methacryloxypropyltrimethoxysilane (MAPTOS), methanol, methylene dichloride, potassium phosphate monobasic, RNase B, sodium cyanoborohydride, N,N,N',N'-tetramethylethylenediamine (TEMED), and trifluoroacetic acid (TFA) from Sigma-Aldrich (St Louis, MO); sodium hydroxide from Fisher Scientific (Pittsburgh, PA); high-purity 8-aminopyrene-1,3,6-trisulfonic acid (APTS) from Beckman Coulter, Inc. (Brea, CA) ; peptide-N-glycosidase F (PNGase F) of *Chryseobacterium menigosepticum* (EC 3.2.2.18) from Northstar BioProducts (East Falmouth, MA); sialidase from ProZyme, Inc. (Hayward, CA); Microposit MF-319 developer from Rohm and Haas Electronic Materials (Midland, MI); Chromium Etchant 1020 and 8002-A, and buffered oxide etchant (BOE) from Transene Co. (Danvers, MA); 353NDT Epoxy from Epoxy Technology (Billerica, MA); and B270 glass substrates and cover plates from Telic Co. (Valencia, CA).

Microfluidic Device Fabrication and Channel Coating. Microfluidic devices, similar in design to what is depicted in **Figure 4-1a**, were fabricated from B270 glass substrates coated with Cr and AZ1518 photoresist as described previously [33]. The substrates were exposed to UV radiation (365 nm, 200 mJ/cm^2) through a photomask (HTA Photomask, San Jose, CA) on a mask aligner (205S, Optical Associates, Inc., San Jose, CA), developed for 2 min in MF-319 developer, and rinsed with water. After development, the channel pattern was transferred to the chromium layer by etching in Cr Etchant 8002-A, and subsequently to the glass layer by etching in BOE until the channels were 15 μm deep. Channel dimensions were measured using a stylus-based profiler (Dektak 6M, Veeco Instruments, Inc., Plainview, NY) which are listed in **Table 4-1**. Fluid access holes were sandblasted at the ends of the channels (AEC Air Eraser, Paasche Airbrush Co., Chicago, IL). Following sandblasting, the unexposed photoresist layer was removed by rinsing in acetone for 2 min, and the remaining Cr layer was removed in Cr Etchant 1020. The drilled substrate was then bonded to a cover plate by hydrolyzing both pieces in a solution of NH_4OH, H_2O_2, and H_2O (2:1:2), by bringing the substrate and coverplate into contact prior to ramping the temperature to 545° C, and annealing for 10 h. Short segments of glass tubing (6 mm o.d. x 4 mm i.d. x 6 mm tall) were affixed over the sandblasted holes with 353NDT epoxy.

The microchannels were coated with linear poly(acrylamide) to minimize electroosmotic flow (EOF) and to prevent analyte adsorption to the channel walls. The microchannels were cleaned sequentially with 1.0 M sodium hydroxide solution, water, and methanol for 20 min each. The microchannels were then filled with a solution of 45 μL MAPTOS dissolved in 1.5 mL methylene dichloride with 0.02 M acetic acid. After 45

min, the microchannels were rinsed with methanol and water for 15 min each to remove residual silane solution. The channels were then filled with an aqueous solution containing 2.4% (w/w) acrylamide, 1.0 μL/mL TEMED, and 1.0 mg/mL ammonium persulfate. After 2 h, the microchannels were flushed with water for 20 min and filled with the separation buffer.

N-Glycan Sample Preparation and Desialylation. N-glycans were cleaved from RNase B and glycoproteins in the blood sera of an ovarian cancer patient and a disease-free individual with PNGase F [28] and labeled with APTS [34]. Briefly, a 10-μL aliquot of human blood serum was lyophilized and then resuspended in 100 μL of 25 mM ammonium bicarbonate. Next, a 5 mU aliquot of PNGase F was added to the reaction mixture and incubated overnight (18-22 h) at 37 °C. Deionized water was then added to the enzymatically released glycans to bring the total volume of the reaction mixture to 1 mL. Samples were then applied to both C18 Sep-Pak® cartridges (Waters, Milford, MA) and activated charcoal cartridges (Harvard Apparatus, Holliston, MA). The use of C18 Sep-Pak® cartridges is necessary to isolate the glycans from peptides and proteins, which would otherwise interfere with trapping on the activated charcoal cartridges. The reaction mixture was first applied to C18 Sep-Pak® cartridge that had been preconditioned with ethanol and deionized water, as recommended by the manufacturer. The reaction mixture was circulated through the C18 Sep-Pak® cartridge 5-times prior to washing with water. Peptides and O-linked glycopeptides were retained on the C18 Sep-Pak® cartridge, while the released glycans were collected as eluent. Next, the C18 Sep-Pak® cartridge was washed with 1 mL of deionized water. The combined eluents containing the released N-glycans were then passed over activated charcoal microcolumns. The columns were

preconditioned with 1 mL of ACN and 1 mL of 0.1% TFA aqueous solution, as recommended by the manufacturer. After applying the sample, the microcolumn was washed with 1 mL of 0.1% TFA aqueous solution. The samples were then eluted with a 1-mL aliquot of 50% ACN aqueous solution containing 0.1% TFA. Finally, the purified glycans were evaporated to dryness with a vacuum CentriVap Concentrator (Labconco Corporation, Kansas City, MO).

Also, the N-glycan samples derived from the blood serum samples were desialylated with sialidase. The N-glycans derived from a 5-μL aliquot of human blood serum was lyophilized and then resuspended in 10 mM phosphate buffer (pH 6). A 0.2-μL aliquot of sialidase was added, and the mixture was incubated at 37°C for 6 h to allow desialylation. Both the native and desialylated glycans derived from human blood serum were dried prior to APTS derivatization.

N-glycan samples were also derived from 1-μg aliquots of dried glycoprotein RNase B with PNGase F. The glycans were suspended in 2.5 μL phosphate buffer (pH 7) with 1% β-mercaptoethanol and thermally denatured at 95 ºC for 10 min. The solution was cooled to room temperature prior to the addition of a 0.5-μL aliquot of PNGase in phosphate buffer, and the reaction mixture was then incubated overnight at 37 ºC. Next, the released glycans were collected and dried in vacuum and labeled with APTS by adding a 2-μL aliquot of 100 μM APTS solution prepared in 0.9 M citric acid and a 1-μL aliquot of 1 M sodium cyanoborohydride prepared in DMSO. The reaction was allowed to proceed for 2 h at 55 ºC. The derivatization mixture was dialyzed overnight at room temperature using a 1000-Da cut-off cellulose membrane to reduce the amount of unreacted APTS. Finally,

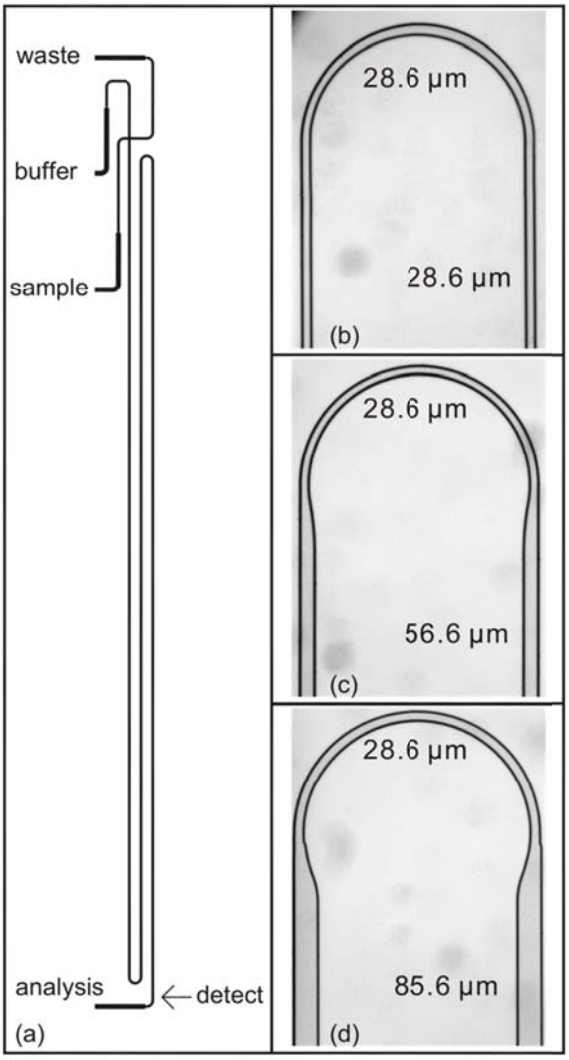

Figure 4-1. (a) Photomask design of a microfluidic device (serp-22-1-2) with a 22-cm serpentine separation channel and two 180° turns with taper ratio 1. See Tables 1 and 2 for device dimensions and details. White light images of asymmetrically tapered, 180° turns with taper ratios (b) 1, (c) 2, and (d) 3.

the dialyzed mixture was dried and resuspended in 15 μL of 1 mM phosphate and 20 mM HEPES buffer (pH 6.8) prior to electrophoretic analysis.

Microchip Electrophoresis. For the electrophoretic separations, a power supply with independent high-voltage outputs supplied the potentials to the sample, buffer, and waste reservoirs. The power supply consisted of a single 10-kV voltage source (10A12-P4-M-C, UltraVolt, Inc., Ronkonkoma, NY) and pairs of optical resistors (OC100, Voltage Multipliers, Inc., Visalia, CA) used as voltage dividers to establish the output potentials. A commercial high voltage power supply (0-30 kV; CZE 1000R, Spellman High Voltage Electronics Corp., Hauppauge, NY) was used to control the potential applied at the analysis reservoir. Applied potentials were controlled with a LabView program and an analog output board (PCI-6713, National Instruments Corp., Austin, TX). Electric field strengths of 750-1750 V/cm in the analysis channel were used to evaluate the separation performance of the microfluidic devices. Standard pinched injections [35] were used to introduce sample to the analysis channel, at the highest applied potentials (30 kV applied to the analysis reservoir), a 20-ms delay was inserted between sample loading and injection to minimize high voltage transients when the potentials applied to the sample, buffer, and waste reservoirs were switched from positive to negative values. The buffer used for the microchip separations was 1 mM phosphate and 20 mM HEPES (pH 6.8). The resistivity of the buffer solution in the microchannels was evaluated by applying potentials from 2–28.5 kV and measuring the current with a picoammeter (6485, Keithley Instruments, Inc., Cleveland, OH).

Separations at a single point in the analysis channel were monitored with an inverted optical microscope (TE-2000U, Nikon, Inc., Melville, NY) equipped with a 20x objective

and an HQ FITC filter cube (Chroma Technology Corp., Bellows Falls, VT). The 488-nm line of an argon ion laser (CVI Melles Griot, Inc., Carlsbad, CA) was attenuated to 1.0 mW with neutral density filters and focused to a point in the analysis channel. The fluorescence signal was spatially filtered with a 600 μm pinhole, detected with a photomultiplier tube (H5783-01, Hamamatsu Corp., Bridgewater, NJ), amplified by a low-noise current preamplifier (SR570, Stanford Research Systems, Inc., Sunnyvale, CA), and recorded with a multifunction data acquisition board (PCI-6032E, National Instruments Corp.) and software written with LabView. The sampling frequency was 100 Hz. To determine separation efficiencies, the data for selected peaks were fitted with a Gaussian function in OriginPro 7.5 software (OriginLab Corp., Northampton, MA). The peak parameters were then used to calculate the velocity, plate height, and plate number.

4.3. Results and Discussion

Turn and Channel Designs. The asymmetrically tapered turns were designed similar to those described previously [30-31]. The inside wall of the 180° turns with taper ratios 2 and 3 were constructed from three arcs that were tangent to one another to provide a smooth transition from the wide straight channel to the narrow turn channel [31]. The first arc reduced the channel width from the wide straight channel to the narrow turn channel. The second arc maintained the narrow turn width. The third arc mirrored the first arc and increased the channel width from the turn channel to the straight channel. The first and third arcs were 300 μm long. The turn radii were 0.5 mm, and thus, the straight channels were spaced 1 mm center-to-center.

The glass substrates were etched isotropically with wet chemical etching, and consequently, the channel width depends on the etch rate and time. We defined the average width of an etched channel, w_{avg}, as

$$w_{avg} = w_{ph} + \frac{\pi}{2} d \qquad (1)$$

where w_{ph} is the channel width on the photomask and d is the channel depth. The channel widths on the photomask were designed such that with a channel depth of 15 μm, the straight channel widths to turn channel widths have taper ratios of 1, 2, and 3. On the photomask, the turn width for the three taper ratios was 5 μm, and the straight widths after etching were 5, 33, and 62 μm to produce taper ratios 1, 2, and 3, respectively. The channel widths for the photomasks and etched channels are summarized in **Table 4-1**, and bright-field images of turns with taper ratios 1, 2, and 3 are shown in **Figure 4-1 b-d**.

To evaluate the impact of taper ratio on dispersion, we fabricated devices with 22-cm serpentine channels, two 180° turns, and taper ratios 1, 2, and 3. A schematic of the device with the 22-cm serpentine channel is shown in **Figure 4-1**. In addition, to test how the separation length and number of turns influenced performance, devices were fabricated with serpentine channels that were 11-cm long with two turns, 18-cm long with four turns, and 36-cm long with four turns. These devices were similar in design to **Figure 4-1a**. The microchip designs, taper ratios, number of turns, and effective separation lengths are summarized in **Table 4-2**.

Table 4-1. Channel widths, taper ratios of 180° turns, and injection lengths.

	Taper ratio of 180° turns		
	1	2	3
Channels on photomask			
Straight width (μm)	5	33	62
Turn width (μm)	5	5	5
Channels after etching			
Straight width (μm)	28.6	56.6	85.6
Turn width (μm)	28.6	28.6	28.6
Taper ratio	1.00	1.98	2.99
Injection length[a)] (μm)	43	71	106

a) Injection length is based on the straight channel width at the cross intersection and increases with taper ratio.

Turn-Induced Sample Dispersion. N-Glycans derived from RNase B were analyzed to evaluate the separation performance of the devices listed in **Table 4-2**. **Figure 4-2** depicts electropherograms acquired with the 22-cm serpentine channel (serp-22-3-2) at 1530 V/cm and 36-cm serpentine channel (serp-36-3-4) at 990 V/cm. Separations on the 36-cm channel were limited to 990 V/cm because of the maximum output of the power supplies. However, we were able to achieve baseline resolution for the structural isomers of mannose 7 and 8 on the 36-cm channel, not the 22-cm channel. From the electropherograms, the plate heights of mannose 5, 6, and 9 were calculated and are plotted as a function of the analyte velocity. These data are also compared to our previous work on the 22-cm spiral separation channel [28]. The primary difference is that we used field strengths of 750-1750 V/cm on the serpentine channels, compared to 75-750 V/cm for the spiral channels.

From **Figure 4-3**, the separations on the serpentine channel with taper ratio 1 had an average plate height that was ~30% larger than the separations on the channels with taper ratios 2 and 3. The average plate heights at field strengths of 1270 and 1530 V/cm were 0.60 μm for taper ratio 1 and 0.46 μm for the taper ratios 2 and 3. Interestingly, the data from the channels with taper ratios 2 and 3 showed similar performance, and turn-induced band dispersion appeared to be minimized. Based on our chip design and previously published work [30], we expected the plate heights from the channel with taper ratio 2 to fall between those for the channels with taper ratios 1 and 3. However, the more general trend of the plate heights approaching an asymptote at field strengths >750 V/cm and linear velocities >8 cm/min was expected as axial diffusion contributed less to the total plate height.

Table 4-2. Device names, separation lengths, taper ratios, and number of 180° turns.

Device[a)]	Separation length (cm)	Taper ratio	Number of 180° turns
serp-22-1-2	21.6	1	2
serp-22-2-2	21.6	2	2
serp-22-3-2	21.6	3	2
serp-11-3-2	11.0	3	2
serp-18-3-4	18.2	3	4
serp-36-3-4	35.8	3	4
spiral-22	22.0	–	–

a) Device names are "channel design – separation length – taper ratio – number of turns" for the serpentine (serp) and spiral channel designs.

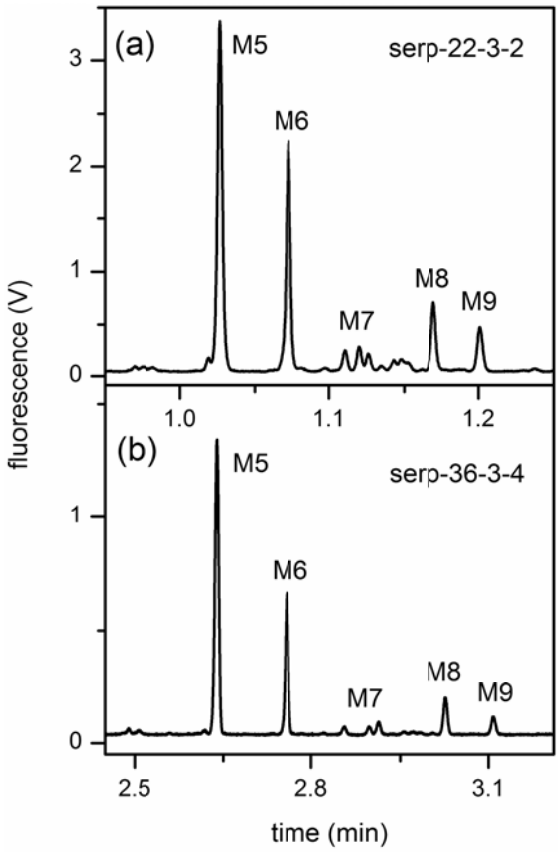

Figure 4-2. Electropherograms of the N-glycans derived from RNase B separated on serpentine channels (a) 22-cm long (serp-22-3-2) and (b) 36-cm long (serp-36-3-4). The separation field strengths on serp-22-3-2 and serp-36-3-4 were 1530 and 990 V/cm, respectively. See Table 2 for device details. The labeled peaks are mannose 5 (M5), mannose 6 (M6), mannose 7 (M7), mannose 8 (M8), and mannose 9 (M9).

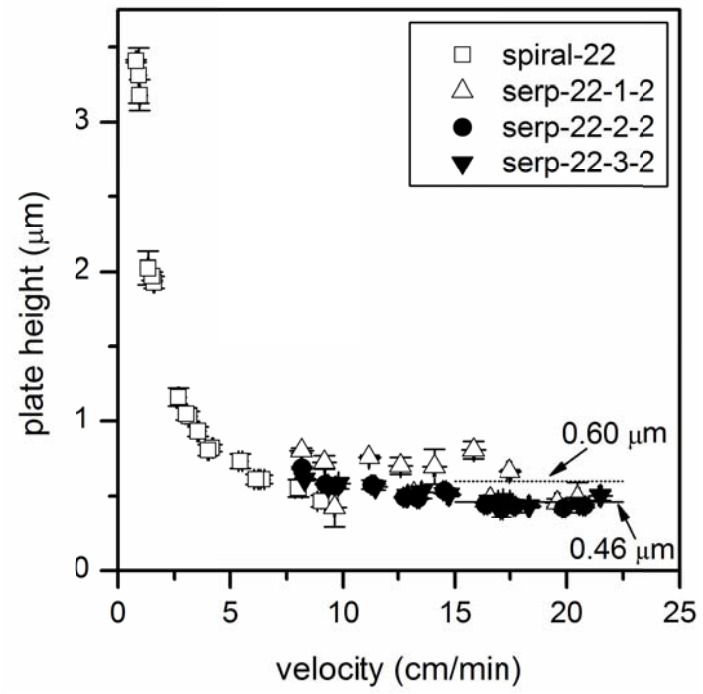

Figure 4-3. Variation of plate height with velocity for serpentine channels with taper ratios 1, 2, and 3. See Table 2 for device details. The solid and dashed lines compare the average plate heights of taper ratio 1 and taper ratios 2 and 3, respectively. Results are compared with data from the 22-cm spiral channel in [28]. Data are from mannose 5, 6, and 9, and error bars are $\pm\sigma$ for $n = 3$ for plate height and velocity.

To study the influence of separation length and number of turns on separation performance, we tested serpentine channels with separation lengths of 11 cm with two turns (serp-11-3-2), 18 cm with four turns (serp-18-3-4), and 36 cm with four turns (serp-36-3-4). **Figure 4-4** compares the plate heights from these channels with the 22-cm serpentine channel with two turns (serp-22-3-2). As seen in the figure, the plate heights for the four channel designs were similar. More importantly, devices with similar separation lengths (22 cm and 18 cm) but twice as many turns (2 and 4) provided similar performance, but in a 50% smaller footprint for serp-18-3-4. If there was a significant amount of turn-induced dispersion, poorer performance would have resulted on the 18-cm channel with four turns (serp-18-3-4).

Contributions to the Plate Height. Equation 2 was fitted to the plate height data from the 22-cm spiral channel shown in **Figure 4-4** to provide an estimate of the dispersion coefficient, D, for mannose 5, 6, and 9.

$$H = A + \frac{2D}{u} \qquad (2)$$

where A includes constant contributions from the injection, detector, and channel geometry and u is the linear velocity. With the fit parameters (A = 1.71 x 10^{-5} cm and D = 2.28 x 10^{-6} cm^2/min), Equation 2 was extrapolated to higher velocities (≥10 cm/min) to compare the plate heights from the serpentine channels. As seen in the figure, the majority of the plate height data lie above the extrapolated curve.

In microchip electrophoresis, contributions to the plate height include axial diffusion (H_{diff}), injection length (H_{inj}), detector path length (H_{det}), Joule heating (H_J), adsorption

(H_{ads}), and geometry (H_{geo}) [36]. The dispersion sources in our system can be estimated with Equation 3.

$$\begin{aligned} H &= H_{diff} + H_{inj} + H_{\det} + H_{geo} + H_J + H_{ads} \\ &= \frac{2D}{u} + \frac{l_{inj}^2}{12L} + \frac{l_{\det}^2}{12L} + \frac{\left(2\theta w_{avg}\right)^2}{12} + C_J \mu E^5 d^6 + C_A u \end{aligned} \quad (3)$$

where l_{inj} is the injected sample plug length, l_{det} is the detection length in the separation channel, L is the separation length, θ is the included angle (180°), C_J is coefficient for Joule heating, μ is the apparent mobility of the analyte, E is the field strength, d is the depth of the microchannel, and C_A is coefficient for adsorption.

For the 22-cm serpentine channel (serp-22-3-2), contributions to the plate height are estimated to be 4.3 nm for a 106 μm long injection plug (see **Table 4-1**) and 0.039 nm for a laser spot with a 10-μm diameter. From Equation 5c in [31], the geometrical dispersion for two 180° turns with taper ratio 3 is calculated to be 25 nm. Although these contributions are negligible, the plates heights for velocities >15 cm/min were ~40% larger than predicted by Equation 2. The two most probable sources are Joule heating and adsorption.

To investigate the extent of Joule heating in our system, the velocity of mannose 5 is plotted against the electric field strength as shown in **Figure 4-5**. Above 1000 V/cm, the velocity deviated from linearity for the channels with taper ratios 2 and 3. Moreover, to evaluate the power dissipation, we measured the ion currents for field strengths up to 1250 V/cm on the 22-cm channels with taper ratios 1, 2, and 3 (see **Figure 4-5**). The field strength at 1530 V/cm was not included due to the input potential limit of the

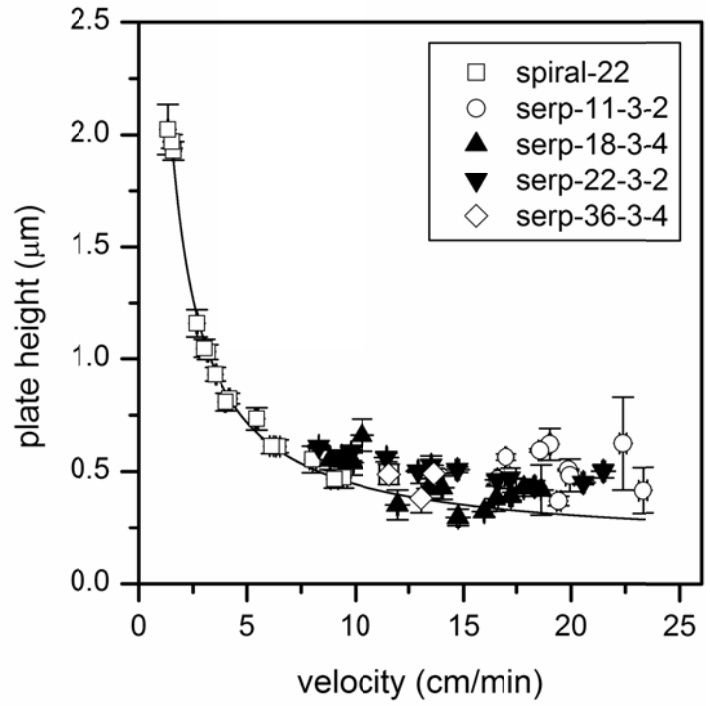

Figure 4-4. Variation of plate height with velocity for the 11, 18, 22, and 36-cm serpentine channels with taper ratio 3. See Table 2 for device details. Results are compared with data from the 22-cm spiral channel in [28], and the solid line is a fit to the spiral data and extrapolated to higher velocities. Data are from mannose 5, 6, and 9, and error bars are $\pm\sigma$ for $n = 3$ for plate height and velocity.

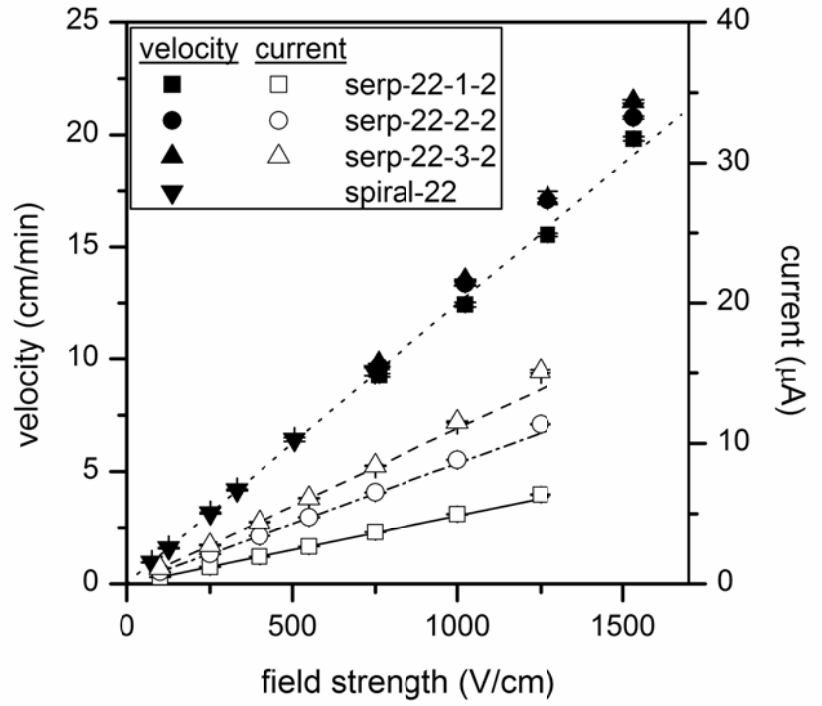

Figure 4-5. Variation of velocity and current with electric field strength for the 22-cm serpentine channels with taper ratios 1, 2, and 3. See Table 2 for device details. For the velocity data, a linear fit of the data from serp-22-1-2 and spiral-22 [28] is shown, and for the current data, linear fits of the first four data points are included. The error bars are $\pm\sigma$ for $n = 3$ for velocity and $n = 30$ for current.

picoammeter. At 1250 V/cm, the power dissipations (power per unit length) for the channels with taper ratios 1, 2, and 3 were 0.80, 1.42, and 1.89 W/m, respectively. In conventional capillaries, Joule heating starts to contribute significantly to the plate height above 1 W/m [37], and in microfluidic devices, separation efficiency begins to degrade at 3 W/m [38].

Another source of the band dispersion is adsorption to the channel walls. In earlier studies on capillaries [39], the onset of adsorption occurred at relatively low field strengths, e.g., 300-400 V/cm. In the studies presented here, adsorption was a relatively minor contribution even at high electric field strengths, e.g., >1000 V/cm. In fact, the plate height did not increase at high field strengths, as observed previously, but simply did not continue to improve. Presently, we are not able to push the separations to higher field strengths to differentiate between Joule heating and adsorption, although both may be present in the separation.

Cancer sample separation. To demonstrate high separation efficiencies for biologically relevant samples, N-glycans derived from the blood serum of an ovarian cancer patient and a disease-free individual were separated on a 22-cm serpentine channel with taper ratio 3 (serp-22-3-2). In addition, portions of both glycan samples were desialylated, separated under similar conditions, and compared to the native samples. The electropherograms of the four N-glycan samples (cancer native, cancer desialylated, disease-free native, and disease-free desialylated) are shown in **Figure 4-6**. When comparing the native and desialylated samples, the desialylated sample separation contained fewer peaks, and the peak intensities were higher due to the reduced sample complexity. The plate heights of five glycan components (labeled 1-5 in **Figure 4-6d**) are

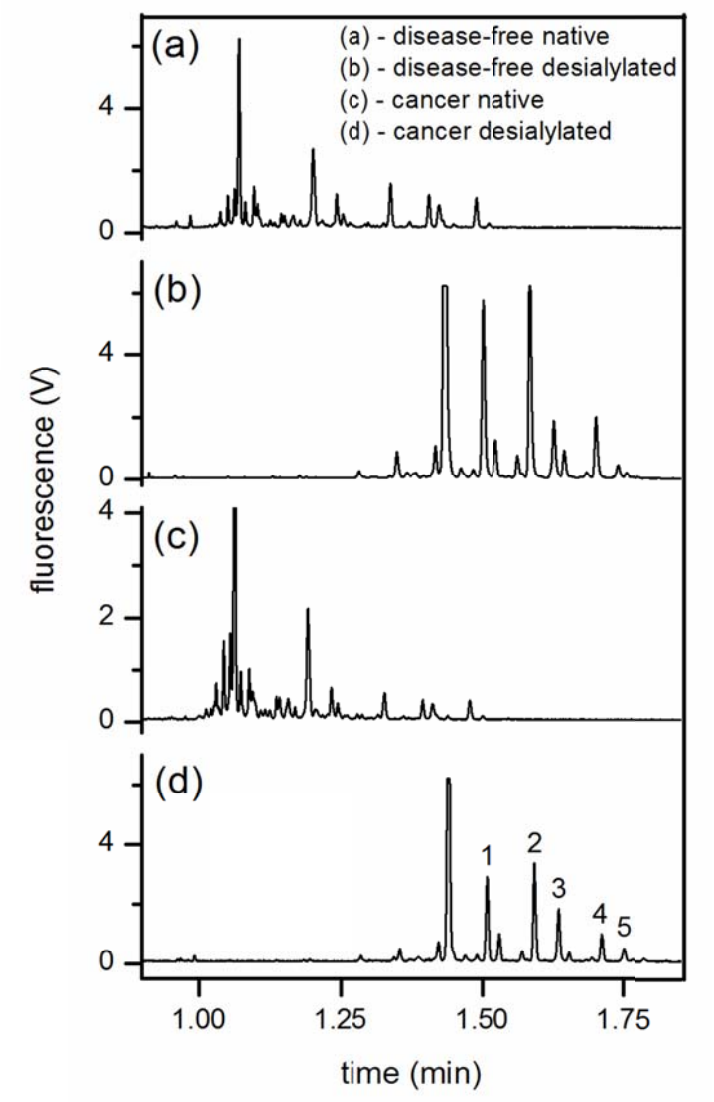

Figure 4-6. Electropherograms of native and desialylated N-glycan samples derived from blood serum samples from an ovarian cancer patient and a disease-free individual. Device serp-22-3-2 and an electric field strength of 1270 V/cm were used. The electropherograms are offset for clarity. Components 1-5 are used to evaluate separation efficiency in **Figure 4-7**.

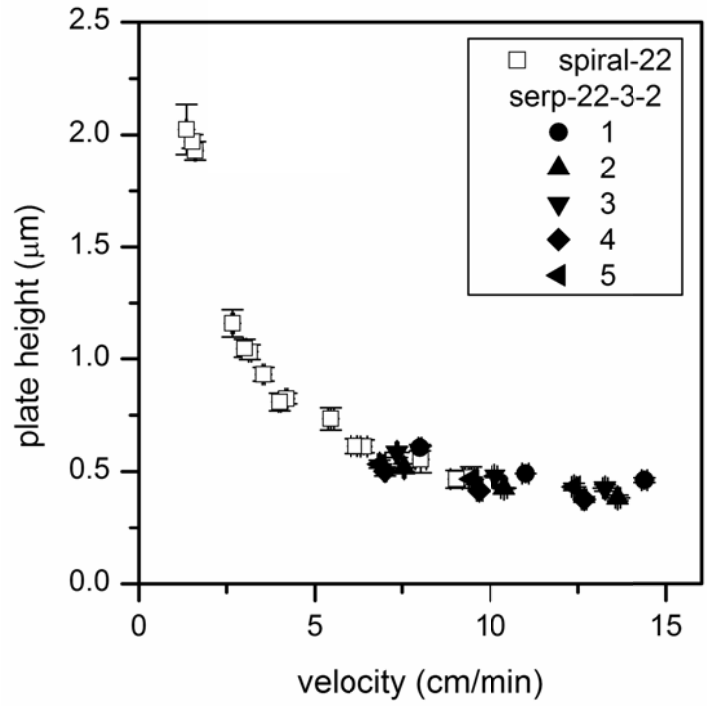

Figure 4-7. Variation of plate height with velocity for the desialylated N-glycan components 1-5 from **Figure 4-6**. See Table 2 for device details of serp-22-3-2. Results are compared with data from the 22-cm spiral channel in [28]. Error bars are $\pm\sigma$ for $n = 3$ for plate height and velocity.

plotted in **Figure 4-7**. As seen in the figure, the plate heights were similar to those from RNase B. These data demonstrated that clinically derived sample can be separated with similar separation efficiencies to model glycans.

4.4. Conclusion

Serpentine channels with asymmetrically tapered turns were evaluated as a function of separation length, electric field strength, taper ratio of the turns, and number of turns. Separations on the 36-cm channel provided the best performance with plate numbers up to 940,000, but separations on the 22-cm channel offered a reasonable compromise between analysis time (under 1.25 min) and separation efficiency (up to 600,000 plates). Interestingly, turns with taper ratios 2 and 3 produced similar efficiencies and minimized turn-induced dispersion, especially compared to turns with taper ratio 1. The separations of N-glycans derived from the blood sera of an ovarian cancer patient and a disease-free individual showed that clinically relevant samples can be separated with performance similar to model glycans from RNase B.

4.5. References

1. Fukui, S.; Feizi, T.; Galustian, C.; Lawson, A. M.; Chai, W. G., Oligosaccharide Microarrays for High-Throughput Detection and Specificity Assignments of Carbohydrate-Protein Interactions. *Nat. Biotechnol.* **2002,** *20* (10), 1011-1017.
2. Dennis, J. W.; Granovsky, M.; Warren, C. E., Protein Glycosylation in Development and Disease. *Bioessays* **1999,** *21* (5), 412-421.
3. Lowe, J. B.; Marth, J. D., A Genetic Approach to Mammalian Glycan Function. *Annu. Rev. Biochem.* **2003,** *72*, 643-691.
4. Miyoshi, E.; Moriwaki, K.; Nakagawa, T., Biological Function of Fucosylation in Cancer Biology. *J. Biochem.* **2008,** *143* (6), 725-729.
5. Meuwis, M. A.; Fillet, M.; Geurts, P.; de Seny, D.; Lutteri, L.; Chapelle, J. P.; Bours, V.; Wehenkel, L.; Belaiche, J.; Malaise, M.; Louis, E.; Merville, M. P.,

Biomarker Discovery for Inflammatory Bowel Disease, Using Proteomic Serum Profiling. *Biochem. Pharmacol.* **2007,** *73* (9), 1422-1433.
6. Kirmiz, C.; Li, B. S.; An, H. J.; Clowers, B. H.; Chew, H. K.; Lam, K. S.; Ferrige, A.; Alecio, R.; Borowsky, A. D.; Sulaimon, S.; Lebrilla, C. B.; Miyamoto, S., A Serum Glycomics Approach to Breast Cancer Biomarkers. *Mol. Cell. Proteomics* **2007,** *6* (1), 43-55.
7. Ferrier, R. J., In *The Organic Chemistry of Sugars*, Levy, D. E.; Fügedi, P., Eds. Taylor & Francis: Boca Raton, 2006; p 17.
8. Bradley, W. P.; Blasco, A. P.; Weiss, J. F.; Alexander, J. C.; Silverman, N. A.; Chretien, P. B., Correlations among Serum Protein-Bound Carbohydrates, Serum Glycoproteins, Lymphocyte-Reactivity, and Tumor Burden in Cancer-Patients. *Cancer* **1977,** *40* (5), 2264-2272.
9. Mrochek, J. E.; Dinsmore, S. R.; Tormey, D. C.; Waalkes, T. P., Protein-Bound Carbohydrates in Breast-Cancer - Liquid-Chromatographic Analysis for Mannose, Galactose, Fucose, and Sialic-Acid in Serum. *Clin. Chem.* **1976,** *22* (9), 1516-1521.
10. An, H. J.; Miyamoto, S.; Lancaster, K. S.; Kirmiz, C.; Li, B. S.; Lam, K. S.; Leiserowitz, G. S.; Lebrilla, C. B., Profiling of Glycans in Serum for the Discovery of Potential Biomarkers for Ovarian Cancer. *J. Proteome Res.* **2006,** *5* (7), 1626-1635.
11. Kyselova, Z.; Mechref, Y.; Al Bataineh, M. M.; Dobrolecki, L. E.; Hickey, R. J.; Vinson, J.; Sweeney, C. J.; Novotny, M. V., Alterations in the Serum Glycome Due to Metastatic Prostate Cancer. *J. Proteome Res.* **2007,** *6* (5), 1822-1832.
12. Kyselova, Z.; Mechref, Y.; Kang, P.; Goetz, J. A.; Dobrolecki, L. E.; Sledge, G. W.; Schnaper, L.; Hickey, R. J.; Malkas, L. H.; Novotny, M. V., Breast Cancer Diagnosis and Prognosis through Quantitative Measurements of Serum Glycan Profiles. *Clin. Chem.* **2008,** *54* (7), 1166-1175.
13. El Rassi, Z., *Carbohydrate Analysis: High Performance Liquid Chromatography and Capillary Electrophoresis*. Elsevier Science B.V.: Amsterdam, 1995.
14. Liu, J. P.; Shirota, O.; Wiesler, D.; Novotny, M., Ultrasensitive Fluorometric Detection of Carbohydrates as Derivatives in Mixtures Separated by Capillary Electrophoresis. *Proc. Natl. Acad. Sci. U. S. A.* **1991,** *88* (6), 2302-2306.
15. Nashabeh, W.; El Rassi, Z., Capillary Zone Electrophoresis of Linear and Branched Oligosaccharides. *J. Chromatogr. A* **1992,** *600* (2), 279-287.
16. Kakehi, K.; Susami, A.; Taga, A.; Suzuki, S.; Honda, S., High-Performance Capillary Electrophoresis of O-Glycosidically Linked Sialic Acid-Containing Oligosaccharides in Glycoproteins as Their Alditol Derivatives with Low-Wavelength Uv Monitoring. *J. Chromatogr. A* **1994,** *680* (1), 209-215.
17. Hutterer, K. M.; Birrell, H.; Camilleri, P.; Jorgenson, J. W., High Resolution of Oligosaccharide Mixtures by Ultrahigh Voltage Micellar Electrokinetic Capillary Chromatography. *J. Chromatogr. B* **2000,** *745* (2), 365-372.
18. Palm, A.; Novotny, M. V., Macroporous Polyacrylamide Poly(Ethylene Glycol) Matrixes as Stationary Phases in Capillary Electrochromatography. *Anal. Chem.* **1997,** *69* (22), 4499-4507.
19. Yang, C. M.; El Rassi, Z., Capillary Electrochromatography of Derivatized Mono- and Oligosaccharides. *Electrophoresis* **1998,** *19* (12), 2061-2067.

20. Suzuki, S.; Yamamoto, M.; Kuwahara, Y.; Makiura, K.; Honda, S., Separation of 1-Phenyl-3-Methyl-5-Pyrazolone Derivatives of Monosaccharides by Capillary Electrochromatography. *Electrophoresis* **1998,** *19* (15), 2682-2688.
21. Que, A. H.; Mechref, Y.; Huang, Y. P.; Taraszka, J. A.; Clemmer, D. E.; Novotny, M. V., Coupling Capillary Electrochromatography with Electrospray Fourier Transform Mass Spectrometry for Characterizing Complex Oligosaccharide Pools. *Anal. Chem.* **2003,** *75* (7), 1684-1690.
22. Tegeler, T. J.; Mechref, Y.; Boraas, K.; Reilly, J. P.; Novotny, M. V., Microdeposition Device Interfacing Capillary Electrochromatography and Microcolumn Liquid Chromatography with Matrix-Assisted Laser Desorption/Ionization Mass Spectrometry. *Anal. Chem.* **2004,** *76* (22), 6698-6706.
23. Mechref, Y.; Novotny, M. V., Glycomic Analysis by Capillary Electrophoresis-Mass Spectrometry. *Mass Spectrom. Rev.* **2009,** *28* (2), 207-222.
24. Dang, F. Q.; Zhang, L. H.; Jabasini, M.; Kaji, N.; Baba, Y., Characterization of Electrophoretic Behavior of Sugar Isomers by Microchip Electrophoresis Coupled with Videomicroscopy. *Anal. Chem.* **2003,** *75* (10), 2433-2439.
25. Callewaert, N.; Contreras, R.; Mitnik-Gankin, L.; Carey, L.; Matsudaira, P.; Ehrlich, D., Total Serum Protein N-Glycome Profiling on a Capillary Electrophoresis-Microfluidics Platform. *Electrophoresis* **2004,** *25* (18-19), 3128-3131.
26. Dang, F. Q.; Kakehi, K.; Nakajima, K.; Shinohara, Y.; Ishikawa, M.; Kaji, N.; Tokeshi, M.; Baba, Y., Rapid Analysis of Oligosaccharides Derived from Glycoproteins by Microchip Electrophoresis. *J. Chromatogr. A* **2006,** *1109* (2), 138-143.
27. Culbertson, C. T.; Jacobson, S. C.; Ramsey, J. M., Microchip Devices for High Efficiency Separations. *Anal. Chem.* **2000,** *72* (23), 5814-5819.
28. Zhuang, Z.; Starkey, J. A.; Mechref, Y.; Novotny, M. V.; Jacobson, S. C., Electrophoretic Analysis of N-Glycans on Microfluidic Devices. *Anal. Chem.* **2007,** *79* (18), 7170-7175.
29. Paegel, B. M.; Emrich, C. A.; Weyemayer, G. J.; Scherer, J. R.; Mathies, R. A., High Throughput DNA Sequencing with a Microfabricated 96-Lane Capillary Array Electrophoresis Bioprocessor. *Proc. Natl. Acad. Sci. U. S. A.* **2002,** *99* (2), 574-579.
30. Griffiths, S. K.; Nilson, R. H., Low-Dispersion Turns and Junctions for Microchannel Systems. *Anal. Chem.* **2001,** *73*, 272-278.
31. Molho, J. I.; Herr, A. E.; Mosier, B. P.; Santiago, J. G.; Kenny, T. W.; Brennen, R. A.; Gordon, G. B.; Mohammadi, B., Optimization of Turn Geometries for Microchip Electrophoresis. *Anal. Chem.* **2001,** *73*, 1350-1360.
32. Emrich, C. A.; Tian, H. J.; Medintz, I. L.; Mathies, R. A., Microfabricated 384-Lane Capillary Array Electrophoresis Bioanalyzer for Ultrahigh-Throughput Genetic Analysis. *Anal. Chem.* **2002,** *74* (19), 5076-5083.
33. Zhuang, Z.; Jacobson, S. C., Serial-to-Parallel Interfaces for Efficient Sample Transfer on Microfluidic Devices. *Anal. Chem.* **2009,** *81* (4), 1477-1481.
34. Guttman, A.; Pritchett, T., Capillary Gel-Electrophoresis Separation of High-Mannose Type Oligosaccharides Derivatized by 1-Aminopyrene-3,6,8-Trisulfonic Acid. *Electrophoresis* **1995,** *16* (10), 1906-1911.

35. Jacobson, S. C.; Hergenröder, R.; Koutny, L. B.; Warmack, R. J.; Ramsey, J. M., Effects of Injection Schemes and Column Geometry on the Performance of Microchip Electrophoresis Devices. *Anal. Chem.* **1994,** *66* (7), 1107-1113.
36. Jacobson, S. C.; Culbertson, C. T., Microfluidics: Some Basics. In *Separation Methods in Microanalytical Systems*, Kutter, J. P.; Fintschenko, Y., Eds. CRC Press: Boca Raton, FL, 2006.
37. Monnig, C. A.; Jorgenson, J. W., On-Column Sample Gating for High-Speed Capillary Zone Electrophoresis. *Anal. Chem.* **1991,** *63* (8), 802-807.
38. Fan, Z. H.; Harrison, D. J., Micromachining of Capillary Electrophoresis Injectors and Separators on Glass Chips and Evaluation of Flow at Capillary Intersections. *Anal. Chem.* **1994,** *66* (1), 177-84.
39. Liu, J. P.; Dolnik, V.; Hsieh, Y. Z.; Novotny, M., Experimental Evaluation of the Separation Efficiency in Capillary Electrophoresis Using Open Tubular and Gel-Filled Columns. *Anal. Chem.* **1992,** *64* (13), 1328-1336.

Chapter 5. Serial-to-Parallel Interfaces for Efficient Sample Transfer on Microfluidic Devices[1]

5.1. Introduction to Multidimensional Separations on Microfluidic Devices

Multidimensional separations using conventional[2] and microfluidic[3] platforms are of considerable interest because they offer increased peak capacity and information content. With microfluidic separations, the two most common formats for combining separation techniques are serial and planar coupling. Serial coupling is the simpler approach because it takes advantage of the precise and rapid fluid handling that microfluidics offers. Micellar electrokinetic chromatography (MEKC) and capillary electrophoresis (CE),[4-5] open channel electrochromatography and CE,[6] isoelectric focusing and CE,[7-8] isotachophoresis and CE,[9] and capillary gel electrophoresis and MEKC[10] have been successfully integrated on microfluidic devices, and to date, these serially coupled techniques have produced the highest peak capacities. However, serial coupling suffers from the second dimension (2D) separation having to be operated approximately 10 times faster than the first dimension (1D) separation in order to properly sample the 1D effluent. Often, this limitation results in the 1D separation being run below its optimum velocity, resulting in poorer overall performance. For systems where the 1D separation operates continuously, a second drawback is that only a small fraction (1-10%) of the sample is typically transferred from the 1D to 2D separation,[5-6] leading to a loss of information and sensitivity.

An alternative approach uses a planar format that mimics traditional two-dimensional electrophoretic separations.[11] In the planar format, the 1D separation propagates along one axis of the separation space, and the 2D separation is run

orthogonal to the 1D separation, usually in an array of parallel channels. Advantages of the planar format include independent time frames for the two separation techniques, i.e., the separations do not have to be correlated as with the serially coupled separations, and preservation of nearly all the information generated during the 1D separation. Several planar systems have been designed and tested,[12-16] but so far, the performance of these systems has lagged behind serially coupled microfluidic systems.

By developing a serial-to-parallel interface, we combine the fluid handling capabilities of microfluidic devices as seen in the serially coupled separations with the array format for the 2D separation on the planar devices. The serial-to-parallel interface directs the sample from a single channel to one of several parallel channels by controlling potentials applied to two routing channels. As depicted in **Figure 5-1**, we designed and tested a serial-to-parallel interface (basic interface), an interface with a tee valve (tee interface), and an interface with a gated valve (gated interface). As discussed below, the tee valve[17] and gated valve[18] were added to the basic interface to enhance injection performance. With these devices, injection frequencies up to 10 Hz and injection times from 20 to 300 ms were evaluated. The results show both the injection amount (peak area) and injection length (peak width) are linearly proportional to the injection time. These interfaces may have application not only in multidimensional separations, but also for continuous monitoring scenarios, e.g., cell secretions over time,[19-20] where high throughput analysis is sought. In both cases, the serial-to-parallel interface allows rapid transfer of sample from a single sample channel to multiple parallel analysis channels.

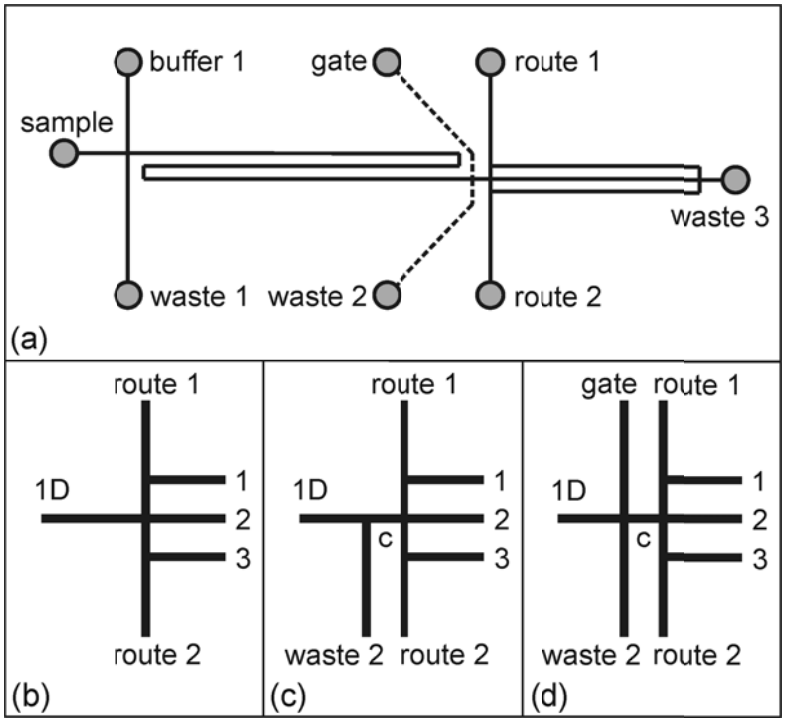

Figure 5-1. (a) Schematic of the microfluidic devices with serial-to-parallel interfaces. Enlarged view of the (b) basic interface, (c) interface with a tee valve (tee interface), and (d) interface with a gated valve (gated interface). In part a, the dashed lines show where the waste 2 and gate channels are for the tee and gated interface designs. In parts b-d, the parallel channels are labeled 1, 2, and 3, and in parts c and d, the connect channel is labeled *c*.

5.2. Experimental Section

Materials. We purchased ammonium hydroxide (30%), hydrogen peroxide (30%), 4-(2-hydroxyethyl)-1-piperazineethanesulfonic acid (HEPES), methanol, sodium tetraborate, and rhodamine B from Sigma-Aldrich Co.; sodium hydroxide from Thermo Fisher Scientific, Inc.; Microposit MF 319 developer from Rohm and Haas Electronic Materials; Chromium Etchant 1020 and Buffered Oxide Etchant from Transene Co., Inc.; and B270 glass substrates and cover plates from Telic Co.

Microfluidic Device Fabrication. Figure 5-1 shows schematics of the three serial-to-parallel interfaces, which were fabricated as previously reported.[21] The device substrates were B270 white crown glass covered with a thin chromium film (120 nm), an anti-reflective coating, and a positive tone photoresist (list photoresist here). The channel designs were transferred onto the glass substrate with a UV exposure of 200 mJ/cm^2 (Optical Associates, Inc.) through a photomask (HTA Photomask). The photoresist was developed, and the exposed patterns were etched into the chromium film. Microchannels were etched into the glass substrate using a stirred buffered oxide etchant. Depending on the etching time, the microchannels were 10-15 μm deep and 30-50 μm wide at the top, as measured with a stylus profiler (Dektak 6M, Veeco Instruments Inc.). Access holes were sandblasted at the ends of the channels (AECR Eraser, Paasche Airbrush Co.). The drilled substrates were bonded to cover plates by hydrolyzing both in a solution of NH_4OH, H_2O_2, and H_2O (2:1:2), rinsing with water, bringing them into contact with each other, and annealing at 550° C for 10 h. Short segments of glass tubing (6 mm o.d. x 4 mm i.d. x 6 mm tall) were epoxied to the drilled side of the bonded substrates for fluid reservoirs.

After thermal annealing, the channels were cleaned with a 1 M sodium hydroxide solution with vacuum applied at each reservoir for 5 min and rinsed with water to remove the sodium hydroxide. These cleaning procedures were repeated after each experiment. After cleaning, the channels were filled with buffer (1 mM sodium tetraborate and 20 mM HEPES, pH 6.2). Channel conductivities were measured by applying 10 V (6487 Keithley Instruments, Inc.) between each pair of reservoirs and measuring the current with a picoammeter (6485, Keithley Instruments, Inc.). The channel lengths were measured with linear scales (2-LMH and Microcode II, Boeckeler Instruments, Inc.) mounted on the stage of an inverted microscope (TE2000-U, Nikon, Inc.). The channel lengths, resistances, applied potentials, and electric field strengths for a typical device with a gated interface are shown in **Table 5-1**. After channel characterization, the buffer in the sample reservoir was replaced with a 10 μM solution of rhodamine B for fluorescence imaging.

Interface Characterization. As shown in **Figure 5-1**, the basic interface has two route channels to direct sample into the parallel channels, the tee interface adds the waste 2 channel to inject sample into the parallel channels, and the gated interface adds the waste 2 and gate channels to inject sample into the parallel channels. Temporal profiles of the potentials applied to each reservoir are shown in **Figure 5-2** for a 1 Hz injection frequency and 100 ms injection time. To continuously deliver sample to the interface, the potentials at the sample, buffer 1, waste 1, and waste 3 reservoirs were 1, 0.9, 0.9, and 0 kV, respectively. For the basic interface, potentials were applied only to the route 1 and 2 reservoirs, but potentials were also applied to the waste 2 reservoir for the tee interface and to the waste 2 and gate reservoirs for the gated interface. As seen in **Figure 5-2**, the

Table 5-1. Channel lengths (L), resistances (R), applied potentials (V), and electric field strengths[1] (E) for the sample loading and injection modes.[2]

			Sample Loading		Injection	
Channel	L (mm)	R (MΩ)	V (kV)	E (V/cm)	V (kV)	E (V/cm)
sample	6.8	46	1.0	148	1.0	148
buffer 1	12.9	86	0.90	10	0.90	10
waste 1	17.1	88	0.90	10	0.90	10
1D	73.1	297	–	168	–	169
gate	12.4	83	0.70	540	0.52	80
waste 2	12.2	83	0.30	479	0.48	22
route 1	8.8	53	0.95	416	0.95	417
route 2	9.0	54	0.95	416	0.95	417
parallel 1	11.1	66	–	353	–	352
parallel 2	11.0	66	–	357	–	356
parallel 3	11.1	66	–	352	–	352
waste 3	11.5	67	0.0	1062	0.0	1060
connect	0.1		–	230	–	227

[1] The electric field strengths are positive when following the arrow directions in **Figure 5-5**.

[2] The applied potentials and calculated electric field strengths are for injections into parallel channel 2.

potentials at the gate and waste 2 reservoirs were switched at the same time as the potentials at the route 1 and 2 reservoirs. In addition, note that the potentials shown in **Figure 5-2** are nominal values and varied slightly depending on the actual channel resistances of each microchip.

The potentials were applied to the microfluidic device using a power supply with four independent high voltage outputs. The power supply consisted of a single 10 kV voltage source (10A12-P4-M-C, UltraVolt, Inc.) and four pairs of optical resistors (OC100, Voltage Multipliers, Inc.). The optical resistors were used as voltage dividers to regulate the potentials applied to the reservoirs. The 10 kV voltage source and optical resistors were controlled through LabView software and an analog output board (PCI-6713, National Instruments Corp.).

To monitor the injections, we used an inverted optical microscope (TE-2000U, Nikon, Inc.) equipped with 4x and 10x objectives and an HQ TRITC filter cube (Chroma Technology Corp.). A metal halide lamp (X-Cite 120, EXFO, Inc.) was used for exciting fluorescence, the fluorescence signal was recorded with a CCD camera (Cascade 512B, Photometrics), and images were captured and processed using MetaMorph software (Molecular Devices). Measurements at a single point were made 300 μm downstream from the interface in the parallel channels, using the same microscope. The fluorescence signal was spatially filtered with a 600 μm pinhole, detected with a photomultiplier tube (H5783-01, Hamamatsu Corp.), amplified by a low-noise current preamplifier (SR570, Stanford Research Systems, Inc.), and recorded using a multifunction data acquisition board (PCI-6032E, National Instruments Corp.) and software written with LabView. The sampling frequency was 1000 Hz.

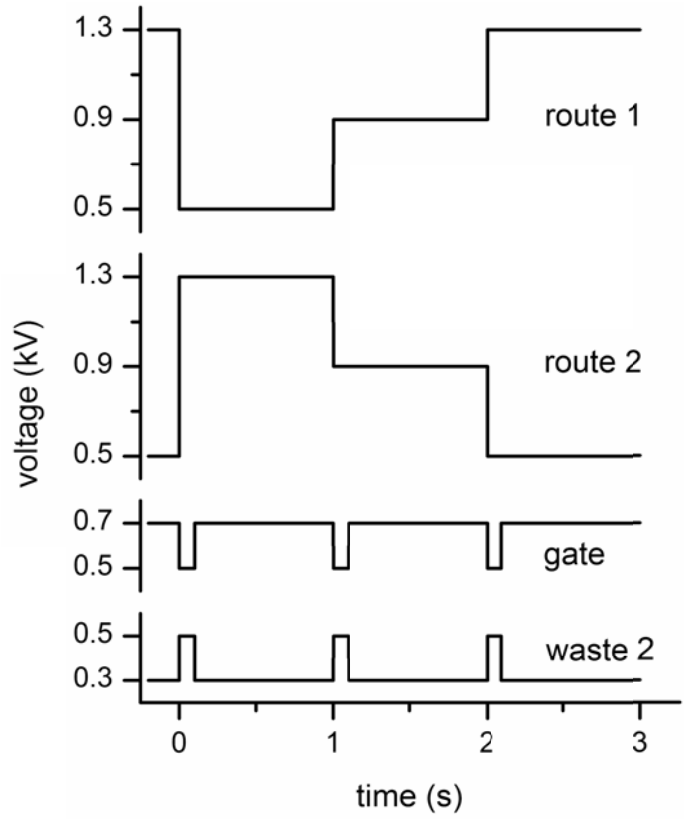

Figure 5-2. Variation of the applied potentials with time for operation of the serial-to-parallel interfaces. The injection frequency is 1 Hz, and the injection times are 1 s for the basic interface and 100 ms for the tee and gated interfaces. Route 1 and route 2 potentials are needed for the basic interface; route 1, route 2, and waste 2 potentials for the tee interface; and route 1, route 2, waste 2, and gate potentials for the gated interface.

Injection frequencies of 1, 2, 5, and 10 Hz and injection times of 20, 50, 100, 200, and 300 ms were evaluated. All data were analyzed using the peak fitting module in OriginPro 7.5 software (OriginLab Corp.). The peak widths were measured using the full width at half maximum of the peak profile, and the peak areas were obtained by integration.

5.3. Results and Discussion

The basic concept behind these interfaces is to connect a single channel (1D) to an array of parallel channels with two routing channels to direct the sample through the interface. To evaluate this concept, we designed the basic interface, tee interface, and gated interface (**Figure 5-1**). The gate and waste 2 channels in the tee and gated interfaces were added to facilitate injections into all three parallel channels as discussed below. The parallel channels are referred to as channels 1, 2, and 3 as shown in **Figure 5-1b,c,d**. In all three designs, the route channels operate similarly. When the potentials at the route 1 and 2 reservoirs are low and high, respectively, the sample is directed into channel 1. When the potentials at the route 1 and 2 reservoirs are the same, the sample is directed into channel 2, and when the potentials at the route 1 and 2 reservoirs are high and low, respectively, the sample is directed into channel 3. While operating the interface, the potential drop between the interface and waste 3 reservoir was kept constant to maintain uniform electric field strengths and flows in parallel channels 1, 2, and 3 (see **Table 5-1**). The parallel channels rejoin near the waste 3 reservoir, which was held at ground for all experiments.

Figure 5-3 shows the operation of the basic interface, which injected sample into channels 1 and 3 and used channel 2 as a common or waste channel. In this mode of operation, the sample continuously flows into channel 2 and is switched to channel 1 (**Figure 5-3c**) and channel 3 (**Figure 5-3e**) by adjusting the potentials at the route 1 and 2 reservoirs. After each injection, sample flow is returned to channel 2, and the injected plug travels down channel 1 (**Figure 5-3d**) or channel 3 (**Figure 5-3f**). Unfortunately, the basic interface is limited to this mode of operation where the channel sequence is 2, 1, 2, 3, 2, 1, 2,... with the sample returning to channel 2 after each injection. If the potentials at the route 1 and 2 reservoirs are configured to send sample down parallel channels with the sequence 1, 2, 3, 1, 2, 3,..., the sample leaks into channel 2 when passing from channel 3 to 1. To overcome this limitation, we designed the tee and gated interfaces.

Operation of the tee interface is shown in **Figure 5-4**. In this design, the waste 2 channel is added to provide a means to inject sample into the interface. During sample loading, the sample is fed from the 1D channel into the waste 2 channel (**Figure 5-4b**). To inject sample, the potential at the waste 2 reservoir is raised to allow sample to pass into the parallel channels, and the potentials at the route 1 and 2 reservoirs are set to direct the sample down channel 1, 2, or 3 (**Figure 5-2**). **Figure 5-4c,d** shows the sample routed into channel 1, **Figure 5-4e,f** into channel 2, and **Figure 5-4g,h** into channel 3. Taking the relative field strengths in the connect and waste 2 channels, we estimate that 75% of the sample was transferred from the 1D channel to the parallel channels and 25% continued into the waste 2 channel during the injection. The fraction of sample injected can easily be varied by raising or lowering the potential applied to the waste 2 reservoir. Although the tee interface permits all three parallel channels to receive discrete injections,

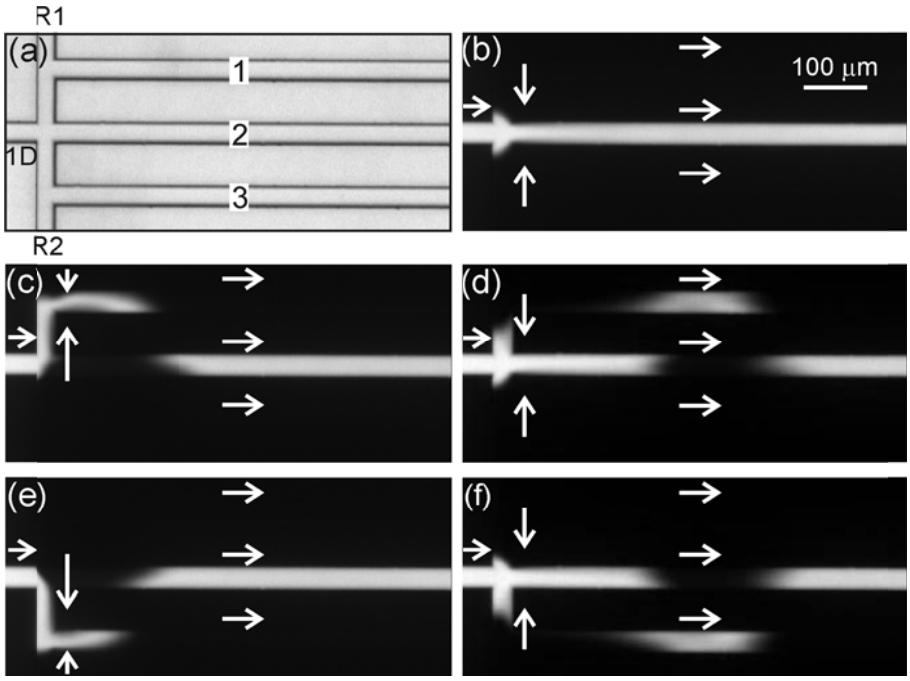

Figure 5-3. (a) Transmitted light image of the serial-to-parallel interface (basic design). Fluorescence images of (b) sample loading and injections into (c,d) channel 1 and (e,f) channel 3. In part a, the channels are labeled first dimension (1D), route 1 (R1), route 2 (R2), and parallel (1, 2, and 3). The injection time was 100 ms, and the arrows depict the flow directions.

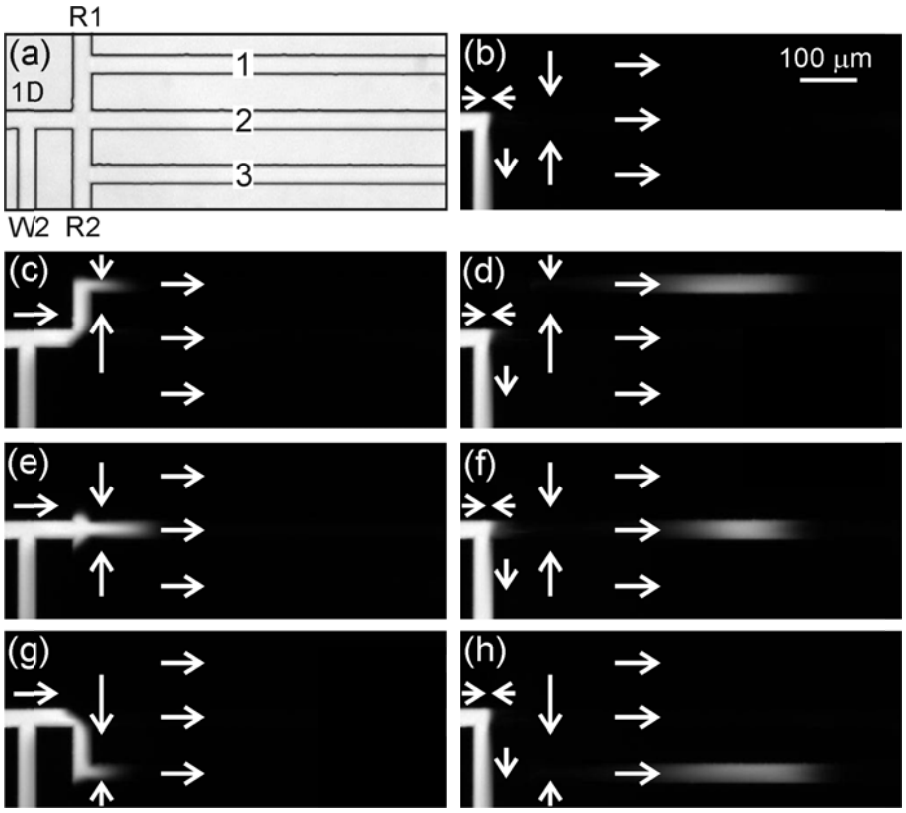

Figure 5-4. (a) Transmitted light image of the serial-to-parallel interface with a tee valve (tee interface). Fluorescence images of (b) sample loading and injections into (c,d) channel 1, (e,f) channel 2, and (g,h) channel 3. In part a, the channels are labeled first dimension (1D), route 1 (R1), route 2 (R2), waste 2 (W2), and parallel (1, 2, and 3). The injection time was 100 ms, and the arrows depict the flow directions.

operation requires careful balancing of the potentials applied to the route 1, route 2, and waste 2 reservoirs in order to inject equal amounts of sample into each of the parallel channels. To make the sample injection independent of the route 1 and 2 potentials, we designed the gated interface.

Figure 5-5 shows the operation of the gated interface. In addition to the waste 2 channel used in the tee interface, the gated interface has the gate channel added to effect a gated injection[18] prior to sample routing. During sample loading (**Figure 5-5b**), the sample flow is fed into the waste 2 channel with buffer flow from the gate channel, which prevents sample leaking into the interface. To dispense sample into the parallel channels, the potentials at the gate and waste 2 reservoirs are lowered and raised, respectively (**Figure 5-2**). The potentials at the route 1 and 2 reservoirs are set to direct sample into channel 1 (**Figure 5-5c,d**), channel 2 (**Figure 5-5e,f**), and channel 3 (**Figure 5-5g,h**). Videos of the gated interface dispensing 100 ms injections at 1 Hz and 50 ms injections at 10 Hz were taken and are available on the *Analytical Chemistry* website (see below). As seen in **Table 5-1**, tuning the potentials applied to the reservoirs minimizes the differences in field strengths in the 1D, connect, and parallel channels when switching between the sample loading and injection modes. This reduces the degree to which previously injected sample plugs are disturbed when subsequent injections are made into the same or adjacent channels. Interface performance was similar to the tee interface; however, uniform dispensing of the sample into channels 1, 2, and 3 was not dependent on the relative potentials applied to the route 1, route 2, and waste 2 reservoirs.

With all three interfaces, we were able to achieve injection frequencies of 1, 2, 5, and 10 Hz. **Figure 5-6** shows fifteen injections (five into each parallel channel) with an

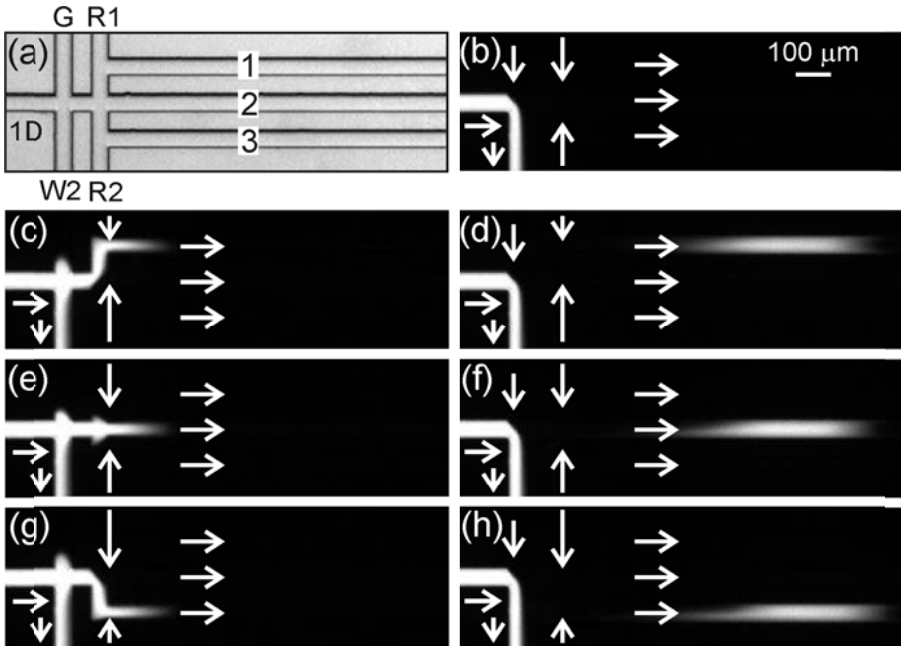

Figure 5-5. (a) Transmitted light image of the serial-to-parallel interface with a gated valve (gated interface). Fluorescence images of (b) sample loading and injections into (c,d) channel 1, (e,f) channel 2, and (g,h) channel 3. In part a, the channels are labeled first dimension (1D), route 1 (R1), route 2 (R2), waste 2 (W2), gate (G), and parallel (1, 2, and 3). The injection time was 100 ms, and the arrows depict the flow directions.

injection frequency of 10 Hz and an injection time of 20 ms, demonstrating that the gated interface can deliver high quality injections at 10 Hz into all three parallel channels. The real-time switching capability of the gated interface can be seen in the video of the 50 ms, 10 Hz injections, and faster frequencies are possible with higher applied potentials or shorter connecting channels in the interfaces. The video also demonstrates the ability to pass 50% of the sample from a single channel to the parallel channels, compared to 3% and 9% in prior work.[5-6] Assuming a sampling frequency of 1 injection per standard deviation (σ) for the peaks eluting from the 1D separation,[22] operating the interface at 10 Hz would allow the 1D peaks to be as narrow as 0.4 s wide while maintaining appropriate sampling. Because the interface is controlled electrically, changes in the mobile phase composition, especially under gradient conditions, can influence the amount sampled from the 1D channel into the parallel channels. The conductivity and electroosmotic mobility in the 1D and waste 2 channels may change with mobile phase composition; however, the amount injected can be calibrated prior to the analysis or with internal standards at different points along the 1D separation.

To further evaluate interface performance, we have investigated injections into the parallel channels with injection times of 20, 50, 100, 200, and 300 ms. The peak widths and peak areas were determined, and **Figure 5-7** shows the variation of the peak widths and areas with injection time for the gated interface. Each data point is an average of 10 consecutive injections into channel 1, 2, or 3, totaling 30 injections for each injection time. Combining the data from all three channels, $R^2 = 0.999$ for the variation of the peak width and area with time, and the relative standard deviations (RSDs) are 2.0% and 0.5% for the peak width (injection plug length) and peak area (injection volume), respectively.

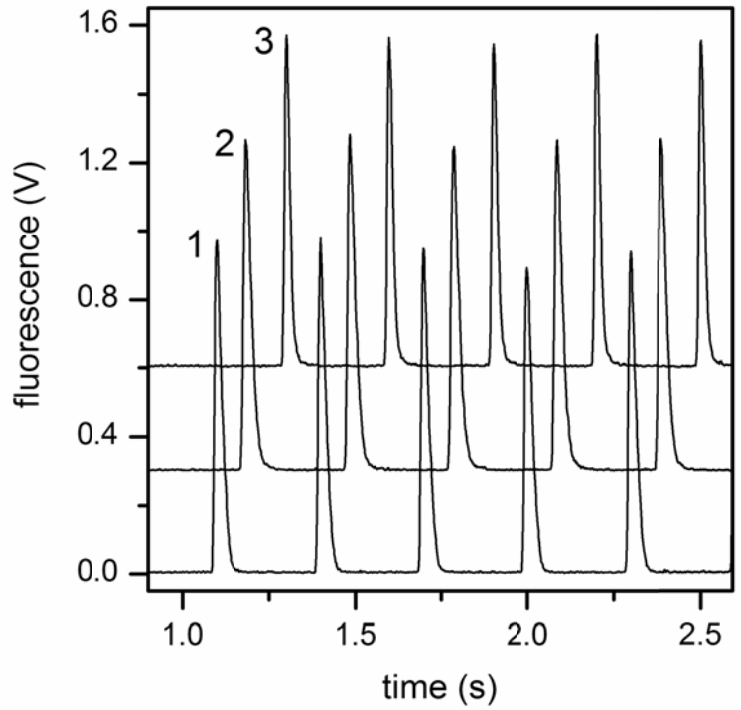

Figure 5-6. Fifteen 20 ms, 10 Hz injections into the three parallel channels of the gated interface. The profiles for channels 2 and 3 are offset for clarity.

The quality of the combined data for the tee interface is similar with $R^2 = 0.998$ and RSD = 1.9%for the peak width and $R^2 = 0.999$ and RSD = 0.4% for the peak area. To determine how much the peak broadens while passing through the interface, we can compare the expected peak widths (the injection times) with the measured peak widths in **Figure 5-7** by multiplying the injection time by the ratio of the field strengths in the connect channel and parallel channels (0.64 from the field strengths listed in **Table 5-1**). Consequently, the peak widths increased an average of 18% from the expected peak width (the injection time) to what was measured in the three parallel channels.

5.4. Conclusion

We have demonstrated the operation of three interfaces that use routing channels to direct the sample into the parallel channels. Overall, operation of the gated interface is most convenient because the gated valve operated independently from the routing function and all three parallel channels could receive sample injections. For example, to allow proper sampling of the 1D MEKC separation in the MEKC/CE system,[5] the 1D separation field strength was only 200 V/cm, well below the optimum. Operating these same separations with the tee or gated interface would allow the 1D MEKC separation to be conducted three times faster at 600 V/cm, improving overall separation performance. With the gated interface, we have used up to four parallel channels and believe eight to ten parallel channels could be incorporated with minimal design change, permitting 1D separations to be operated eight to ten times faster or 2D separations to have eight to ten times longer analysis times. One approach to designing an interface with more parallel channels would be to minimize the distance between parallel channels, which is currently

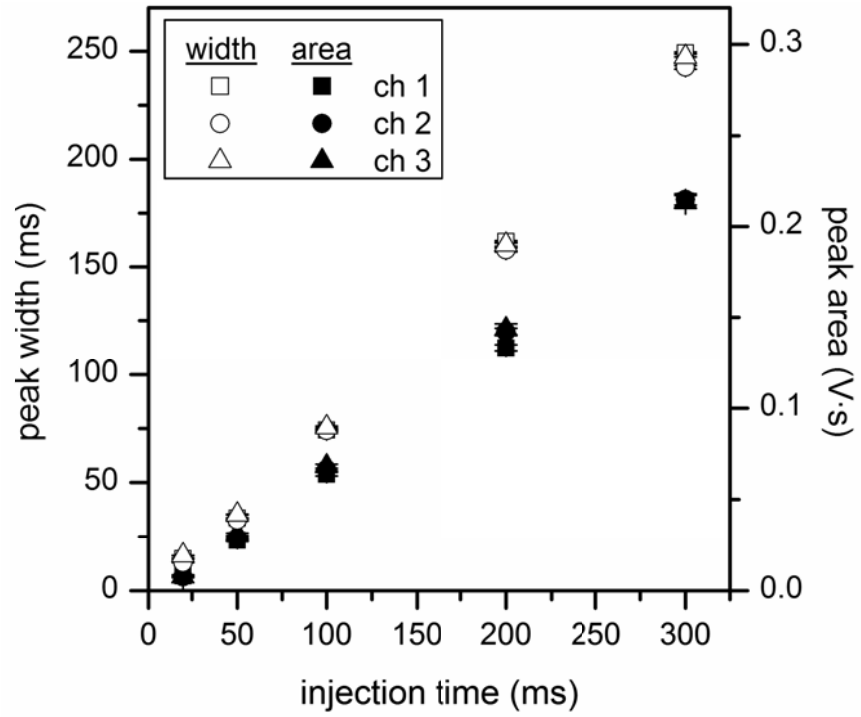

Figure 5-7. Variation of the peak width (open symbols) and peak area (solid symbols) with injection time for the gated interface. Peak widths are full widths at half maximum (FWHM), and error bars are ± σ for n = 10.

100 μm, and to interface with more parallel channels would be to minimize the distance between parallel channels, which is currently 100 μm, and to connect the parallel channels to the interface in a radial pattern, rather than perpendicularly as in **Figure 5-1**. The number of channels emanating from the interface is limited by the ability of the route channels to effectively deliver the sample into one of the parallel channels without sample leaking into an adjacent parallel channel. Overall, the gated interface adds some complexity to device operation, but the enhanced performance outweighs implementing additional control. N-glycans derived from model glycoproteins such as ribonuclease B, asialofetuin, and α_1-acid glycoprotein and derived from blood sera of cancer patients were previously analyzed on the spiral and serpentine microchannels with one dimensional microchip electrophoresis. The serial-to-parallel interfaces can be used for two-dimensional separation of the above N-glycans for better peak capacities.

Supporting Information Available. Videos of the gated interface dispensing 100 ms injections at 1 Hz (gated_interface_100ms_1Hz.avi) and 50 ms injections at 10 Hz (gated_interface_50ms_10Hz.avi). This material is available on the American Chemical Society website at http://pubs.acs.org/doi/suppl/10.1021/ac801774p.

5.5. References

1. This chapter reproduced in part with permission from Zhuang, Z., and Jacobson, S. C., Serial-to-Parallel Interfaces for Efficient Sample Transfer on Microfluidic Devices. *Anal. Chem.* **2009,** *81* (4), 1477-1481. Copyright 2009 American Chemical Society.
2. Cohen, S. A.; Schure, M. R., *Multidimensional Liquid Chromatography*. John Wiley & Sons: 2008.
3. Freire, S. L. S.; Wheeler, A. R., Proteome-on-a-Chip: Mirage, or on the Horizon? *Lab Chip* **2006,** *6* (11), 1415-1423.

4. Rocklin, R. D.; Ramsey, R. S.; Ramsey, J. M., A Microfabricated Fluidic Device for Performing Two-Dimensional Liquid-Phase Separations. *Anal. Chem.* **2000,** *72*, 5244-5249.
5. Ramsey, J. D.; Jacobson, S. C.; Culbertson, C. T.; Ramsey, J. M., High-Efficiency, Two-Dimensional Separations of Protein Digests on Microfluidic Devices. *Anal. Chem.* **2003,** *75*, 3758-3764.
6. Gottschlich, N.; Jacobson, S. C.; Culbertson, C. T.; Ramsey, J. M., Two-Dimensional Electrochromatography/Capillary Electrophoresis on a Microchip. *Anal. Chem.* **2001,** *73*, 2669-2674.
7. Herr, A. E.; Molho, J. I.; Drouvalakis, K. A.; Mikkelsen, J. C.; Utz, P. J.; Santiago, J. G.; Kenny, T. W., On-Chip Coupling of Isoelectric Focusing and Free Solution Electrophoresis for Multidimensional Separations. *Anal. Chem.* **2003,** *75* (5), 1180-1187.
8. Wang, Y. C.; Choi, M. N.; Han, J. Y., Two-Dimensional Protein Separation with Advanced Sample and Buffer Isolation Using Microfluidic Valves. *Anal. Chem.* **2004,** *76* (15), 4426-4431.
9. Kaniansky, D.; Masar, M.; Dankova, M.; Bodor, R.; Rakocyova, R., Column Switching in Zone Electrophoresis on a Chip. *J. Chromatogr. A* **2004,** *1051* (1-2), 33-42.
10. Shadpour, H.; Soper, S. A., Two-Dimensional Electrophoretic Separation of Proteins Using Poly(Methyl Methacrylate) Microchips. *Anal. Chem.* **2006,** *78* (11), 3519-3527.
11. O'Farrell, P. H., High-Resolution Two-Dimensional Electrophoresis of Proteins. *J. Biol. Chem.* **1975,** *250*, 4007-4021.
12. Tsai, S.-W.; Loughran, M.; Karube, I., Development of a Microchip for 2-Dimensional Capillary Electrophoresis. *J. Micromech. Microeng.* **2004,** *14* (12), 1693-1699.
13. Buch, J. S.; Rosenberger, F.; Highsmith, W. E.; Kimball, C.; DeVoe, D. L.; Lee, C. S., Denaturing Gradient-Based Two-Dimensional Gene Mutation Scanning in a Polymer Microfluidic Network. *Lab Chip* **2005,** *5* (4), 392-400.
14. Li, Y.; Buch, J. S.; Rosenberger, F.; DeVoe, D. L.; Lee, C. S., Integration of Isoelectric Focusing with Parallel Sodium Dodecyl Sulfate Gel Electrophoresis for Multidimensional Protein Separations in a Plastic Microfludic Network. *Anal. Chem.* **2004,** *76* (3), 742-748.
15. Chen, X. X.; Wu, H. K.; Mao, C. D.; Whitesides, G. M., A Prototype Two-Dimensional Capillary Electrophoresis System Fabricated in Poly(Dimethylsiloxane). *Anal. Chem.* **2002,** *74* (8), 1772-1778.
16. Emrich, C. A.; Medintz, I. L.; Chu, W. K.; Mathies, R. A., Microfabricated Two-Dimensional Electrophoresis Device for Differential Protein Expression Profiling. *Anal. Chem.* **2007,** *79* (19), 7360-7366.
17. Harrison, D. J.; Manz, A.; Fan, Z. H.; Ludi, H.; Widmer, H. M., Capillary Electrophoresis and Sample Injection Systems Integrated on a Planar Glass Chip. *Anal. Chem.* **1992,** *64* (17), 1926-1932.
18. Jacobson, S. C.; Hergenröder, R.; Moore Jr., A. W.; Ramsey, J. M., Precolumn Reactions with Electrophoretic Analysis Integrated on a Microchip. *Anal. Chem.* **1994,** *66* (23), 4127-4132.

19. Dishinger, J. F.; Kennedy, R. T., Serial Immunoassays in Parallel on a Microfluidic Chip for Monitoring Hormone Secretion from Living Cells. *Anal. Chem.* **2007,** *79* (3), 947-954.
20. Shackman, J. G.; Dahlgren, G. M.; Peters, J. L.; Kennedy, R. T., Perfusion and Chemical Monitoring of Living Cells on a Microfluidic Chip. *Lab Chip* **2005,** *5* (1), 56-63.
21. Zhuang, Z.; Starkey, J. A.; Mechref, Y.; Novotny, M. V.; Jacobson, S. C., Electrophoretic Analysis of N-Glycans on Microfluidic Devices. *Anal. Chem.* **2007,** *79* (18), 7170-7175.
22. Murphy, R. E.; Schure, M. R.; Foley, J. P., Effect of Sampling Rate on Resolution in Comprehensive Two-Dimensional Liquid Chromatography. *Anal. Chem.* **1998,** *70* (8), 1585-1594.

Chapter 6. Two-Dimensional Electrochromatography-Electrophoresis Microchip Separations of N-Glycans with a Serial-to-Parallel Interface

6.1. Introduction to Two Dimensional Separation of Glycans and Capillary Electrochromatography with Monolithic Stationary Phases

Previously, N-glycans derived from model glycoproteins and blood sera of cancer patients have been electrophoretically separated on microfluidic devices with spiral[1] and serpentine microchannels . The separation efficiencies of the glycan components ranged from 400,000 to 940,000, and the average peak capacity was 160-240. The electrophoretic profiles of the clinically derived glycans were very complex, and with higher separation efficiencies, the components can be better resolved. The length of the spiral and serpentine channels can be increased without substantially increasing the microchip footprint, but the analysis time will be increased with a longer separation length. An alternative approach to increase the separation performance is to incorporate two-dimensional (2D) separations. A few 2D separations of glycans have been developed.[2-5] The separation techniques used were reverse phase liquid chromatography (RPLC), hydrophilic interaction liquid chromatography (HILIC), and anion exchange chromatography. These separations were developed on conventional liquid chromatography and capillary platforms.

Microfluidic devices can integrate multiple functions on a single chip and precisely distribute fluids to designated locations. Precise fluid handling was demonstrated with serial-to-parallel interfaces developed for 2D biomolecular separations.[6] The interface incorporated two serially connected separation dimensions, where the first dimension was

a serpentine channel, and the second dimension was three parallel straight channels. The interface was best suited for a slower first dimension and a faster second dimension, because only a portion of the effluent from the first dimension was transferred to the second dimension. With that in mind, capillary electrochromatography (CEC) with monolithic stationary phases and capillary electrophoresis (CE) were evaluated as the first and second dimension separation techniques, respectively.

CEC combines the benefits of CE and liquid chromatography: the flat profile of the electroosmotic flow (EOF) reduces band broadening and various stationary phases can be incorporated for different analytes. In the 1990s, CEC became more popular, especially with monolithic stationary phases. The technique was applied to microscale biomolecular separations, e.g., peptides and proteins.[7-9] Glycans have also been separated by CEC with monolithic stationary phases, e.g., methacrylate[10] and acrylamide[11-13] monoliths. The separation mode was normal phase. This separation mode provided better separation efficiencies than reverse phase chromatography since glycans have multiple hydroxyl groups, which render the molecule more hydrophilic. Monolithic stationary phases have become attractive on capillary and microchip platforms because the *in situ* fabrication is fritless, the permeability is much higher compared to packed beds, the selectivity is controlled by the surface chemistry, and the permeability is varied by the pore diameter.[14] Especially in microfluidic devices, particle packing is extremely difficult, and monolithic phases can be formed by UV exposure, which conveniently enables fabrication at designated locations.

In this work, we investigated CEC with acrylamide monolithic phases and CE for 2D glycan analysis. APTS-labeled glycans were analyzed on monoliths with the

electroosmotic flow suppressed, and 2-AMAC labeled glycans were analyzed on monoliths with the electroosmotic flow enabled.

6.2. Experimental

Materials. Acetic acid, acrylamide, 2-acrylamido-2-methyl-1-propanesulfonic acid (AMPS), ammonium persulfate, 2-aminoacridone (2-AMAC), azobisisobutyronitrile (AIBN), citric acid, dextrin 10, dimethylsulfoxide (DMSO), 2-heptanol, dodecanol, 4-(2-hydroxyethyl)-1-piperazine-ethanesulfonic acid (HEPES), β-mercaptoethanol, γ-methacryloxypropyltrimethoxysilane (MAPTOS), methanol, 2-(methacryloyloxy)ethyl trimethyl ammonium methyl sulfate (MEAMS), N,N-methylenebisacrylamide, methylene dichloride, potassium phosphate diabasic, RNase B, sodium cyanoborohydride, and N,N,N',N'-tetramethylethylenediamine (TEMED) were purchased from Sigma-Aldrich. High-purity 8-amino-1,3,6-trisulfonic acid (APTS) was obtained from Beckman Coulter, Inc., and peptide-N-glycosidase F (PNGase F) of *Chryseobacterium menigosepticum* (EC 3.2.2.18) from Northstar BioProducts. Sodium hydroxide was purchased from Fisher Scientific, Microposit MF-319 developer from Rohm and Haas Electronic Materials, Chromium Etchant 1020 and buffered oxide etchant (BOE) from Transene Co., and B270 glass substrates and cover plates from Telic Company.

Microfluidic Device Fabrication. Microfluidic devices with the gated serial-to-parallel interfaces are shown in **Figure 6-1**. The 180° turns in the serpentine separation channels were asymmetrically tapered to minimize band dispersion. The microchips were fabricated by standard photolithography and wet chemical etching as previously described.[15] The device substrates were B270 white crown glass covered with a thin

chromium film (120 nm), an anti-reflective coating, and a positive tone photoresist. The channel designs were transferred onto the glass substrate with a UV exposure of 200 mJ/cm^2 (Optical Associates, Inc.) through a photomask (HTA Photomask). The photoresist was developed, and the exposed patterns were etched into the chromium film. Microchannels were etched into the glass substrate with a stirred buffered oxide etchant. Depending on the etching time, the microchannels were 10-15 μm deep and 40-100 μm wide at the top, as measured with a stylus profiler (Dektak 6M, Veeco Instruments Inc.). Access holes were sandblasted at the ends of the channels (AECR Eraser, Paasche Airbrush Co.). The drilled substrates were bonded to cover plates by hydrolyzing both in a solution of NH_4OH, H_2O_2, and H_2O (2:1:2), rinsing with water, bringing them into contact with each other, and annealing at 550° C for 10 h. A chip holder was manufactured to permit fluidic access to the reservoirs and apply pressure (4-6 bar) for monolith cleaning.

Channel Coating. The microchip was first coated with a silane to covalently link the monolith to the channel wall and to increase the mechanical stability of the monolith column. For some experiments, the microchannels were coated with linear polyacrylamide to minimize electroosmotic flow, according to a procedure modified slightly from Hjertén's method[16] and described in reference 1.

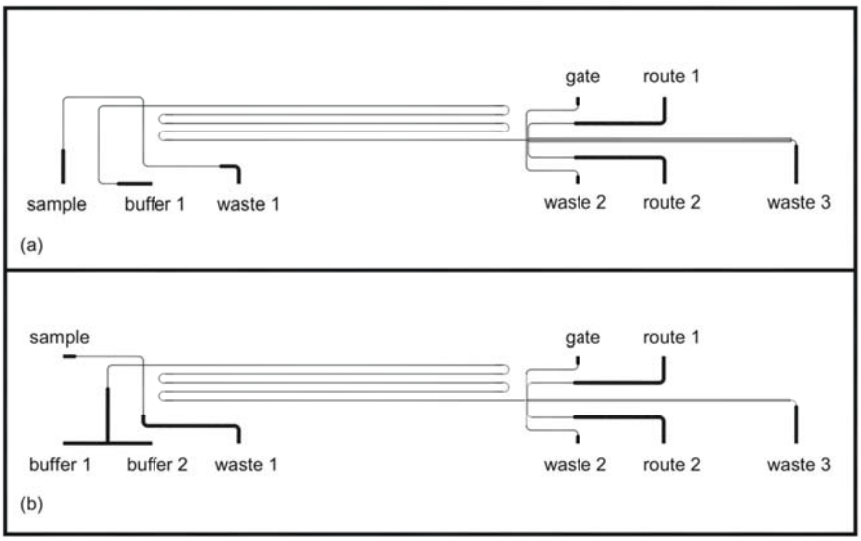

Figure 6-1. AutoCAD drawings of microfluidic devices with the gated serial-to-parallel interface for 2D glycan separations. (a) Basic design of the 2D microchip with a gated serial-to-parallel interface. (b) Temporal gradient elution was incorporated in the first dimension by adding buffer 2 reservoir. The turns in the 1D serpentine channels were asymmetrically tapered with a taper ratio of 3.

Monolith Fabrication. The monolithic column was prepared from a polymerization mixture typically containing 55 mg acrylamide, 35 mg methylenebisacrylamide, 10 mg AMPS, 1 mg AIBN, 550 μL DMSO, and 450 μL 2-heptanol. The mixture was sonicated for 5 min and purged with nitrogen for 5 min. The microchannels were filled with the polymerization mixture, and the microchannels were covered with electrical tape, except for the first dimension serpentine channel. The microchip was exposed to 1.2 J/cm^2 of UV light. The monolith was sequentially cleaned with DMSO, methanol, and water for 0.5 h each with 6 bar applied pressure.

Sample Preparation. A 1-μg aliquot of dextrin 10 was labeled with APTS by adding a 2-μL aliquot of 100 mM APTS solution prepared in 0.9 M citric acid and a 1-μL aliquot of 1 M sodium cyanoborohydride prepared in DMSO. The reaction was allowed to proceed for 2 h at 55 ºC. The derivatization mixture was dialyzed overnight at room temperature with a 1000-Da cut-off cellulose membrane to reduce the amount of unreacted APTS. Finally, the dialyzed mixture was dried and resuspended in 50 μL of running buffer prior to electrophoretic analysis.

A 1-μg aliquot of dextrin 10 was labeled with 2-AMAC by adding a 2-μL aliquot of 500 μM 2-AMAC solution prepared in 3:17 (v/v) mixture of glacial acetic acid and DMSO and a 1-μL aliquot of 1 M sodium cyanoborohydride prepared in DMSO. The reaction was allowed to proceed for 2 h at 75 ºC. The labeled sample was resuspended in 50 μL of running buffer, and the supernatant was obtained for electrophoretic analysis.

Microchip Operation and Detection. The separation buffer typically contained 10 mM phosphate (pH 6.8) and 60% (v/v) acetonitrile (ACN). A pinched or modified

pinched injection was used to dispense samples for the first dimension CEC separation. The high voltage outputs were controlled with a program written in LabView 8.0 (National Instruments Corp.) and an analog output board (PCI-6713, National Instruments Corp.).

To detect the first dimension CEC separation, an inverted optical microscope (TE-2000U, Nikon, Inc.) was configured for epifluorescence and equipped with 20x and 40x objectives and an HQ FITC filter cube (Chroma Technology Corp.). The 488-nm line of an argon ion laser (Melles Griot, Inc.) was attenuated to 0.5 mW with neutral density filters and focused to a point in the analysis channel 22 cm downstream from the cross intersection. The fluorescence signal was spatially filtered with a 600 μm pinhole, detected with a photomultiplier tube (H5783-01, Hamamatsu Corp.), amplified by a low-noise current preamplifier (SR570, Stanford Research Systems, Inc.), and recorded with a multifunction data acquisition board (PCI-6032E, National Instruments Corp.) and software written in LabView. The sampling frequency was 100 Hz. To detect the second dimension parallel channels simultaneously, a Powell lens (5° fan angle; StockerYale) was used to expand the 488-nm line of an argon ion laser (Melles Griot, Inc.) into a line. The fluorescence signal was detected with a CCD camera (Cascade 512B, Photometrics), and images were captured and processed using IPLab software (BD Biosciences Bioimaging). The CCD camera was triggered by a +5 V TTL pulse from a digital I/O channel on the PCI-6713 analog output LabView board.

Data Analysis. To calculate the separation efficiencies, the data for selected peaks were fitted with a Gaussian function using OriginPro 7.5 software (OrignLab Corp., Northampton, MA).

6.3. Results and Discussion

Monolith Fabrication and Cleaning. To clean the monolith after fabrication, a subambient pressure was initially used to draw solutions though the microchannel containing the monolith. The subambient pressure was sufficient to clean a 2-cm long monolith thoroughly, but was not adequate to clean a 20-cm long monolith. Multiple porogens were tested to form the acrylamide-bisacrylamide monolith to investigate whether the monolith can be fabricated with an aqueous phase porogen. The porogens tested are listed in **Table 6-1**. The monolith can be formed in DMSO/water and pure water in addition to the DMSO/heptanol and DMSO/dodecanol porogens.

Electroosmotic flow was applied to facilitate the cleaning of the monolith with a 10 mM phosphate buffer with 80% (v/v) methanol. During cleaning, a clear plastic gel formed after the monolith column. A higher pressure was needed to clean a monolith column with the 22-cm length of the 1D serpentine channel. A chip holder was designed and fabricated to apply higher pressures to the reservoirs on the chip. In the chip holder, a chip was clamped between two plastic or metal plates. An o-ring was placed between the reservoir and the holder to ensure good seal. A nitrogen cylinder was used to apply the pressure, and the regulator was used to monitor the pressure. A pressure of 4-6 bar was sufficient to generate enough flow to clean the 22-cm monolith columns.

Table 6-1. Porogen mixtures tested with the acrylamide/bisacrylamide monolith.

porogen mixture	result
DMSO/water	regular monolith
pure water	transparent gel
methanol/water	regular monolith
DMSO/heptanol	regular monolith
DMSO/dodecanol	regular monolith
DMSO/methanol	not formed
DMSO/isopropanol	not formed
pure methanol	not formed

Reversed Electroosmotic Flow with MEAMS. MEAMS carries a positive charge and can be incorporated in the monolith to generate reverse electroosmotic flow. For the negatively charged APTS-labeled glycans, the reverse electroosmotic flow is in the same direction as their electrophoretic mobilities and can be used to drive the 1D CEC separation. Initially, MEAMS was mixed with acrylamide (1:1 mass ratio) and used to coat the channel walls to suppress the electroosmotic flow. An APTS-labeled dextrin 10 mixture was separated in the coated channel. The running buffer was 10 mM phosphate and 100 mM potassium chloride with and without 50% (v/v) ACN. The separations are shown in **Figure 6-2**. Potassium chloride was added to reduce the charge interaction between the sample and the MEAMS coating. When 50% ACN was added to the buffer, the migration times increased, and the resolution improved, which indicated ACN promoted hydrophilic interactions.

APTS-labeled dextrin 10 separation on a monolith with electroosmotic flow suppressed. A serpentine microchannel was coated with linear polyacrylamide to suppress the electroosmotic flow. Subsequently, a 12-cm monolith column was formed in the channel from a polymerization mixture of 40 mg acrylamide, 40 mg methylenebisacrylamide, 2 mg AIBN, 0.5 mL DMSO, and 0.5 mL heptanol. An APTS-labeled dextrin mixture was separated on the monolith with a buffer of 1 mM phosphate and 20 mM HEPES with and without 40% (v/v) ACN. The separation with ACN in the buffer is shown in **Figure 6-3**. In the separation without ACN in the buffer, one broad peak was observed with the elution time spanning 4-7 min. When 40% ACN was added to the buffer, five major peaks were observed in the electropherogram, and the elution times spanned 2-4 min. ACN promoted hydrophilic chromatographic interaction on the

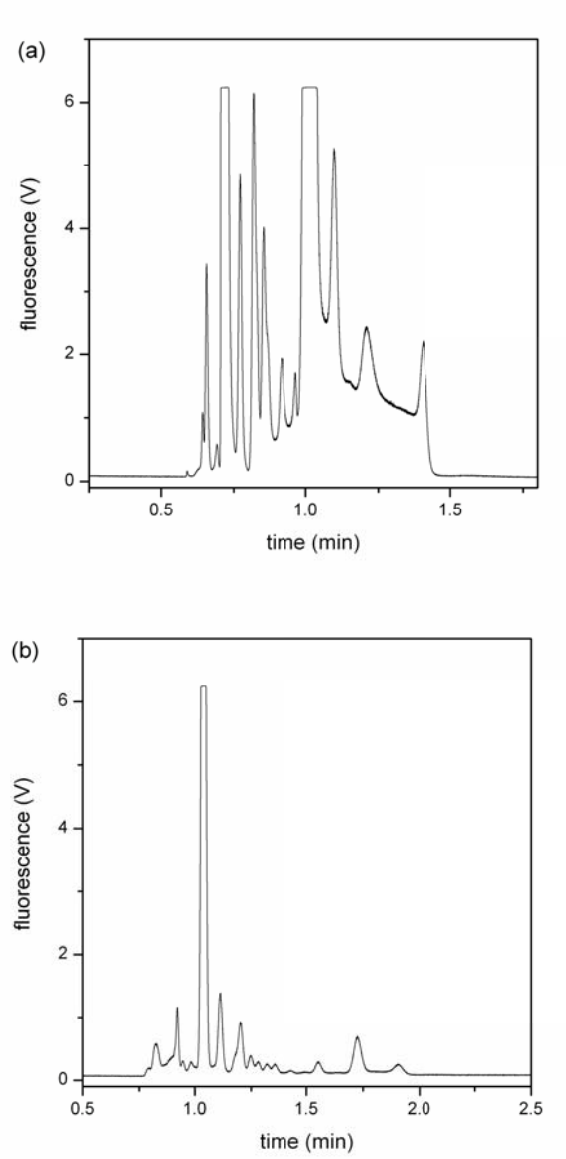

Figure 6-2. Chromatograms of APTS-labeled dextrin 10 separated on a microchannel coated with MEAMS and linear polyacrylamide. The separation field strength was 300 V/cm, and the separation length was 3 cm. (a) Buffer was 10 mM phosphate and 100 mM potassium chloride. (b) Buffer was 10 mM phosphate and 100 mM potassium chloride with 50% (v/v) ACN.

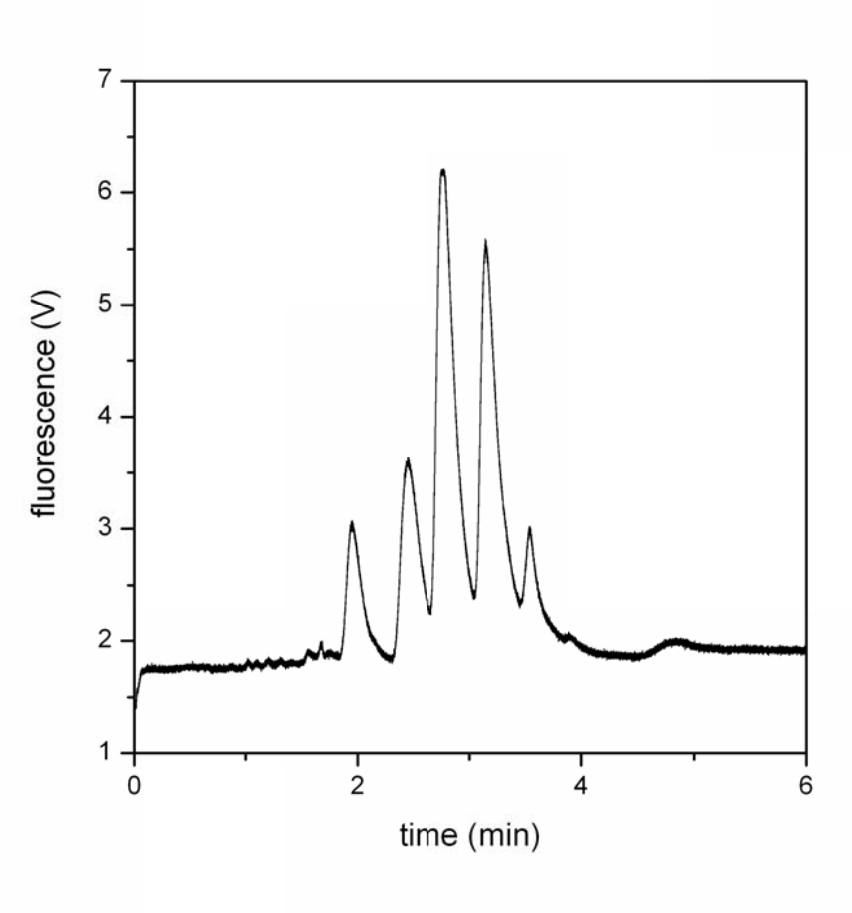

Figure 6-3. Chromatogram of APTS-labeled dextrin 10 separated on a 12-cm monolith in a serpentine microchannel. The separation field strength was 500 V/cm. The separation buffer was 1 mM phosphate and 20 mM HEPES with 40% (v/v) ACN.

monolithic stationary phase, and several components in the dextrin 10 mixture were separated.

2-AMAC-labeled dextrin 10 separation on a monolith with electroosmotic flow enabled. A serpentine microchannel was coated with silane, and subsequently, a 20-cm monolith column was formed in the channel from a polymerization mixture of 60 mg acrylamide, 40 mg methylenebisacrylamide, 1 mg AMPS, 2 mg AIBN, 0.5 mL DMSO, and 0.5 mL heptanol. AMPS was added to generate electroosmotic flow on the monolithic column. A 2-AMAC-labeled dextrin 10 mixture was separated on this monolith, and the electropherogram is shown in **Figure 6-4**. The excess 2-AMAC label eluted before the labeled glycans. The separation performance may be improved by adding more hydrophilic groups in the monolith, such as polyethylene glycol.

2-AMAC-labeled dextrin 10 CE separation. To evaluate using CE as the second dimension after the monolithic CEC separation, a 2-AMAC-labeled dextrin 10 mixture was electrophoretically separated, and the electropherogram is shown in **Figure 6-5**. The excess 2-AMAC label was separated from the labeled glycans, and the elution order is the same as the CEC separation.

Simultaneous detection for the second dimension. A Powell lens was used to expand the laser beam into a line. The line of laser light is shown in **Figure 6-5** during sample loading for a pinched injection. White light shows the outline of the channels, and the mercury lamp illuminates the sample during the loading process. The length of the expanded line was enough to cover the three parallel channels and detect the 2D separations simultaneously.

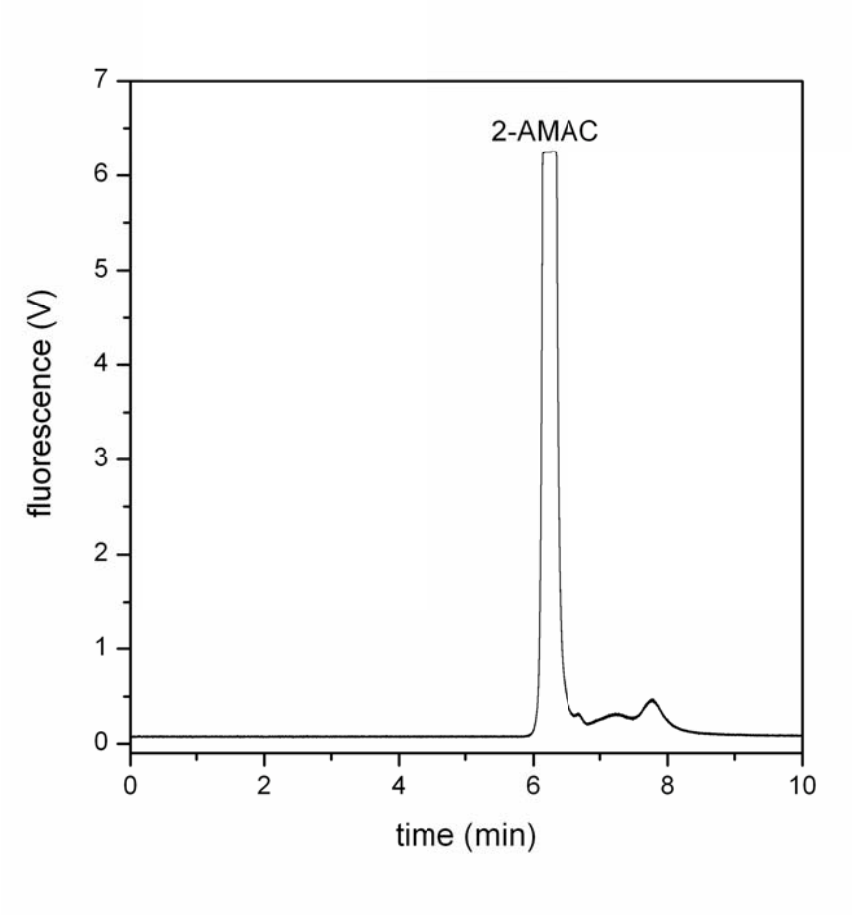

Figure 6-4. Chromatogram of a 2-AMAC-labeled dextrin 10 mixture separated on a 20-cm monolith in a serpentine microchannel. The separation field strength was 375 V/cm. The separation buffer was 10 mM phosphate with 60% (v/v) ACN.

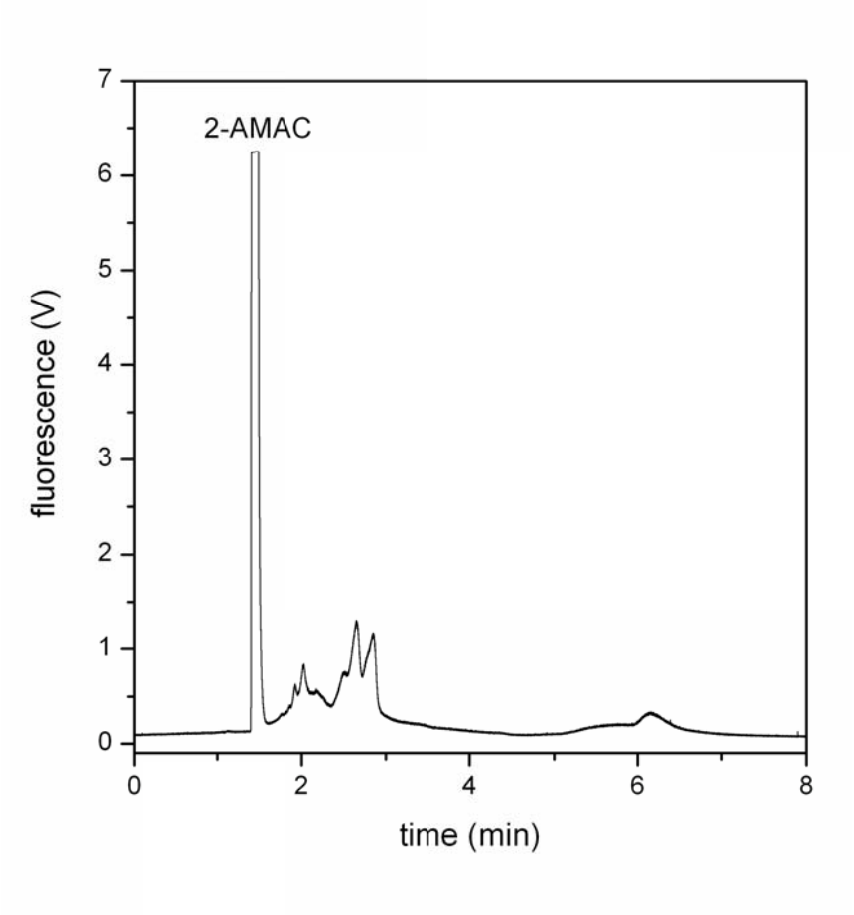

Figure 6-5. Electropherogram of a 2-AMAC-labeled dextrin 10 mixture separated on a 11-cm serpentine microchannel. The separation field strength was 300 V/cm, and the separation buffer was 10 mM phosphate with 60% (v/v) ACN.

Figure 6-5. Fluorescence image of the cross intersection showing the expanded laser line by the Powell lens. The intersection was illuminated with white light to show the channel edges, and a mercury lamp to illuminate the sample stream during sample loading for a pinched injection. The sample loading direction was from top to bottom.

6.4. Conclusion

Monolithic phases of acrylamide and bisacrylamide have been tested for CEC separation for the first dimension. A chip holder was designed and made for monolith cleaning with higher pressures. Preliminary first dimension CEC and second dimension CE separation of a 2-AMAC-labeled dextrin 10 mixture were tested. More work is needed to improve the separation performance of each dimension and to couple the separations in two dimensions.

6.5. References

1. Zhuang, Z.; Starkey, J. A.; Mechref, Y.; Novotny, M. V.; Jacobson, S. C., Electrophoretic Analysis of N-Glycans on Microfluidic Devices. *Anal. Chem.* **2007,** *79* (18), 7170-7175.
2. Tomiya, N.; Awaya, J.; Kurono, M.; Endo, S.; Arata, Y.; Takahashi, N., Analyses of N-Linked Oligosaccharides Using a Two-Dimensional Mapping Technique. *Anal. Biochem.* **1988,** *171* (1), 73-90.
3. Charlwood, J.; Birrell, H.; Tolson, D.; Camilleri, P., Two-Dimensional Chromatography in the Analysis of Complex Glycans from Transferrin. *Anal. Chem.* **1998,** *70* (13), 2530-2535.
4. Tomiya, N.; Lee, Y. C.; Yoshida, T.; Wada, Y.; Awaya, J.; Kurono, M.; Takahashi, N., Calculated 2-Dimensional Sugar Map of Pyridylaminated Oligosaccharides - Elucidation of the Jack Bean Alpha-Mannosidase Digestion Pathway of Man9glcnac2. *Anal. Biochem.* **1991,** *193* (1), 90-100.
5. Guile, G. R.; Wong, S. Y. C.; Dwek, R. A., Analytical and Preparative Separation of Anionic Oligosaccharides by Weak Anion-Exchange High-Performance Liquid-Chromatography on an Inert Polymer Column. *Anal. Biochem.* **1994,** *222* (1), 231-235.
6. Zhuang, Z.; Jacobson, S. C., Serial-to-Parallel Interfaces for Efficient Sample Transfer on Microfluidic Devices. *Anal. Chem.* **2009,** *81* (4), 1477-1481.
7. Kasicka, V., Recent Advances in Ce and Cec of Peptides (2007-2009). *Electrophoresis* **2010,** *31* (1), 122-146.
8. Miksik, I.; Sedlakova, P., Capillary Electrochromatography of Proteins and Peptides. *J. Sep. Sci.* **2007,** *30* (11), 1686-1703.
9. El Rassi, Z., Electrophoretic and Electrochromatographic Separation of Proteins in Capillaries: An Update Covering 2007-2009. *Electrophoresis* **2010,** *31* (1), 174-191.

10. Zhong, H. W.; El Rassi, Z., Neutral Polar Methacrylate-Based Monoliths for Normal Phase Nano-Lc and Cec of Polar Species Including N-Glycans. *J. Sep. Sci.* **2009,** *32* (1), 10-20.
11. Que, A. H.; Mechref, Y.; Huang, Y. P.; Taraszka, J. A.; Clemmer, D. E.; Novotny, M. V., Coupling Capillary Electrochromatography with Electrospray Fourier Transform Mass Spectrometry for Characterizing Complex Oligosaccharide Pools. *Anal. Chem.* **2003,** *75* (7), 1684-1690.
12. Que, A. H.; Novotny, M. V., Separation of Neutral Saccharide Mixtures with Capillary Electrochromatography Using Hydrophilic Monolithic Columns. *Anal. Chem.* **2002,** *74* (20), 5184-5191.
13. Que, A. H.; Novotny, M. V., Structural Characterization of Neutral Oligosaccharide Mixtures through a Combination of Capillary Electrochromatography and Ion Trap Tandem Mass Spectrometry. *Anal. Bioanal. Chem.* **2003,** *375* (5), 599-608.
14. Eeltink, S.; Svec, F., Recent Advances in the Control of Morphology and Surface Chemistry of Porous Polymer-Based Monolithic Stationary Phases and Their Application in Cec. *Electrophoresis* **2007,** *28* (1-2), 137-147.
15. Jacobson, S. C.; Hergenröder, R.; Koutny, L. B.; Warmack, R. J.; Ramsey, J. M., Effects of Injection Schemes and Column Geometry on the Performance of Microchip Electrophoresis Devices. *Anal. Chem.* **1994,** *66* (7), 1107-1113.
16. Hjerten, S., High-Performance Electrophoresis. Elimination of Electroendosmosis and Solute Adsorption. *J. Chromatogr.* **1985,** *347*, 191-198.

Chapter 7. Summary of Research Progress and Future Directions

7.1. Summary of Research Progress

This dissertation discusses development of several microfluidic devices for applications of faster and more efficient biomolecule separations, especially glycan profiling. Microfluidic devices have unique advantages for chemical separation techniques, such as a small footprint, low reagent consumption, fast heat dissipation, and precise fluidic handling capabilities. Various separation techniques have been developed[1-3] and many types of samples[4-6] have been analyzed on microfluidic platforms, among which glycans are of considerable interest. Chapter 1 summarizes our motivation and the progress with the development of the microfluidic devices, and subsequent chapters describe detailed contributions to each individual technique and device.

For systems that cannot support electrokinetic transport, such as organic solvents, high conductivity solutions, and low pH buffers, pressure-driven flow control and valving on microfluidic devices was developed. Chapter 2 describes a pressure-driven gated valve. The pressure source is applied to the microchip through a gas manifold, on which solenoids are mounted to control the pressure on or off, needle valves to finely adjust applied pressures, pressure transducers to monitor the pressures applied to the reservoirs of the microchip. Pressure-driven valving was tested for 10 μM rhodamine B in 10 mM sodium tetraborate solution. A parabolic flow profile was seen in the fluorescence images, and a linear relationship between the velocity and applied pressure was observed. Pressure-driven injections of different volumes at a flow rate of ~ 500 pL/s were reproducible with a relative standard deviation less than 0.7%.

In Chapter 3, we report rapid and efficient electrophoretic separations of N-glycans on microfluidic devices. Using a separation length of 22 cm and an electric field strength of 750 V/cm, analysis times were less than 3 min, and separation efficiencies were between 400,000 and 655,000 plates for the N-glycans and up to 980,000 plates for other sample components. These high efficiencies were necessary to separate positional isomers derived from ribonuclease B and linkage isomers from asialofetuin. Structural isomers of N-glycans derived from a blood serum sample of a cancer patient were also analyzed to demonstrate clinically relevant, complex samples could be separated on-chip with efficiencies similar to samples derived from model glycoproteins. In addition, we compared microchip and capillary electrophoresis under similar separation conditions, and the microchips performed as well as the capillaries. These results confirmed that the non-circular cross-section of the microchannel did not hamper separation performance. For all experiments, the glycan samples were derivatized with 8-aminopyrene-1,3,6-trisulfonic acid (APTS) to impart charge for electrophoresis and a fluorescent label for detection.

Other channel designs that minimize the racetrack effect include serpentine channel layouts with low dispersion turns with symmetric[7] and asymmetric[8-10] tapering of the channel in the turns. Chapter 4 describes the evaluation of several serpentine microchannels with asymmetrically tapered turns having different taper ratios. N-glycans derived from ribonuclease B (RNase B) were separated on these serpentine microchips at electric field strengths ranging from about 760 to 1530 V/cm. At 1530 V/cm, mannose components derived from RNase B were separated in less than 1.2 min with plate numbers of 500,000-600,000. Compared to separations at 750 V/cm, separation time was

reduced by 55% and plate numbers increased by 16-41%. N-glycans derived from the blood serum of an ovarian cancer patient and a healthy individual were separated at 1270 V/cm, and similar separation efficiencies to the RNase B glycans were observed. Native and desialylated glycan samples were easily resolved as seen in the electropherograms.

For the spiral and serpentine microchannels, separation length was increased to achieve better separation efficiency. An alternative approach is to incorporate two dimensional separations for which the total peak capacity will be the product of the two individual dimensional peak capacities. On microfluidic platforms, two common formats for combining multidimensional separation techniques are serial and planar coupling. To date, serially coupled formats have provided superior separation performance than the planar formats.

In Chapter 5, we report serial-to-parallel interfaces for rapidly and efficiently transferring samples from a single microfluidic channel to multiple parallel channels. Three designs and operation modes were evaluated to determine the most efficient transfer process. All designs employed two routing channels to direct the sample into the parallel channels and to prevent sample from leaking into adjacent channels. For two of the three designs, a tee valve and gated valve were added to the interface prior to routing the samples to assist with sample injections into the parallel channels. Injection times as short as 20 ms and injection frequencies up to 10 Hz were achieved with relative standard deviations less than 0.5% for the injected area. With an injection time of 50 ms and injection frequency of 10 Hz, up to 50% of the sample is efficiently transferred. Among the three designs, the interface with the gated valve provided the highest performance and reproducibility.

Chapter 6 described preliminary efforts to integrate two dimensional (2D) separation techniques on the device with the gated serial-to-parallel interface. We investigated capillary electrochromatography (CEC) with acrylamide monolithic phases and capillary electrophoresis (CE) for 2D glycan analysis. APTS-labeled glycans were analyzed on monoliths with electroosmotic flow (EOF) suppressed, and 2-aminoacridone (2-AMAC) labeled glycans were analyzed on monoliths with the electroosmotic flow enabled. A Powell lens was used to expand the laser from a spot to a line so that the parallel channels in the second dimension could be detected simultaneously with a CCD camera.

7.2. Future Directions

Improvements for the First Dimension CEC. APTS-labeled glycans were analyzed on a monolith with the electroosmotic flow suppressed by coating the channel with linear polyacrylamide. Initial separation of the glycans showed the electrochromatography was functioning to resolve the glycan mixture. However, the increase in the background baseline demonstrated some components in the sample were adsorbed onto the monolith and not eluting with the separation buffer. The separation is based on hydrophilic interaction[11] and glycan mixtures have difference in hydrophilicity. The APTS-labeled glycans contained some unreacted labels, which are shown in **Figure 3-3**. The unreacted labels are highly charged and may be the cause of the high background. Solid phase extraction can be tested to purify the APTS-labeled glycans and remove the unreacted labels and salts.

2-AMAC-labeled glycans were separated on the acrylamide monolith formed with acrylamide as the monomer , methylenebisacrylamide as the crosslinker, 2-acrylamido-2-

methyl-1-propanesulfonic acid (AMPS) as the electroosmotic flow generator , and azobisisobutyronitrile (AIBN) as the UV initiator. The separation resolution can be improved by adjusting the morphology and surface chemistry of the monolithic phases, which can be controlled by carefully selecting the polymerization mixture components and varying the concentrations of each.[12] Increasing the crosslinker concentration and lowering the porogen polarity both decrease the microglobule and pore sizes, and subsequently, decrease the plate height and improve the separation performance. In preliminary results, the glycan peaks eluted close to the unreacted label. Functional groups,[13-15] such as amino and hydroxyl containing compounds, can be added to be polymerization mixture to change the hydrophilicity of the monolithic stationary phase.

Immobilization of Enzyme and Lectin on the Monolith. Glycans of interest are present on glycoproteins. Glycan profiling can be carried out with glycans released from the glycoprotein or with glycopeptides generated by enzymatic digestion. Previously, glycans have been separated from the glycoproteins with peptide-N-glycosidase F during sample preparation. The process takes 24 h at 37 °C. The enzyme can be immobilized on a monolithic support by a single step fabrication[16] or two step photografting.[17] The immobilized enzyme was able to cleave off the glycans under room temperature in seconds to minutes and is also reported to be stable and reusable over time periods of months. In addition to PNGase F, proteolytic enzymes such as trypsin can also be immobilized on a monolithic support and achieve much faster digestion under room temperature.[18]

With enzymes and lectins immobilized on monolithic supports, glycan analysis can be streamlined and integrated entirely on a microfluidic device. Labor and time

consuming sample preparation steps can be eliminated, and the analysis can start with loading glycoproteins directly to the microchip. Glycan cleavage, protein digestion, sample labeling, separation, and detection can all be integrated on the same microfluidic device.

Reverse Phase Separation on the Monolith. To analyze the glycan content in clinical samples, glycans can be cleaved from the sample directly, and the whole glycan pool can be profiled. Alternatively, glycoproteins or glycopeptides can be separated and collected prior to glycan release.[19] Compared to glycans, glycoproteins and glycopeptides are often more hydrophobic, and reverse phase electrochromatography can be used to separate them. Instead of a polyacrylamide monolith, polymethacrylate monolith can be used to provide a more hydrophobic backbone and used for reserve-phase separation of glycans, glycoproteins, and glycopeptides.

7.3. References

1. Tia, S.; Herr, A. E., On-Chip Technologies for Multidimensional Separations. *Lab Chip* **2009,** *9* (17), 2524-2536.
2. Reyes, D. R.; Iossifidis, D.; Auroux, P. A.; Manz, A., Micro Total Analysis Systems. 1. Introduction, Theory, and Technology. *Anal. Chem.* **2002,** *74* (12), 2623-2636.
3. Auroux, P. A.; Iossifidis, D.; Reyes, D. R.; Manz, A., Micro Total Analysis Systems. 2. Analytical Standard Operations and Applications. *Anal. Chem.* **2002,** *74* (12), 2637-2652.
4. Tran, N. T.; Ayed, I.; Pallandre, A.; Taverna, M., Recent Innovations in Protein Separation on Microchips by Electrophoretic Methods: An Update. *Electrophoresis* **2010,** *31* (1), 147-173.
5. Toriello, N. M.; Douglas, E. S.; Thaitrong, N.; Hsiao, S. C.; Francis, M. B.; Bertozzi, C. R.; Mathies, R. A., Integrated Microfluidic Bioprocessor for Single-Cell Gene Expression Analysis. *Proc. Natl. Acad. Sci. U. S. A* **2008,** *105* (51), 20173-8.
6. Sanders, G. H. W.; Manz, A., Chip-Based Microsystems for Genomic and Proteomic Analysis. *Trac-Trends Anal. Chem.* **2000,** *19* (6), 364-378.

7. Paegel, B. M.; Emrich, C. A.; Weyemayer, G. J.; Scherer, J. R.; Mathies, R. A., High Throughput DNA Sequencing with a Microfabricated 96-Lane Capillary Array Electrophoresis Bioprocessor. *Proc. Natl. Acad. Sci. U. S. A.* **2002,** *99* (2), 574-579.
8. Griffiths, S. K.; Nilson, R. H., Low-Dispersion Turns and Junctions for Microchannel Systems. *Anal. Chem.* **2001,** *73*, 272-278.
9. Molho, J. I.; Herr, A. E.; Mosier, B. P.; Santiago, J. G.; Kenny, T. W.; Brennen, R. A.; Gordon, G. B.; Mohammadi, B., Optimization of Turn Geometries for Microchip Electrophoresis. *Anal. Chem.* **2001,** *73*, 1350-1360.
10. Ramsey, J. D.; Jacobson, S. C.; Culbertson, C. T.; Ramsey, J. M., High-Efficiency, Two-Dimensional Separations of Protein Digests on Microfluidic Devices. *Anal. Chem.* **2003,** *75*, 3758-3764.
11. Alpert, A. J., Hydrophilic-Interaction Chromatography for the Separation of Peptides, Nucleic-Acids and Other Polar Compounds. *J. Chromatogr.* **1990,** *499*, 177-196.
12. Eeltink, S.; Svec, F., Recent Advances in the Control of Morphology and Surface Chemistry of Porous Polymer-Based Monolithic Stationary Phases and Their Application in Cec. *Electrophoresis* **2007,** *28* (1-2), 137-147.
13. Que, A. H.; Konse, T.; Baker, A. G.; Novotny, M. V., Analysis of Bile Acids and Their Conjugates by Capillary Electrochromatography/Electrospray Ion Trap Mass Spectrometry. *Anal. Chem.* **2000,** *72* (13), 2703-2710.
14. Que, A. H.; Novotny, M. V., Separation of Neutral Saccharide Mixtures with Capillary Electrochromatography Using Hydrophilic Monolithic Columns. *Anal. Chem.* **2002,** *74* (20), 5184-5191.
15. Que, A. H.; Mechref, Y.; Huang, Y. P.; Taraszka, J. A.; Clemmer, D. E.; Novotny, M. V., Coupling Capillary Electrochromatography with Electrospray Fourier Transform Mass Spectrometry for Characterizing Complex Oligosaccharide Pools. *Anal. Chem.* **2003,** *75* (7), 1684-1690.
16. Palms, A. K.; Novotny, M. V., A Monolithic Pngase F Enzyme Microreactor Enabling Glycan Mass Mapping of Glycoproteins by Mass Spectrometry. *Rapid Commun. Mass. Sp.* **2005,** *19* (12), 1730-1738.
17. Krenkova, J.; Lacher, N. A.; Svec, F., Multidimensional System Enabling Deglycosylation of Proteins Using a Capillary Reactor with Peptide-N-Glycosidase F Immobilized on a Porous Polymer Monolith and Hydrophilic Interaction Liquid Chromatography-Mass Spectrometry of Glycans. *J. Chromatogr. A* **2009,** *1216* (15), 3252-3259.
18. Peterson, D. S.; Rohr, T.; Svec, F.; Frechet, J. M. J., Enzymatic Microreactor-on-a-Chip: Protein Mapping Using Trypsin Immobilized on Porous Polymer Monoliths Molded in Channels of Microfluidic Devices. *Anal. Chem.* **2002,** *74* (16), 4081-4088.
19. Rudd, P. M.; Guile, G. R.; Kuster, B.; Harvey, D. J.; Opdenakker, G.; Dwek, R. A., Oligosaccharide Sequencing Technology. *Nature* **1997,** *388* (6638), 205-207.

Curriculum Vitae

Zexi Zhuang

EDUCATION

Indiana University, Bloomington, IN Jun 2010

Ph.D. candidate; Major: Analytical Chemistry; GPA: 3.72/4.0

Fudan University, Shanghai, China May 2003

B.S.; Major: Applied Chemistry; GPA: 3.44/4.0

RESEARCH EXPERIENCE

Stephen C. Jacobson Group, Indiana University, Bloomington, IN Sep 2003 ~ Present

Graduate Research Assistant

- Developed a pressure-driven microfluidic device for pressure pumping, valving, and dispensing small volume (picoliter) injections.
- Designed a serial-to-parallel 2D separation microfluidic device for fast 2D separations and 1-10 Hz sampling rate was achieved at the interface to minimize information loss.
- Achieved ultra high efficiency separation of N-glycans for discovering cancer biomarkers with spiral and serpentine microchannels by resolving structural and linkage isomers.
- Programmed labview codes for voltage control and data acquisition for the whole lab.
- Improved protocols for glass microchip fabrication

Xiangmin Zhang Group, Fudan University, Shanghai Jun 2001 ~ Jun 2003

Undergraduate Research Assistant

- Developed a temperature gradient liquid chromatography for novel applications
- Analyzed traditional Chinese medicines using HPLC
- Separated peptides with capillary electrophoresis and HPLC

TEACHING EXPERIENCE

Indiana University, Bloomington, IN Sep 2003 ~ May 2005

Associate Instructor

- Lectured “Intro to Chemical Principles”

- Supervised “Principles of Chemistry and Biochemistry II” lab sessions
- Lectured and graded “Chromatography”, graduate level class

Fudan University, Shanghai, China Sep 2002 ~ May 2003

Undergraduate Teaching Assistant

- Performed general chemistry experiments to verify and improve design of student experiments and served as an assistant for student biochemistry experiments.

PUBLICATIONS

5. Z. Zhuang Y. Mechref, M.V. Novotny and Jacobson S.C., “Electrophoretic Analysis of N-Glycans on Serpentine Microchannels with Different Taper Ratio Turns”, In Preparation.
4. Sudhoff S.B., Zhuang Z. and Jacobson S.C., “Fast Slewing High Voltage Power Supplies with Optical Resistors as Voltage Dividers”, In Preparation.
3. Z. Zhuang and Jacobson S.C., “Pressure-Driven Flow Control and Valving on Microfluidic Devices”, In Preparation.
2. Z. Zhuang and Jacobson S.C., “Serial-to-Parallel Interfaces for Efficient Sample Transfer on Microfluidic Devices”, Anal. Chem., 2009, 81 (4), 1477-1481
1. Z. Zhuang, J.A. Starkey, Y. Mechref, M.V. Novotny and Jacobson S.C., “Electrophoretic Analysis of N-Glycans on Microfluidic Devices”, *Anal. Chem.*, 2007, 79 (18), 7170-7175

PRESENTATIONS

6. Z. Zhuang, J.A. Starkey, Y. Mechref, M.V. Novotny and Jacobson S.C, “Electrophoretic Glycan Separations on Serpentine Microchannels with Low Dispersion Turns”, Turkey Run Analytical Chemistry Conference 2008
5. Z. Zhuang, J.A. Starkey, Y. Mechref, M.V. Novotny and Jacobson S.C., “High Performance One- and Two-Dimensional Microfluidic Separations”, PITTCON 2008
4. Z. Zhuang and Jacobson S.C., “Serial-to-Parallel Interfaces on Microfluidic Devices”, PITTCON 2007
3. Z. Zhuang and Jacobson S.C., “Fast Sampling Serial-to-Parallel Interfaces on Microfluidic Devices”, Turkey Run Analytical Chemistry Conference 2007
2. Z. Zhuang, J.A. Starkey, Y. Mechref, M.V. Novotny and Jacobson S.C., “Glycan Analysis on Microfluidic Devices”, Turkey Run Analytical Chemistry Conference 2006
1. Z. Zhuang and Jacobson S.C., “Serial-to-Parallel Interfaces on Microfluidic Devices”, Turkey Run Analytical Chemistry Conference 2005